INAUGURAL–DISSERTATION
zur
Erlangung der Doktorwürde
der
Naturwissenschaftlich–Mathematischen
Gesamtfakultät
der
Ruprecht–Karls–Universität
Heidelberg

vorgelegt von
M.–Eng. Hai-Wen Ge (Thermophys. Engr.)
aus Zhejiang, V. R. China

Tag der mündlichen Prüfung: 05.05.2006

Probability Density Function Modeling of Turbulent Non–reactive and Reactive Spray Flows

Gutachter: Prof. Dr. Eva Gutheil
Prof. Dr. Jürgen Wolfrum

Abstract

Turbulent spray flows are frequently encountered in practical combustion systems. The features of turbulent spray flows such as droplet size distribution and mixing process of fuel and air are very important for combustion efficiency, combustion stability, and pollutant emission. Turbulent spray flow is a very complex process which includes turbulence, heat and mass transfer, and phase change. For reactive cases, chemical reactions need to be considered. All processes are strongly coupled. Many aspects in such processes are unsolved.

In the present thesis, turbulent spray flows are investigated using probability density function (PDF) methods. Two methodologies are used: the presumed and the transported PDF method. The presumed PDF methods adopt empirical distributions. The parameters of the distributions are computed from the first several moments which are determined by solving the transport equations of these moments. The transported PDF methods directly solve the transport equation of the single/joint PDF. The statistics are determined from the solutions.

A PDF of the mixture fraction for turbulent spray flows is proposed. The PDF transport equation is deduced. The molecular mixing is described using an extended Interaction-by-Exchange-with-the-Mean (IEM) model. The PDF transport equation is closed through coupling with an extended $k-\epsilon$ model, and is solved using a hybrid finite volume/Lagrangian Monte-Carlo particle method. A turbulent non-reactive spray jet is simulated. The numerical results of the transported PDF method are in good agreement with experimental data from the literature, and they improve the results from the moment closure method. Furthermore, the shapes of the PDF of the mixture fraction at different positions, which are computed by the transported PDF method, are presented and analyzed. It appears that the spray source changes the value of the mean mixture fraction, but it does not change the shape of its PDF. A comparison of the results of the transported PDF method with the standard β function shows that the standard β function fails to describe the shape of the PDF of mixture fraction. With the definition of appropriate local maximum and minimum values of the mixture fraction, a modified four-parameter β function is suitable to reflect the shape of the PDF very well.

A joint velocity-scalar PDF for turbulent spray flows is proposed. Its transport equation is deduced and modeled. The simplified Langevin model is extended to model the gas velocity. The molecular mixing is modeled using the extended IEM model. The simulation of a turbulent non-reactive spray flow shows that the profiles of the gas velocity are well predicted by this joint PDF model.

A joint enthalpy-mixture fraction PDF for turbulent spray flames is proposed.

Its transport equation is deduced. The molecular mixing is modeled using the extended IEM model. A turbulent methanol/air spray flame is simulated. A detailed methanol/air combustion mechanism consisting of 23 species and 168 elementary reactions is implemented through a spray flamelet model. The numerical results of the gas velocity, the gas temperature, the mass fraction of fuel vapor, and the Sauter mean radius are compared with experimental data from the literature and with results from the moment closure method. Good agreement with the experiment is observed. The transported PDF method improves the results of the moment closure method with respect to the mass fraction of the methanol vapor. The presumed PDFs of mixture fraction used in the moment closure method are compared with the computed PDFs of the mixture fraction from the transported PDF method. The results show that the latter ones are more accurate.

The applications of the presumed PDF methods in turbulent spray flows are discussed. The normal distribution, log-normal distribution, Nukiyama-Tanasawa distribution, Rosin-Rammler distribution, standard β distribution, and the modified four-parameter β distribution are discussed and analyzed. The relationships between them are pointed out.

A turbulent ethanol/air spray flow is simulated using $k-\epsilon$ model. A conventional Eulerian/Lagrangian formulation is used. The numerical results of the non-reactive case are compared with the measurements obtained by phase Doppler anemometry. The Sauter mean radius, mean droplet velocity as well as droplet size distribution in the non-reactive case are well predicted. For the reactive case, the detailed chemistry is implemented in the simulation through a spray flamelet model, in which 38 species and 337 elementary reactions are considered. The profiles of the gas temperature are compared with the experimental data which is measured using 2D NO-LIF. Good agreement with the experimental data is found.

Especially, an implicit scheme is designed to compute the particle velocity in convective environment. A numerical test shows that the implicit scheme is more robust, accurate and efficient than the conventional explicit scheme.

Keywords: turbulent spray flow, Monte-Carlo method, PDF method, probability density function, flamelet model

Zusammenfassung

Turbulente Sprays werden häufig im praktischen Verbrennungsystem angetroffen. Die Eigenschaften der turbulenten Sprays, wie Verteilung der Tröpfchengrößen und die Vermischung von Kraftstoff und Luft sind für die Effizienz, die Stabilität, und das Emissionsverhalten der Verbrennungprozesse sehr wichtig. Dies stellt ein sehr komplexes Problem dar. Die Prozesse Turbulenz, Wärme- und Stoffübertragung und Phasenänderung müssen dazu behandelt werden. Für reagierende Stömungen müssen chemische Reaktionen berücksichtigt werden. Diese Prozesse sind stark mit einander gekoppelt und viele Aspekte dieser Prozesse sind bislang unbekannt.

In dieser Arbeit werden turbulente Sprays mit Hilfe einer Wahrscheinlichkeitsdichtefunktion (Probability Density Function, PDF) dargestellt. Zwei Ansätze werden dabei verwendet, angenommene und transportierte PDF Methoden.

Zunächst wird eine PDF für die Mischungsbrüche des turbulenten Sprays vorgeschlagen. Die PDF Transportgleichung wird dazu abgeleitet. Das molekulare Mischen wird mit einem erweitertem (Interaction-by-Exchange-with-the-Mean, IEM) Modell behandelt. Die PDF Transportgleichung wird mit einem erweiterten $k - \epsilon$ Modell geschlossen. Es wird durch eine hybride Finite-Volumen/Lagrange Monte-Carlo Methode gelöst. Ein turbulentes, nicht reagierenden Sprays wird damit simuliert. Die numerischen Resultate der PDF Methode sind in guter Übereinstimmung mit den experimentellen Daten aus der Literatur und verbessern die des Momentenmodells. Außerdem werden die mittels der Monte-Carlo Methode berechneten Formen der Wahrscheinlichkeitsdichtefunktion des Mischungsbruchs in unterschiedlichen Positionen dargestellt und analysiert. Es ergibt sich, dass die Sprayquelle den Wert des mittleren Mischungsbruchs ändert, aber sie ändert nicht die Form seiner PDF. Ein Vergleich der Monte-Carlo PDF mit der Standard-Betafunktion zeigt, dass die Standard-Betafunktion die Form der PDF nicht beschreiben kann. Mit der Definition von geeigneten lokalen Maxima und Minima des Mischungsbruchs ist eine modifizierte Betafunktion mit vier Parametern sehr gut geeignet, die Form der Monte-Carlo PDF darzustellen.

Weiterhin wird eine gebundene Wahrscheinlichkeitsdichteverteilung zwischen Geschwindigkeit und skalaren Größen für turbulente Sprays vorgeschlagen. Die Transportgleichung hierfür wird abgeleitet und modelliert. Ein vereinfachtes Langevin-Modell wird erweitert, um die Gasgeschwindigkeit zu modellieren. Das molekulare Mischen wird mit dem erweiterten IEM-Modell beschrieben. Simulationen des turbulenten nicht-reaktiven Sprays zeigen, dass die numerischen Resultate für die Gasgeschwindigkeit durch dieses Modell verbessert werden.

Des Weiteren wird eine gebundene Enthalpie-Mischungsbruch-PDF für turbulente Sprayflammen vorgeschlagen. Die entsprechende Transportgleichung wird hergeleitet.

Das molekulare Mischen wird mit dem modifizierten IEM-Modell beschrieben. Eine turbulente Methanol/Luft Sprayflamme wird simuliert. Der verwendete Methanol-Luft-Mechanismus umfasst 23 Spezies und 168 Elementarreaktionen. Er wird durch ein Sprayflammen-Schichtenmodell integriert. Die numerischen Resultate für die Gasgeschwindigkeit, die Gastemperatur, den Massenbruch des Kraftstoffdampfs und den Sauterradius werden mit experimentellen Daten aus der Literatur und den Resultaten der Momentenmethode verglichen. Es ergibt sich eine gute Übereinstimmung mit den experimentellen Daten. Die verwendete Methode verbessert die Resultate des Momentenmodells in Bezug auf den Massenbruch des Methanoldampfes. Die angenommene PDF des Mischungsbruchs, die im Momentenmodell verwendet wird, wird mit den berechneten-PDFs des Mischungsbruchs aus der transportierten PDF-Methode verglichen. Die Resultate zeigen, dass die letztere zuverlässiger ist. So sind die Zusammensetzung des Gemischs, die durch die verwendete PDF-Methode berechnet wird, genauer.

Die Anwendungen der angenommene PDF Methode in den turbulenten Sprays werden diskutiert. Die Normalverteilung, logarithmisch-normal-Verteilung, Nukiyama-Tanasawa-Verteilung, Rosin-Rammler-Verteilung, Standard-Beta-Verteilung, modifizierte Vierparameter Beta-Verteilung werden besprochen und analysiert. Die Verbindungen zwischen ihnen werden dargestellt.

Eine turbulente Ethanols/Luft-Spray wird sowohl experimentell, als auch durch numerische Simulation untersucht. Ein herkömmliches Euler/Lagrange Modell wird verwendet. Der mittlere Sauterradius, die mittlere Tröpfchengeschwindigkeit sowie die Verteilung der Tröpfchengrößen werden gut vorausgesagt. Der detaillierte Reaktionsmechanismus wird in der Simulation der Sprayverbrennung durch ein Sprayflammen-Schichtenmodell behandelt, in dem 38 Spezies und 337 Elementarreaktionen betrachtet werden. Es ergibt gute Übereinstimmung zu den experimentellen Daten.

Zusätzlich wird ein implizites Schema entworfen, um die Partikelgeschwindigkeit des Sprays zu berechnen. Ein numerischer Test zeigt, dass der implizite Schema robuster, genauer und leistungsfähiger ist als ein herkömmliches explizites Schema.

Schlüsselwörter: turbulente Sprays, Monte-Carlo-Methode, PDF-Methode, Wahrscheinlichkeitsdichtefunktion, Flamelet-Modell

Contents

List of Tables

List of Figures

1. Introduction

1.1 Background

Combustion is presently the major source of mechanical and electrical energy and it will remain the major source in the foreseeable future. Currently, more than 90% of the primary energy is provided by combustion [1]. According to the World Energy Council the energy demand will increase by 65% until 2020. Therefore, it is of utmost interest to make economic use of the available resources. The impact of pollutant emission and other detriments should be minimized.

Liquid fuels occupy a large portion of modern energy supplement, because of its convenience in transport, flexibility in storage, and availability. In 2002, oil occupied 34.9% of the total primary energy supply [1]. Combustion of liquid hydrocarbon fuels occurs in many practical combustion systems, such as gas turbines, automotive engines, industrial furnaces, and liquid-fueled rockets. The liquid fuels are injected as a spray into the combustion chamber. Almost all the flows in practical devices are turbulence. The resulting turbulent non-reactive and reactive spray flows are very complex. Diverse complex phenomena are involved, such as the hydrodynamic characteristics of fuel injection and spray formation, the transport characteristics of droplets, the interaction between phases, the interaction of heat and mass transfer with turbulence and chemical reactions. These factors have significant effect on the performance of the combustion system. The liquid atomization, droplet size distribution in the spray, spray angle, spray pattern, and mixing of fuel and air are crucial for combustion efficiency, stability, and pollutant emission in spray combustion.

Modern combustion systems are designed with the following goals: high combustion efficiency, high reliability, and minimum emission of the air pollutants. Numerical prediction is a feasible and economic way to establish the criteria for designing the combustors under these detriments. Application of numerical simulation in industry has grown rapidly during the last half century. The numerical simulations are now truly on par with experiment and theory as a research tool for fluid dynamics. The numerical simulations bridge the gaps between the theory and experiment. The weaknesses of each method are complemented by the strengths of the others. The numerical simulation complements the theoretical investigations where the nonlinearity, high degrees

of freedom, or lack of symmetry are of importance, and complements the experiment where the devices are expensive, the data is inaccessible, or the phenomenon is very complex. For the study of combustion, numerical simulations improve our understanding of flame structures and dynamics. The numerical results provide multi-scale information of the flows that is not available using any other technique. The influences of individual parameters in the combustion processes can be established via numerical simulations. Now the numerical simulations are widely used in the design and optimization of the practical combustion system. Compared to the experimental testing and prototyping, the development costs of numerical simulation are very low. Today, no real progress in design or optimization can be made without numerical simulations.

In the present work, turbulent non-reactive and reactive spray flows are investigated by numerical simulations and theoretical analysis with the help of the available experimental data. The transported PDF method and moment closure method are used to simulate the turbulent non-reactive and reactive spray flows. The numerical results are compared with the experimental data and numerical results from the literature. The results of statistical distributions are analyzed using the presumed PDF method. In the following three sections, the numerical simulations of turbulent spray flows, PDF methods, and turbulent combustion models are reviewed. In Chapter 2, the governing equations and physical models are presented, including the gas phase, liquid phase, as well as the transported PDF method, presumed PDF method, and spray flamelet model. Chapter 3 presents the numerical methods solving the governing equations. Chapter 4 shows the numerical results and the discussions. Turbulent methanol/air and ethanol/air spray flows as well as spray flames are simulated. Numerical results are compared with the experimental data and other results available in the literature. Finally, conclusions and perspectives are given in Chapter 5.

1.2 Numerical Simulations of Turbulent Spray Flows in Air

The status of spray and droplet modeling has been reviewed in [2, 3, 4, 5, 6, 7, 8]. In this section, numerical methods to simulate the turbulent spray flows are reviewed.

There are several ways to couple the carrier phase and the dispersed phase. The simplest way is a one-way coupling which predicts the dispersion behavior of transported discrete particles within a given turbulent gas flow (carrier phase $\rightarrow$ dispersed phase). The effects of dispersed particles on the carrier phase are neglected. However, such effects should not be neglected in many cases. The turbulence modifies dispersed particles behavior, which in return modifies turbulence, because micro turbulence is produced due to the presence of the particles. At the interface of the particles, gas-

phase boundary layers and wakes develop because of relative motion between the particle center and the carrier phase. If there is heat and mass transfer between particles and carrier phase, two-way coupling should be used (carrier phase ↔ dispersed phase). Furthermore, when the particle number density is sufficiently large and the effect of the particle-particle interaction cannot be neglected, four-way coupling must be used (carrier phase ↔ dispersed phase ↔ dispersed phase). In the present work, only dilute spray flows are considered. The droplet interactions are neglected. The effects of two-way coupling are taken into account.

The locally homogeneous flow (LHF) model neglects the slip effect between the liquid phase and gas phase. The two phases are in dynamic and thermodynamic equilibrium. At each point in the flow field, they have the same velocity and temperature. LHF condition is the limiting case with infinitely small droplets.

To take into account the effects of the finite rate transportation between the two phases, the separated flow (SF) model is proposed. In general, there are three different approaches in the SF model: discrete-droplet model (DDM); continuous droplet model (CDM); continuous formulation model (CFM). CDM is applicable only when a few phenomena must be considered. Otherwise, the computational cost will be very high. CFM treats the two phases as continuous phases and solve both of them with an Eulerian formulation. It is referred to as an "Eulerian approach" in mathematics, distinguishing it from the "Lagrangian approach". Both of them will be discussed later. It is inconvenient when a range of droplet sizes, and effects of droplet heat-up, etc. must be considered. It is also difficult to establish the representation of the turbulent stresses and transport in liquid phase. DDM corresponds to another category of approach: the "Lagrangian approach". In DDM, the spray is represented by a finite number of droplet groups. The motion and transport of these droplet groups are tracked through flow field using a Lagrangian formulation. The mean quantities of the liquid phase are computed through the statistical methods. An Eulerian formulation or a Lagrangian formulation is employed to solve the gas phase. The effects of the liquid phase are considered by introducing appropriate spray source terms into the governing equations of the gas phase. DDM eliminates errors due to the numerical diffusion in the solution of liquid phase. It is convenient for DDM to construct physical model and numerical algorithm. Thus it is widely used in current numerical simulation of multiphase flows [2, 7]. Considering turbulent dispersion, DDM is further subdivided into deterministic separated-flow (DSF) models and stochastic separated-flow (SSF) models. DSF models neglect the droplet-turbulence interaction which is not satisfying in the most cases. They give unphysical results with laminar-like behavior. Therefore, SSF models dominate this field [2, 7]. In present work, only SSF models are considered.

The mathematical approaches for multiphase flow are usually divided into two

main categories: Eulerian approach (or two-fluid model) and Lagrangian approach (or particle-tracking method) [9, 10, 11]. They are categorized by the way of description of the dispersed phase. Eulerian approach takes the dispersed phase as a continuous fluid. It introduces several continuous scalar fields to represent the particles. The particle characteristics are defined at nodes, which are generally coincident with those used for the continuous-phase grid. The mean field equations are derived for both phases. Therefore, the dispersed phase is modeled at the macroscopic level by this way. The Lagrangian approach is performed at a mesoscopic level. In the Lagrangian approach, the mean field equations are only used for the continuous phase. The particle characteristics are defined along the particle path lines. The particles are tracked individually by using a set of equations which describe their dynamical behaviour. The stochastic particles are tracked to reproduce the same statistics as the real one. The time evolution of the variables of interest is described by stochastic differential equations (SDEs).

The Eulerian approach relies more on the physical models while the Lagrangian approach remains closer to the physics. The computational cost of the Eulerian approach is lower than the Lagrangian approach. The Eulerian approach is well suited to simulate the dense multiphase flow. However, it is less general because of the assumption of a dispersion tensor. It is difficult for the Eulerian approach to account for complex phenomena. The previous studies [9, 10, 11] show that the Lagrangian approach is well suited for the simulation of complex phenomena, for instance, vaporization, combustion, particle/wall interaction, coalescence, break up. Compared to the Eulerian approach, the Lagrangian approach avoids a significant increase of the model constants [9]. The non-physical numerical diffusion of Eulerian particle density in regions of high gradients can be eliminated because of Lagrangian particles' point-wise spatial accuracy. In the present work, the Lagrangian approach with point-volume model is used.

In both the classical Eulerian and Lagrangian approach, the continuous phase is described using the Navier-Stokes equations. Direct numerical simulation (DNS), large eddy simulation (LES), Reynolds-averaged numerical simulation (RANS) method, and probability density function (PDF) method are widely used to solve the continuous phase. Direct numerical simulation (DNS) resolves all time and length scales of the flows [12, 13, 14]. Each simulation produces a single realization of the flow. DNS is a powerful research tool. It is extremely valuable in helping us understand the dynamics because of it unrivaled accuracy. DNS was first used for multiphase flow in 1970's [15]. Many aspects of the multiphase flows are investigated by DNS, including particle dispersion [16, 17, 18, 19, 20], turbulence modification [21, 22, 23, 24], particle interaction [25, 26]. The heat transfer [27, 28, 29, 30], mass transfer [31, 32, 33, 34,

35, 36, 37, 38, 39], multicomponent effects [40, 41], supercritical effects [42, 43, 44], Soret and Dufour effects [44] and heterogeneous reaction [45, 46, 47, 48, 49, 50] were considered in DNS since the end of the last century. However, the application range of DNS is severely limited, because the computational cost of DNS increases as Re^3. A large number of degrees of freedom have to be considered in turbulent non-reactive or reactive flows. This problem becomes much more serious for the turbulent multiphase flows. A full DNS of a practical system is extremely difficult for current computational facilities. Therefore, averaging techniques and simplification are necessary to reduce the computational costs. As a result, unclosed terms arise. Special models are then developed to close the problems. Reynolds averaged numerical simulation (RANS) method only describes the time averaged quantities of the flow field. The effects of the fluctuating variables are described through a turbulent viscosity model or Reynolds-stress model. In the turbulent viscosity models, the turbulent viscosity is obtained from an algebraic relation or from turbulent quantities such as turbulent kinetic energy and its dissipation rate, which is solved using a modeled transport equation. Among the turbulent viscosity model, the two-equation $k - \epsilon$ model is the most frequently used. In the Reynolds-stress models, the modeled transport equations are solved for each component of the Reynolds stress and for the dissipation rate which provides a length or time scale of the turbulence [51]. Therefore, the turbulent viscosity hypothesis is not needed any longer. For the compressible flows, the density cannot be taken as a constant. Therefore, we must consider the density in the same statistical fashion as the other fluid-mechanical quantities. If we directly apply the time-averaging on the Navier-Stokes equation, a wide variety of quantities involving density fluctuation occur in the averaged equations. Favre (mass) weighted averaging is used to solve this problem. In Favre averaging, all fluid-mechanical quantities except the pressure are mass averaged. The correlations with the density fluctuation are eliminated. RANS methods are widely used in the simulation of engineering flows because of their computational simplicity. Unfortunately, many unsteady behavior cannot be captured by the RANS methods. For turbulent combustion, the knowledge of steady statistical means is not always sufficient. An alternative is to use large eddy simulation (LES). LES explicitly computes the large structures of the flows, usually the ones larger than the grid size. The effects of the smaller one are modeled using a subgrid-scale (SGS) model. The large structures in turbulent flows generally depend on the geometry of the system, while the small ones are more universal. Therefore, the models for LES may be more efficient and more global. LES is a powerful tool to predict the unsteady phenomena in turbulent flow which is connecting to the combustion instability, turbulent mixing, and turbulence-chemistry interaction. LES has been applied to the complex flows that occur in engineering applications [52, 53, 54, 55, 56]. LES was applied to multiphase flow in last decade

[57]. To simplify the problem, the effects of particles on the carrier phase and the effects of carrier phase subgrid fluctuations on the particles are neglected in the simulation [57, 58]. Two-way coupling was considered later in [59, 60, 61, 62, 63]. Recently, LES has been used to simulate secondary breakup [64].

PDF method provides an attractive alternative. It will be discussed in detail in the following section.

1.3 Probability Density Function Methods

Suppose a certain physical phenomenon is of interest, and an experiment is conducted to obtain an observed value of this phenomenon. It may be possible to develop a deterministic mathematical model to predict the outcome with the known conditions. However, the outcome cannot be determined on the basis of the available knowledge of the physical phenomenon. Or the outcome is very sensitive to the initial conditions and boundary conditions. This is very common in the fluid dynamics in which the nonlinear effects play a very important role. Theoretically, the flows will be the same if they have exactly the same initial conditions and boundary conditions. Unfortunately, in most practical flows, the conditions cannot be exactly controlled. A small perturbation will be enlarged by the nonlinear effects, which will lead to a completely different flow field. A flow exhibiting such properties is called as a turbulent flow. All the phenomenal properties of the turbulent (multi-phase) flows fluctuate in a non-deterministic manner due to the fluctuations in the initial conditions and boundary conditions. If we measure one physical variable in a turbulent flow with the variation of time, we may get a result like the one illustrated in Fig. 1.1 (left). For such cases, deterministic models are too complex to develop. This is the motivation for modeling the turbulent (multi-phase) flow as a random medium and describing it with probabilistic mathematical model.

The probability theory and statistical theory are the basis of judgement when certainty is not available or not possible. The main object of the probability method is to generalize from a given set of data to a more broadly applicable statement. The main object of the statistical theory is to estimate the properties of a population from tests on the samples drawn from that population. In statistical analysis, the physical variables can take on many possible values, like the one shown in Fig. 1.1 (left). With the knowledge of the statistical theory, the original time-dependent coordinate is transformed into a PDF coordinate (Fig. 1.1) by dividing the whole range of this fluid variable into several class intervals. The class frequency in each interval is counted. The PDF at the ith class interval is evaluated by:

$$f = \frac{N_i}{N_{total}} \cdot \frac{1}{\Delta x_i}, \tag{1.1}$$

where N_i is the frequency of class i; N_{total} is the total number of the available data; Δx_i is the width of the ith class interval. Therefore, PDF is theoretically independent of the choice of the width of class interval while the frequency distribution function is not. When evaluating one PDF, identical class interval is not necessary. The unit of the PDF is the reciprocal of this variable's unit, $[x]^{-1}$.

Giving a joint PDF of N independent variables $\Psi_1, \Psi_2, ...\Psi_N$, the integral of the PDF in whole space is normalized to unity:

$$\int_{\Psi_1,\Psi_2,...\Psi_N} f(\Psi_1, \Psi_2, ...\Psi_N) d\Psi_1 d\Psi_2 ... d\Psi_N = 1. \tag{1.2}$$

The mean of an arbitrary function Q defined in $\mathbf{\Psi}$-space can be calculated from the PDF:

$$\langle Q \rangle = \int_{\Psi_1,\Psi_2,...\Psi_N} Q(\Psi_1, \Psi_2, ...\Psi_N) f(\Psi_1, \Psi_2, ...\Psi_N) d\Psi_1 d\Psi_2 ... d\Psi_N. \tag{1.3}$$

The joint PDF contains all the required information to describe the flow fields. These PDFs can be extracted from experimental data, or the numerical results of direct numerical simulations, LES, transported PDF method.

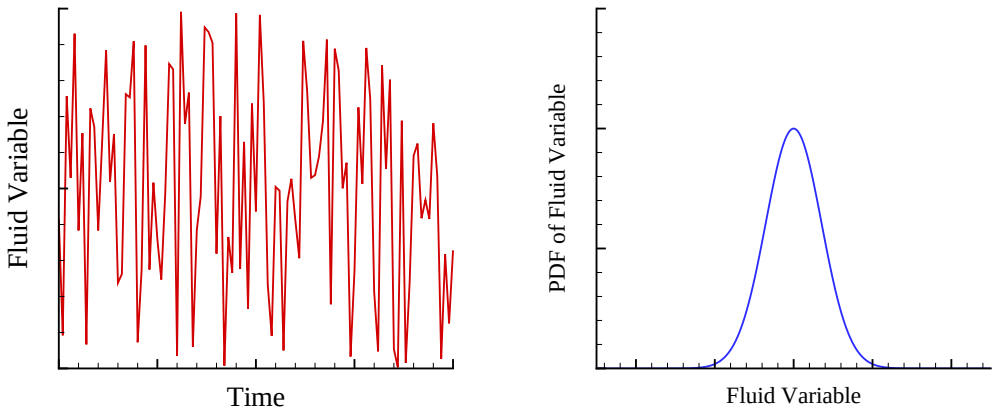

Fig. 1.1: Transformation from time-dependent coordinate (left) to PDF coordinate (right)

Now, the next step is to describe the shape of the PDF with mathematical tools. There are two different ways to do it. One way is to use probability theory. We presume an empirical expression which fits the real PDF. This is the so-called "presumed PDF method". Since the shape of the PDF usually depends on the local physical conditions, a few parameters of the PDF are computed at each location based on the balance equations of the first several moments [65], usually the mean and variance. The presumed PDF method is often used to model one variable. It will become much more difficult to model more than one variable with a presumed joint PDF. For such

problem, people usually assume that they are statistical independent and model the single variable with presumed PDF:

$$f(\Psi_1, \Psi_2, ...\Psi_N) \approx f_1(\Psi_1) f_2(\Psi_2) ... f_N(\Psi_N). \tag{1.4}$$

The presumed PDF method for fluid dynamics is briefly presented in Section 2.2.2. Several popular presumed PDFs are discussed. The relationships between them are analyzed.

Another way is to use statistical theory. We derive the transport equation of this PDF, and solve it numerically. This method is the "transported PDF method" (in many situations, it is referred to as the "PDF method"). When complex processes are involved in the continuous phase, for instance, compressible turbulent reactive flow, this method is a better choice for simulation.

With the PDF method, the local instantaneous variables are simulated explicitly and writing closure laws directly at the macroscopic level is avoided. PDF methods take full account of the stochastic nature of turbulence by describing the flow at each point in terms of the joint PDF of fluid variables, such as velocity, temperature, compositions. Because of this complete description, the most important processes can be modeled without any assumptions, including the terms of convection, body force, mean pressure gradient, chemical reaction source, and spray source for turbulent spray flows. Especially, the PDF methods exactly treat the arbitrary complex chemistry, which makes the PDF methods very attractive in the research of reactive flows. The spray source terms appear in closed forms in the PDF transport equation. In this sense, PDF methods have the potential to be efficient simulating tools for turbulent non-reactive/reactive spray flows.

The joint PDF provides much more information than the conventional method. The independent turbulent fluctuation of all considered fluid variables can be completely represented. All the moments of fluid variables can be determined from the joint PDF, if the moments exist. However, in general, the joint PDF cannot be determined from a finite number of moments. The turbulence-chemistry interaction, turbulence-droplet interaction, chemistry-droplet interaction can be well modeled through the solution of the transport equation for this joint PDF [66].

The models developed for PDF methods are more universal. They depend little on the external conditions, such as combustor configuration, inflow conditions. The PDF methods can handle many different inflow streams of unrelated velocities, temperature and compositions. For instance, the combustion in the gas turbine engines cannot be simply categorized into classical premixed or non-premixed combustion. Most of the turbulent combustion models are designed for special flame type, for instance, the flamelet models for turbulent diffusion flames [67], flame surface density models for

premixed flame [68]. The conventional methods meet the difficulties of deciding which models to be used. Whereas for the PDF methods, this is not a problem. Therefore, the PDF methods have the potential to be novel methods for the computation of turbulent flows.

The multi-time Lagrangian joint PDF completely describes the past history of all fluid particles, which motivates the application of PDF method for unsteady problem [69, 70]. The computational cost of the PDF method compared to direct numerical simulations is considerably lower and affordable for modern computers [71, 72]. Sometimes their computational costs are even lower than the presumed PDF methods [72].

Hopf [73] proposed a PDF transport equation for turbulent flow first in 1952. In some literature, the PDF transport equation is referred to as "Hopf's functional differential equation". Several attempts were made to give an asymptotic solution for the PDF transport equation of simplified cases [74, 75]. Lundgren [76, 77] derived, modeled, and solved a transport equation of the joint PDF of velocity for turbulent flow. Dopazo and O'Brien [78, 79, 80], and Pope [81] derived, modeled and solved the transport equation for the joint PDF of composition. The PDF methods became very popular in numerical simulation of turbulent flow since Pope's work [71, 82, 72, 51, 83, 84].

PDF methods for turbulent single-phase flows have reached the level of maturity. They have become a very active and fruitful research area [84]. The transport equation of the joint velocity-turbulent frequency-composition PDF of turbulent flows has been derived and modeled [85]. A complete closure is provided by the resulting modeled transport equation [86]. Advanced mixing model, including Euclidean minimum spanning tree (EMST) model [87], has been developed. The change in particle composition is determined by particle interactions along the edges of a Euclidean minimum spanning tree constructed in composition space. A new near-wall model has been developed [88, 89]. A fully consistent hybrid finite volume/Monte-Carlo algorithm has been developed to solve the transport equation of the joint velocity-turbulent frequency-composition PDF on structured meshes [90, 91, 92] and unstructured meshes [93, 94]. The computational efficiency of the PDF method is improved significantly by using the consistent hybrid algorithm. Multiple mapping conditioning (MMC) approach has been developed in the context of the turbulent mixing by combining conditional moment closure and amplitude mapping closure [95]. The MMC model represents a logical combination of the PDF method and the conditional moment closure method. The mapping between Gaussian reference fields and species fields is constructed to yield a one-point joint PDF. The statistics of the species fields are determined from the joint PDF and the mapping. The detailed chemical reaction has been adopted through computationally efficient numerical schemes [96, 97, 98] or laminar flamelet model [99, 100, 101]. Turbulent-radiation interactions have been modeled through a

joint velocity-composition PDF [102] and a composition PDF [103]. The concept of the transported PDF method has been introduced into the context of LES, which led to the filtered density function (FDF) method [104]. The FDF method has become a very popular topic in combustion community because of its ability to deal with unsteady phenomena [105, 106, 107, 108, 109, 56]. The PDF method has also been coupled with unsteady Reynolds averaged numerical simulation (U-RANS) to investigate the unsteady phenomena in turbulent non-reactive/reactive flows [69, 70]. Recently, Mura and Borghi [110] proposed a partial PDF concept, in which the whole PDF is decomposed into several partial PDFs. Each PDF has a relative weight. The transport equation of the partial PDFs and the weighting coefficients were deduced.

However, there are still significant areas requiring careful research in PDF methods, especially in application to the multi-phase flows. PDF methods were introduced into the field of multiphase flow at the beginning of 1990's. PDF methods were used to describe the dispersed phase. Derevich and Zaichik [111] derived the joint PDF transport equation of particle's velocity and temperature. Assuming that the fluctuation of the gas velocity seen by particles is a Gaussian random process, the conditional average of the gas fluctuation velocity is closed using the Furutsu-Novikov-Donsker formula. Nevertheless, the assumption of Gaussian random process lacks a solid foundation. Reeks and his co-workers [112, 113] derived the PDF transport equation of particle's velocity in analogy with the kinetic theory. The effects of velocity fluctuation of carrier phase were modeled using Kraichnan's direct interaction approximation (DIA) and Lagrangian history direct interaction (LHDI) approximation. Hyland *et al.* [114] modeled the PDF equation of particle's velocity using Furutsu-Novikov-Donsker formula and obtained an equation that is identical to the one obtained by Reeks [115] in LHDI framework. Pandya and Mashayek [116] used Van Kampen's cumulant expansion method to obtain an approximate equation of PDF to predict the droplet evaporation in isothermal and isotropic turbulent flows. Consequently, the macroscopic equations of the moments for interesting particle properties were derived from the particle PDF equations [115, 117, 118, 119, 120, 121, 122, 123, 124, 125]. Jones and Sheen [126] deduced a joint PDF of particle's velocity, temperature, and mass (size). The effects of turbulent fluctuation were taken into account using a Wiener process. The PDF transport equation is solved using a Monte-Carlo method. Simonin [127] described the dispersed phase in terms of a particle PDF of velocity, temperature and mass obeying a kinetic equation including the effects from the fluid turbulence and inter-particle collisions. The quantities of the continuous phase occurring in the particle PDF transport equation are replaced with so-called "particle-seen" quantities. The particle-seen quantities are determined by introducing appropriate physical models. The particle-seen fluid velocity is modeled by using a Langevin equation, which

is identical to the one used in the stochastic trajectory models and the one used in the PDF equation of single-phase flows [71]. The resulting closed form of the kinetic equation is used to derive an Eulerian transport equation for the mean and turbulent correlations of the dispersed phase variables [128]. Minier and Pozorski [129, 130, 131] followed Simonin's idea and improved the coefficients in the Langevin equations. The corresponding stochastic model is still in development [129, 130, 131, 132]. Combining with second-order moment closure of fluid turbulence, Liu *et al.* [133, 134] solved the joint PDF transport equation of droplets and droplet-seen gas properties with a hybrid finite-volume and Monte-Carlo method. The crossing-trajectory effect and the continuity effect is taken into account by the Langevin equation proposed by Simonin [127]. A well-specified case of spray evaporation in a sudden-expansion chamber is simulated for validation.

On the other hand, PDF methods were used to describe the carrier phase in multiphase flows. Raju [135, 136, 137] deduced and solved joint composition PDF transport equation of turbulent spray flows. Interaction-by-exchange-with-the-mean (IEM) mixing model was used to account the effects of molecular mixing. A single-step mechanism was used for the reactive cases. The PDF transport equation was solved using a hybrid finite-volume and Monte-Carlo method on unstructured meshes. Taut *et al.* [138] deduced and solved joint composition PDF transport equation of the turbulent spray flows too. Modified Curl's model was used for molecular mixing. Detailed chemistry was implemented using intrinsic low-dimensional manifolds (ILDM) method. Monte-Carlo method was implemented into the KIVA III code to solve the PDF transport equation. Durand *et al.* [139] suggested a joint composition PDF for Diesel engine combustion. Modified Curl's model was extended to account the effects of vaporizing droplets. The PDF transport equation was solved using an Eulerian Monte-Carlo method which was implemented into KIVA II code. Ge and Gutheil deduced, modeled, and solved a single scalar (mixture fraction) PDF [140] and a joint velocity-scalar PDF [141] for the turbulent spray flows. IEM model was extended to take into account the effects of molecular mixing. For the joint velocity-scalar PDF, Langevin model was extended to model the gas velocities. A hybrid finite volume and Lagrangian Monte-Carlo method was used to solve the PDF transport equation. Recently, Ge and Gutheil [142] deduced joint mixture fraction-enthalpy PDF for turbulent spray flame. Detailed chemistry was implemented through spray flamelet model.

Zhu *et al.* [143, 144] deduced and solved a single joint PDF transport equation of all liquid-phase and gas-phase random variables. A phase-indicator function was used to capture the interface of the multiphase flow. The effects of turbulent fluctuation were neglected. Rumberg and Rogg [145] suggested to describe the multiphase flow with two separate density function. Both phase density functions and their transport

equations were defined in the overall two-phase flow field. Effects of interfacial surfaces interaction, including heat and mass transfer, on the overall flow were taken into account by source terms in the transport equation. Following this idea, Roekaerts and his co-workers [146, 147] adopted a joint velocity-composition PDF for the continuous phase and the joint PDF of droplet velocity, droplet temperature, droplet-seen gas velocity, and droplet-seen gas composition for dispersed phase. A Reynolds-stress model was used to close the problem. A turbulent spray flow with evaporation was simulated in which the effects of two-way coupling were neglected [148].

1.4 Turbulent Combustion Models

Combustion processes in gaseous phase evolve many complex physical and chemical phenomena: reaction chemistry, turbulence transportation, diffusion of heat and species, and thermodynamics. These processes are strongly coupled. The interaction between them cannot be neglected, especially the turbulent-chemistry-interaction. The chemical reaction rates are strongly coupled to molecular diffusion at the smallest scales of turbulence. The heat release from the chemical reactions affects the turbulent flow, both from variations in density field and from the effects of local dilatation. The study of turbulence-chemistry interaction is one of the most important topics in combustion community. To reduce its complexity, a simplified chemistry of single-step reaction or two-step reaction is often used in engineering simulation. The mean heat release rate and the species mass fraction are of great practical interest. Because either RANS or LES, the combustion occurs at the unresolved scales of the computations, the mean reaction rates should be approximated using combustion models. The simplest and direct approach is to develop the chemical rate in taylor series as a function of species mass fraction and temperature [149]:

$$\begin{aligned} \bar{\dot{\omega}}_F &= -A\bar{\rho}^2\tilde{T}^b\tilde{Y}_F\tilde{Y}_O\exp\left(-\frac{T_A}{\tilde{T}}\right) \\ &\quad\times\left[1+\frac{\widetilde{Y_F''Y_O''}}{\tilde{Y}_F\tilde{Y}_O}+(P_1+Q_1)\left(\frac{\widetilde{Y_F''T''}}{\tilde{Y}_F\tilde{T}}+\frac{\widetilde{Y_O''T''}}{\tilde{Y}_O\tilde{T}}\right)+...\right]. \end{aligned} \tag{1.5}$$

This equation leads to various difficulties. Because of strong non-linearities, large errors exist if only few terms of the series expansion are retained. Many new unclosed quantities arise that must be modeled using algebraic expressions or additional transport equations.

Due to the growing awareness concerning combustion related pollutant emissions and global warming, detailed chemistry is necessary for the numerical simulation. On the other hand, if the detailed chemistry is implemented, the computational cost becomes very high because of the high degree of freedom of the system. In the most

common formulation, a time-dependent differential equation is used to calculate the concentration of each chemical species. These coupled equations are characterized with widely disparate characteristic time scale, which increase the difficulties in computation. Such character, referred as "stiffness", needs special numerical treatment [150, 151]. Actually, Eq. (1.5) is only valid for a simple irreversible reaction. When a detailed chemical reaction mechanism is considered, the expression involving hundreds of species will be extremely complicated. Models with solid physical meanings are required. These models must be designed to describe turbulent flames and have to provide an estimation of the mean production/consumption rates of chemical species. They should base on the known quantities or on the quantities which may be easily modeled or obtained from closed balance equations. Basic concepts include the mixture fraction for non-premixed flames and progress variable for premixed combustion.

The simplest approach is the "no model" (Arrhenius) approach, which neglects the effects of turbulence on combustion and retains only the first term in the Eq. (1.5). In other words, it assumes that the chemical time scales are larger than turbulent time scales ($\tau_c \gg \tau + t$, Da$\rightarrow \infty$).

The eddy breakup (EBU) model [152] is based on a phenomenological analysis of turbulent combustion assuming high Re number (Re $\gg 1$) and high Da number (Da $\gg 1$). EBU model assumes a homogeneous and isotropic turbulence. The reaction zone is viewed as a collection of fresh and burnt gas pockets. The mean reaction rate is mainly controlled by the turbulent mixing time and does not depend on the chemical characteristics. The mean reaction rate is written as a function of known quantities without any additional transport equations. However, it contains limited information about kinetics and ignores turbulent fluctuations. The EBU model is widely used in engineering simulation because of its simplicity. It is available in most commercial CFD codes. Eddy dissipation concept (EDC) [153] is directly extended from EBU. It cannot be used in premixed flame and cannot describe any ignition mechanism.

Another category of modeling strategy is statistical approach. The statistical properties of intermediate states are described using a probability density function. With the joint composition PDF $\tilde{f}(\rho, Y_1^*, ..., Y_N^*, T^*; \mathbf{x}, t)$, the mean burning rate can be estimated as

$$\begin{aligned} \bar{\dot{\omega}}_{Y_i}(\mathbf{x}, t) &= \int_\rho \int_{Y_1} ... \int_{Y_N} \int_T \dot{\omega}_{Y_i}(\rho^*, Y_1^*, ..., Y_N^*, T^*) \\ &\quad \times \tilde{f}(\rho^*, Y_1^*, ..., Y_N^*, T^*; \mathbf{x}, t) d\rho^* dY_1^* \dots dY_N^* dT^*. \end{aligned} \tag{1.6}$$

Then the turbulent flame is fully described by this joint PDF. Similar to the problem described in Section 1.3, the PDF here can be determined by presumed PDF method or transported PDF method.

Theoretically, the transported PDF method can treat the arbitrary complex chem-

istry without any assumption. However, computing $\dot{\omega}_{Y_i}(\rho^*, Y_1^*, ..., Y_N^*, T^*)$ is still a difficult task for current computers. Special numerical strategies are developed to reduce the computational time in calculating the mean reaction rate. Two methodologies are often used, the storage-retrieval algorithm and the dimension reduction method. The storage-retrieval algorithm bases on the fact that two close points in the composition space will evolve to the new points which are very close, too. If one composition vector is close enough to another one whose new state has been computed directly and has been stored in a structured library, then the new state of this composition vector is retrieved from the library. Otherwise, the new state is computed directly and stored in the library. The storage-retrieval algorithm includes *in situ* adaptive tabulation (ISAT) [97], artificial neural networks (ANN) [154, 98], repro-modelling [155], piecewise implementation of solution mapping [156], etc. The dimension reduction method aims to reduce the number of differential equations to be solved directly. Some species are assumed to be in steady state or some reactions to be in particle equilibrium. The concentration of these species are determined from the algebraic equations. The dimension reduction method includes quasi-steady state approach [157, 158], intrinsic low-dimensional manifolds (ILDM) [96], trajectory-generated low-dimensional manifolds (TGLDM) [159], computational singular perturbation (CSP) [160], flamelet generated manifolds [161], flame prolongation of ILDM [162], Roussel and Fraser algorithm [163], rate-controlled constrained equilibrium (RCCE) [164, 165], pre-image curves [166] etc..

On the other hand, great efforts have been taken to simplify the expression of the joint PDF $\tilde{f}(\rho^*, Y_1^*, ..., Y_N^*, T^*; \mathbf{x}, t)$. For instance, the composition space $Y_1^*, ..., Y_N^*$ is replaced with a conserved scalar; the joint PDF is presumed to a empirical expression.

Bray-Moss-Libby model [167] combines a statistical approach (presumed PDF) and a physical analysis. It corresponds to an infinitely thin flame front. It has evidenced some special features of turbulent premixed combustion.

Another group of combustion model assumes that the chemical reaction occurs in thin layers separating fresh gases from fully burnt ones (high Damköhler number limit). The reaction zone is viewed as a collection of laminar flamelets. Coherent flamelet and flame surface density models are introduced for turbulent premixed combustion [168, 169, 68, 84]. For non-premixed flames, hypotheses formulated to construct models may be organized into three groups [68]:

- mixed is burnt: assuming infinitely fast chemistry;
- flamelet assumption: finite rate chemistry assuming a local diffusive-reactive layer similar to the one observed in laminar flames;
- PDF method: finite rate chemistry with the treatments of molecular and heat

transport separated from the chemical reactions. The chemical reaction is treated without any assumption while molecular diffusion is modeled through a micro-mixing model.

In many turbulent reactive flows, departures from chemical equilibrium appear at conditions where the characteristic turbulent mixing time scalar is comparable with the characteristic chemical reaction time scale. Modeling these highly turbulent flames with the fast chemistry assumption may fail to predict the concentrations of the free radicals that are considerably higher than their equilibrium values. In this sense, the first group is questionable.

Flamelet assumption takes into account the non-equilibrium effects. Instead of calculating the reaction rate, the composition space is determined from a pre-calculated laminar flamelet library. The coupling between non-equilibrium chemistry and turbulence is achieved by the statistical description of two parameters: the mixture fraction and the instantaneous scalar dissipation rate. The mean compositions are calculated by [67]

$$\tilde{Y}_i = \int_{\xi_C} \int_{\chi} Y_i^{SLFM}(\xi_C, \chi) \tilde{f}(\xi_C, \chi; \mathbf{x}, t) d\xi_C d\chi. \tag{1.7}$$

Here $\tilde{f}(\xi_C, \chi; \mathbf{x}, t)$ is the joint PDF of the mixture fraction and the scalar dissipation rate. Usually, we assume that these two parameters are statistically independent [67]:

$$f(\xi_C, \chi; \mathbf{x}, t) = f_{\xi_C}(\xi_C; \mathbf{x}, t) f_{\chi}(\chi; \mathbf{x}, t). \tag{1.8}$$

A β function [170] and a log-normal function [171] are used to describe the mixture fraction and scalar dissipation rate, respectively. It is well-known that the assumption of the mixture fraction and scalar dissipation rate being statistical independent is incorrect. In this sense, the assumption of statistical independence is questionable. An alternative way to avoid such assumption is to solve the transport equation of $\tilde{f}(\xi_C, \chi; \mathbf{x}, t)$.

Conditional moment closure (CMC) was proposed in 1990's [172, 173, 174]. The basic concept is that the fluctuations in temperature and composition that occur in turbulent combustion can be closely cross-linked to the fluctuations in one or two key variables. With CMC, the conservation equations for species and enthalpy can be reformulated in terms of conditional averages, which is the average of all these scalars having the same value of the key variable(s). The PDF $\tilde{f}$ in Eq. (1.6) is replaced by a conditional PDF. For the non-premixed combustion, the mixture fraction is the key variable of interest. CMC has been used to simulate spray auto-ignition [175].

For the turbulent spray flame, the combustion model is few. Musculus and Rutland [176] extended the coherent flamelet model to diesel combustion. The mean reaction rate is calculated from the transport equation of the flame area density. The effects

of turbulence are taken into account in the formation of the flame area. Gutheil and co-workers [177, 178] and Chang *et al.* [179] extended the classical flamelet model for the spray combustion. Gutheil and co-workers [180] developed spray flamelet model which takes into account the effects of droplets on the flamelet. The flamelet library is built up from the results of counter-flow spray combustion with detailed transport and detailed chemistry [181, 182, 183]. The spray flamelet model has been applied in the simulation of the turbulent methanol/air spray flames [180] and turbulent ethanol/air spray flames [184]. Recently, it has been implemented into the PDF code for spray combustion [142].

2. Governing Equations and Models

In this chapter, the governing equations of gas-phase and liquid-phase are presented as well as the transported PDF formulation. Physical models used in the present thesis are described. Presumed PDF method for fluid dynamics is discussed.

2.1 Gas Phase Flow

2.1.1 Thermo-Chemistry

We assume the gas flow to be an ideal gas mixture. In this section the thermo-chemistry of an ideal gas mixture is described.

Thermo-chemical state of the gas mixture is characterized by the pressure, p, temperature, T, and the mass fraction, $\mathbf{Y} = (Y_1, Y_2, \ldots, Y_{N_s})^T$ of the N_s species. The molecular weight of species α is W_α. Its gas constant is

$$R_\alpha = \frac{\mathcal{R}}{W_\alpha}, \tag{2.1}$$

where $\mathcal{R} = 8.31451\text{J/(mol·K)}$ is the universal gas constant.

Specific total stagnant enthalpy consists of the kinetic energy, sensible enthalpy, h_s, and chemical enthalpy (the enthalpy of formation), Δh_f^0 [185],

$$h = \frac{1}{2}U_i U_i + h_s + \Delta h_f^0. \tag{2.2}$$

The specific sensible enthalpy of species α is given by

$$h_{s,\alpha}(T) = h_{s,\alpha}^0 + \int_{298.15K}^{T} c_{p\alpha}(T')dT', \tag{2.3}$$

where $h_{s,\alpha}^0$ is the sensible enthalpy of species α at the reference temperature $T_0 = 298.15$ K. The value of $h_{s,\alpha}^0$ is taken from the thermodynamic data table [186]. The constant-pressure specific heat $c_{p\alpha}(T)$ is given by a polynomial function of T:

$$c_{p\alpha}(T) = a_{0,\alpha} + a_{1,\alpha}T + a_{2,\alpha}T^2 + a_{3,\alpha}T^3 + a_{4,\alpha}T^4. \tag{2.4}$$

The coefficients $a_{n,i}$ is taken from the literature [187].

The specific sensible enthalpy of a gas mixture is

$$h_s = \sum_{\alpha=1}^{N_s} h_{s,\alpha} Y_\alpha. \tag{2.5}$$

The chemical reaction energy source term $\dot{Q}$ is

$$\dot{Q} = -\sum_{\alpha=1}^{N_s} \Delta h^0_{f,\alpha} S_\alpha. \tag{2.6}$$

Here S_α is the net chemical reaction rate for species α:

$$S_\alpha = M_\alpha \dot{\omega}_\alpha. \tag{2.7}$$

Assumed as a Newtonian fluid, the viscosity coefficient μ is given as a function of temperature. Effect of bulk viscosity is neglected. The dynamic viscosity of species α is

$$\ln \mu_\alpha = \sum_{i=0}^{3} a_{i,\alpha} (\ln T)^i. \tag{2.8}$$

The coefficients $a_{n,i}$ is taken from the table in [188]. The dynamic viscosity of a gas mixture is given as [188]

$$\mu = \frac{1}{2}\left[\sum_{\alpha=1}^{N_s} X_\alpha \mu_\alpha + (\sum_{\alpha=1}^{N_s} \frac{X_\alpha}{\mu_\alpha})^{-1}\right], \tag{2.9}$$

where X_α is the mole fraction of the species α.

Similarly, thermal conductivity λ_α is given as a function of temperature, too, and is determined from a polynomial form with the coefficients $d_{i,\alpha}$ [188]:

$$\ln \lambda_\alpha = \sum_{i=1}^{4} d_{i,\alpha} (\ln T)^{i-1}. \tag{2.10}$$

The coefficients $d_{i,\alpha}$ is taken from the table in [188]. The thermal conductivity of a gas mixture is determined using

$$\lambda = \frac{1}{2}\left[\sum_{\alpha=1}^{N_s} X_\alpha \lambda_\alpha + (\sum_{\alpha=1}^{N_s} \frac{X_\alpha}{\lambda_\alpha})^{-1}\right]. \tag{2.11}$$

Binary diffusion coefficient $D_{\alpha\beta}$ depends on the temperature and is evaluated from a polynomial form with the coefficients $b_{i,\alpha\beta}$ [188]:

$$\ln D_{\alpha\beta} = \sum_{i=1}^{4} b_{i,\alpha\beta} (\ln T)^{i-1}. \tag{2.12}$$

The coefficients $b_{i,\alpha\beta}$ is taken from the table in [188]. The diffusion coefficient of species α in a mixture is estimated from Hirschfelder-Curtiss (or zeroth-order) approximation [189]:

$$D_{\alpha,M} = \frac{1 - Y_\alpha}{\sum_{\beta \neq \alpha} \frac{X_\alpha}{D_{\alpha\beta}}}. \tag{2.13}$$

2.1.2 Conservation Equations

For compressible multiphase flows, the Navier-Stokes equations are written in conservation form:

Continuity Equation

$$\frac{\partial \rho}{\partial t} + \frac{\partial (\rho U_j)}{\partial x_j} = S_{l,1}; \tag{2.14}$$

Momentum Equation

$$\frac{\partial (\rho U_i)}{\partial t} + \frac{\partial (\rho U_i U_j)}{\partial x_j} = -\frac{\partial p}{\partial x_i} + \frac{\partial \tau_{ij}}{\partial x_j} + \rho g_i + S_{l,U_i}; \tag{2.15}$$

Conservation Equation of the Total Stagnant Enthalpy

$$\frac{\partial (\rho h)}{\partial t} + \frac{\partial (\rho U_j h)}{\partial x_j} = \frac{\partial p}{\partial t} + \frac{\partial (\tau_{ij} U_j)}{\partial x_i} - \frac{\partial J^d_{q,j}}{\partial x_j} - \frac{\partial J^c_{q,j}}{\partial x_j} + q_r + S_{l,h}; \tag{2.16}$$

Conservation Equation of Species

$$\frac{\partial (\rho Y_\alpha)}{\partial t} + \frac{\partial (\rho U_j Y_\alpha)}{\partial x_j} - \frac{\partial}{\partial x_j}\left(\rho D_\alpha \frac{\partial Y_\alpha}{\partial x_j}\right) = S_\alpha + S_{l,Y_\alpha}. \tag{2.17}$$

$\rho, \mathbf{U}, h, p$ are the density, velocity, enthalpy and pressure of the gas flows. $g = 9.8\mathrm{m/s}^2$ is the acceleration of gravity. Subscript $\alpha = 1, 2, \ldots, N_s$ indicates the species. $S_{l,1}$, S_{l,U_i}, $S_{l,h}$, S_{l,Y_α} are the source term due to spray evaporation. τ_{ij} is the viscous stress tensor:

$$\tau_{ij} = \mu\left(\frac{\partial U_i}{\partial x_j} + \frac{\partial U_j}{\partial x_i} - \frac{2}{3}\frac{\partial U_k}{\partial x_k}\delta_{ij}\right), \tag{2.18}$$

where δ is the tensorial Kronecker symbol

$$\delta_{ij} = \begin{cases} 1 & : \quad i = j \\ 0 & : \quad i \neq j. \end{cases} \tag{2.19}$$

The viscous and pressure tensor are often combined into a tensor σ_{ij} defined as

$$\sigma_{ij} = \tau_{ij} - p\delta_{ij}. \tag{2.20}$$

In the energy equation (2.16), the term due to friction heating and Dufour effect are neglected. The terms on the right-hand side are the change rate of the pressure, the viscous heating source term, the heat diffusion term, the transport of different sensible enthalpies by individual species, the radiative heat flux, q_r, and the source term due to spray evaporation, S_{l,h_s}, respectively. The head diffusion term is expressed by the Fourier's Law:

$$J^c_{q,j} = -\lambda\frac{\partial T}{\partial x_j} = \frac{\lambda}{\bar{C}_p}\left(\frac{\partial h}{\partial x_j} - \sum_{\alpha=1}^{N_s} h_\alpha \frac{\partial Y_\alpha}{\partial x_j}\right). \tag{2.21}$$

$J^d_{q,j}$ is written as

$$J^d_{q,j} = \sum_{\alpha=1}^{N_s} h_\alpha J^m_\alpha = -\sum_{\alpha=1}^{N_s} \rho h_{s,\alpha} D_{\alpha,M} \frac{Y_\alpha}{\partial x_j}. \tag{2.22}$$

Assuming a unity Lewis number (Le=1) and equal diffusibility of all species, the total heat flux is

$$\begin{aligned} J_q &= J^c_{q,j} + J^d_{q,j} = -\frac{\lambda}{\bar{C}_p}\left(\frac{\partial h}{\partial x_j} - \sum_{\alpha=1}^{N_s} h_\alpha \frac{\partial Y_\alpha}{\partial x_j}\right) - \sum_{\alpha=1}^{N_s} \rho h_{s,\alpha} D_{\alpha,M} \frac{Y_\alpha}{\partial x_j} \\ &= -\frac{\lambda}{\bar{C}_p}\frac{\partial h}{\partial x_j} = -\Gamma_h \frac{\partial h}{\partial x_j}. \end{aligned} \tag{2.23}$$

In the present work, q_r, and the viscous heating source term are neglected. Eq. (2.16) can be simplified as

$$\frac{\partial \rho h}{\partial t} + \frac{\partial (\rho U_j h)}{\partial x_j} = \frac{\partial p}{\partial t} + \frac{\partial}{\partial x_j}\left(\Gamma_h \frac{\partial h}{\partial x_j}\right) + S_{l,h}. \tag{2.24}$$

The terms on the right-hand side of Eq. (2.17) are the diffusive flux described in terms of Fick's law and the source term due to the spray evaporation. A conserved scalar formulation has been used following [67]. With this formulation, the instantaneous thermo-chemical state of the fluid is related to a single conserved scalar quantity, the mixture fraction, ξ_C. It is defined as

$$\xi_C = \frac{Z_C - Z_{C,\min}}{Z_{C,\max} - Z_{C,\min}}, \tag{2.25}$$

where Z_j is the mass fraction of element j in the mixture and is defined as

$$Z_j = \sum_{i=1}^{n} \frac{a_{ij} M_j}{M_i} Y_i. \tag{2.26}$$

Here the reference element is carbon C [1]. With the assumption of equal diffusibility of all species, the conservation equation of the mixture fraction can be deduced from the conservation equation of species:

$$\frac{\partial (\rho \xi_C)}{\partial t} + \frac{\partial (\rho U_j \xi_C)}{\partial x_j} = \frac{\partial}{\partial x_j}\left(\Gamma_M \frac{\partial \xi_C}{\partial x_j}\right) + S_{l,1}, \tag{2.27}$$

where $\Gamma_M = \rho D_M$ is the mass diffusion coefficient of the mixture.

[1] Besides, the reference element can be H or O. However, the element O appears in both fuel and oxidizer. The Lewis number of the hydrogen is too low. Thus, the element C is usually preferred.

2.1.3 Turbulent Viscosity Models

Because of their simplicity, Reynolds-averaged numerical simulation methods are widely used in engineering simulation. The conservation equations in the previous section are transformed into time-averaged formulations. For compressible flow, it is convenient to introduce a density-weighted average, so-called "Favre-average". The Favre-average of a function Φ is defined as

$$\tilde{\Phi} = \frac{\overline{\rho\Phi}}{\bar{\rho}}. \tag{2.28}$$

The fluctuating components are defined as

$$\Phi'' = \Phi - \tilde{\Phi} \tag{2.29}$$

with

$$\widetilde{\Phi''} = 0. \tag{2.30}$$

Applying Favre-average on Eq. (2.14) and (2.15), we obtain

$$\frac{\partial\bar{\rho}}{\partial t} + \frac{\partial(\bar{\rho}\widetilde{U}_j)}{\partial x_j} = \bar{S}_{l,1}; \tag{2.31}$$

$$\frac{\partial(\bar{\rho}\widetilde{U}_j)}{\partial t} + \frac{\partial(\bar{\rho}\widetilde{U}_i\widetilde{U}_j)}{\partial x_j} + \frac{\partial(\bar{\rho}\widetilde{u_i''u_j''})}{\partial x_j} = -\frac{\partial\bar{p}}{\partial x_i} + \frac{\partial\bar{\tau}_{ij}}{\partial x_j} + \bar{\rho}g_i + \bar{S}_{l,U_i}. \tag{2.32}$$

The Reynolds stress tensor $\bar{\rho}\widetilde{u_i''u_j''}$ is unknown. It can be modeled following turbulent-viscosity hypothesis. The Reynolds stress anisotropy $a_{ij} \equiv \bar{\rho}\widetilde{u_i''u_j''} - \frac{2}{3}\bar{\rho}\tilde{k}\delta_{ij}$ is determined by the gradients of the mean velocity through a specific relationship. Zero-equation model (Prandtl mixing length model [190]) use a deterministic expression to determine the Reynolds stress. One-equation models, for instance, Prandtl-Kolmogorov model [191], Spalart-Allmaras model [192], introduce an equation to calculate the Reynolds stress. The most widely used is the $k-\epsilon$ model because of its simplicity and effectiveness [193]. $k-\epsilon$ model is one of the two-equation models. Two additional transport equations are solved for the turbulent kinetic energy k and its dissipation rate ϵ. The length scale and time scale are determined by

$$L = \frac{k^{3/2}}{\epsilon}, \qquad t_\tau = \frac{k}{\epsilon}. \tag{2.33}$$

$k-\epsilon$ model assumes the isotropic turbulence. By introducing a kinematic eddy viscosity μ_t, the Reynolds stress tensor is written as

$$\bar{\rho}\widetilde{u_i''u_j''} = \frac{2}{3}\mu_t\frac{\partial\widetilde{U}_k}{\partial x_k}\delta_{ij} - \mu_t\left(\frac{\partial\widetilde{U}_i}{\partial x_j} + \frac{\partial\widetilde{U}_j}{\partial x_i}\right). \tag{2.34}$$

Turbulent viscosity μ_t is related to the turbulent kinetic energy, $\tilde{k}$, and its dissipation rate, $\tilde{\epsilon}$, via

$$\mu_t = c_\mu \bar{\rho} \frac{\tilde{k}^2}{\tilde{\epsilon}}, \tag{2.35}$$

where c_μ is a model constant listed in Table (2.1). $\tilde{k}$ is the Favre-averaged turbulent kinetic energy:

$$\tilde{k} = \frac{1}{2} \widetilde{u_j'' u_j''}. \tag{2.36}$$

Eeffective viscosity is given by

$$\mu_{\text{eff}} = \mu_t + \mu_l, \tag{2.37}$$

where μ_l is the laminar viscosity of the fluid.

Substituting Eqs. (2.34) and (2.37) into Eq. (2.32), the modeled momentum equation is obtained

$$\frac{\partial(\bar{\rho}\widetilde{U}_j)}{\partial t} + \frac{\partial(\bar{\rho}\widetilde{U}_i\widetilde{U}_j)}{\partial x_j} = -\frac{\partial \bar{p}}{\partial x_i} + \frac{\partial}{\partial x_j}\left[\mu_{\text{eff}}\left(\frac{\partial \widetilde{U}_i}{\partial x_j} + \frac{\partial \widetilde{U}_j}{\partial x_i} - \frac{2}{3}\frac{\partial \widetilde{U}_k}{\partial x_k}\delta_{ij}\right)\right] + \bar{\rho} g_i + \bar{S}_{l,U_i}. \tag{2.38}$$

In the present work, an extended $k-\epsilon$ model is used [194]. The extended $k-\epsilon$ model is based on the standard $k-\epsilon$ model for gas-phase flow. It has been applied to spray flow. The effects of the spray source are taken into account by introducing appropriate source terms into the transport equations of k and ϵ [178]. The new equations are written as

$$\frac{\partial \bar{\rho}\tilde{k}}{\partial t} + \nabla \cdot (\bar{\rho}\widetilde{\mathbf{U}}\tilde{k}) = \nabla \cdot \left(\Gamma_{k,\text{eff}} \nabla \tilde{k}\right) + G_k - \bar{\rho}\tilde{\epsilon} + \bar{S}_{l,k}; \tag{2.39}$$

$$\frac{\partial \bar{\rho}\tilde{\epsilon}}{\partial t} + \nabla \cdot (\bar{\rho}\widetilde{\mathbf{U}}\tilde{\epsilon}) = \nabla \cdot (\Gamma_{\epsilon,\text{eff}} \nabla \tilde{\epsilon}) + c_{\epsilon,1}\frac{\tilde{\epsilon}}{\tilde{k}} G_k - c_{\epsilon,2}\bar{\rho}\frac{\tilde{\epsilon}}{\tilde{k}}\tilde{\epsilon} + \bar{S}_{l,\epsilon}; \tag{2.40}$$

where the effective exchange coefficients $\Gamma_{k,\text{eff}}$ and $\Gamma_{\epsilon,\text{eff}}$ are given as

$$\Gamma_{k,\text{eff}} = \frac{\mu_{\text{eff}}}{\sigma_k}; \tag{2.41}$$

$$\Gamma_{\epsilon,\text{eff}} = \frac{\mu_{\text{eff}}}{\sigma_\epsilon}. \tag{2.42}$$

σ_k and σ_ϵ are the effective Schmidt numbers for k and ϵ. They are assumed to be constants as shown in Table 2.1. Other model constants $c_{\epsilon,1}$, $c_{\epsilon,2}$ are listed in Table 2.1, too. The values of these model constants are take from the literature [191]. The generation term for the turbulent kinetic energy is given by

$$G_k = \mu_t \left[\left(\frac{\partial \tilde{U}_i}{\partial x_j} + \frac{\partial \tilde{U}_j}{\partial x_i}\right) - \frac{2}{3}\frac{\partial \tilde{U}_k}{\partial x_k}\delta_{ij}\right]\frac{\partial \tilde{U}_i}{\partial x_j}. \tag{2.43}$$

$\bar{S}_{l,k}$ and $\bar{S}_{l,\epsilon}$ are the mean spray source terms, which are determined by

$$\bar{S}_{l,k} = \bar{S}''_{l,U_j} u_j'' + \frac{1}{2}\bar{S}_{l,1}\widetilde{u_j'' u_j''} \tag{2.44}$$

c_μ	σ_k	σ_ϵ	$c_{\epsilon,1}$	$c_{\epsilon,2}$
0.09	1.0	1.3	1.44	1.92

Tab. 2.1: Constants in the $k-\epsilon$ model.

and

$$\bar{S}_{l,\epsilon} = C_s \bar{S}_{l,k}. \tag{2.45}$$

The model constant C_s is set to 1.50 [195].

Scalar fluxes are modeled using gradient-diffusion hypothesis. The Favre-averaged energy equation is written

$$\frac{\partial \bar{\rho}\tilde{h}}{\partial t} + \frac{(\bar{\rho}\widetilde{U}_j\tilde{h})}{\partial x_j} = \frac{\partial \bar{p}}{\partial t} + \frac{\partial}{\partial x_j}\left(\Gamma_h \frac{\partial \tilde{h}}{\partial x_j} - \bar{\rho}\widetilde{u_j''h''}\right) + \bar{S}_{l,h}, \tag{2.46}$$

where the thermal diffusion coefficient $\Gamma_h = \bar{\rho}D_M = \lambda/\bar{c}_p$ indicates the molecular transport of the specific enthalpy. The term for the turbulent transport of specific enthalpy is modeled as

$$\bar{\rho}\widetilde{u_j''h''} = -\Gamma_{h,\mathrm{t}} \frac{\partial \tilde{h}}{\partial x_j}. \tag{2.47}$$

By introducing the effective thermal diffusion coefficient $\Gamma_{h,\mathrm{eff}} = \Gamma_h + \Gamma_{h,\mathrm{t}}$, Eq. (2.46) can be written as

$$\frac{\partial \bar{\rho}\tilde{h}}{\partial t} + \frac{(\bar{\rho}\widetilde{U}_j\tilde{h})}{\partial x_j} = \frac{\partial \bar{p}}{\partial t} + \frac{\partial}{\partial x_j}\left(\Gamma_{h,\mathrm{eff}} \frac{\partial \tilde{h}}{\partial x_j}\right) + \bar{S}_{l,h}. \tag{2.48}$$

According to Eq. (2.27), the mean conservation equation for mixture fraction is deduced:

$$\frac{\partial \bar{\rho}\widetilde{\xi_C}}{\partial t} + \frac{(\bar{\rho}\widetilde{U}_j\widetilde{\xi_C})}{\partial x_j} = \frac{\partial}{\partial x_j}\left(\Gamma_M \frac{\partial \widetilde{\xi_C}}{\partial x_j} - \bar{\rho}\widetilde{u_j''\xi_C''}\right) + \bar{S}_{l,1}, \tag{2.49}$$

where the term of turbulent transport of mixture fraction is modeled as

$$\bar{\rho}\widetilde{u_j''\xi_C''} = -\Gamma_{M,\mathrm{t}} \frac{\partial \widetilde{\xi_C}}{\partial x_j}. \tag{2.50}$$

Similarly, by introducing the effective diffusion coefficient $\Gamma_{M,\mathrm{eff}} = \Gamma_M + \Gamma_{M,\mathrm{t}}$, Eq. (2.49) can be written as

$$\frac{\partial \bar{\rho}\widetilde{\xi_C}}{\partial t} + \frac{(\bar{\rho}\widetilde{U}_j\widetilde{\xi_C})}{\partial x_j} = \frac{\partial}{\partial x_j}\left(\Gamma_{M,\mathrm{eff}} \frac{\partial \widetilde{\xi_C}}{\partial x_j}\right) + \bar{S}_{l,1}. \tag{2.51}$$

It should be mentioned that both experiment [196] and theoretical analysis [197] have shown the existence of the counter-gradient scalar turbulent transport in certain situations where the sign in Eq. (2.47, 2.50) is reverse. It could be due to the differential

buoyancy effects on cold, heavy fresh gases and on hot, light burnt gases. Despite these evidences, gradient hypothesis is widely used in practical simulation.

We can determine the Reynolds stress by solving the transport equation for its each component. This method is Reynolds-stress modeling. The length and time scale of the turbulence are determined from the dissipation rate which is computed from a modeled transport equation. Thus, the turbulent viscosity hypothesis is not needed. Recently, the Reynolds-stress model has been extended to multiphase flow [198].

2.2 Probability Density Function Methods

2.2.1 Transported PDF Methods

In this section the PDF transport equation is explained. The consequent models used in the transported PDF method are described.

Basic idea of the transported PDF method is to describe the state of the flow at the location $\mathbf{x} = (x_1, x_2, x_3)$ at the time t in terms of a probability density function f. This f is a one variable PDF or a joint multi-variable PDF. The variables are physical variables of the flow such as velocity, composition, or turbulent frequency. The transport equation of the PDF is deduced from the Navier-Stokes equations [71]. Unclosed conditional expectation are modeled using appropriate physical models. The PDF transport equation is solved using a Monte-Carlo method. The PDF is represented by a large number of gas particles, which form a sample space. The development of the particles in sample space is described by a set of stochastic differential equations, which is transformed from the modeled PDF transport equation. Thus, the gas particles exhibit the same PDF as the solution of the modeled PDF transport equation. Statistics of the flow fields are determined by integration the particle properties in the whole sample space. In the present work, a single-scalar PDF (mixture fraction), a joint scalar PDF (mixture fraction and enthalpy), and a joint velocity-scalar PDF (velocities and mixture fraction) are considered.

2.2.1.1 Single-Scalar PDF Transport Equation

We define a one-point one-time Eulerian mass weighted PDF of mixture fraction by

$$\tilde{f}(\zeta_C; \mathbf{x}, t) = \frac{\rho(\zeta_C)\langle\delta(\xi_C - \zeta_C)\rangle}{\bar{\rho}}, \tag{2.52}$$

where ζ_c is the mixture fraction in the sample space, while ξ_C is the mixture fraction in the physical space. Therefore, the PDF is a bridge connecting the sample space and physical space. All communication processes between the sample space and physical

space are based on this PDF. According to the conservation equation of mixture fraction in turbulent spray flow (2.27), the PDF transport equation of mixture fraction is deduced following the way suggested by Pope [71]:

$$\bar{\rho}\frac{\partial \tilde{f}}{\partial t} + \bar{\rho}V_i\frac{\partial \tilde{f}}{\partial x_i} + \frac{\partial(\bar{S}_{l,1}\tilde{f})}{\partial \zeta_C} = -\frac{\partial}{\partial \zeta_C}\left[\left\langle \frac{\partial}{\partial x_j}\left(\Gamma_M \frac{\partial \xi_C}{\partial x_j}\right)\middle|\zeta_c\right\rangle \tilde{f}\right]. \tag{2.53}$$

The terms on the left-hand side can be solved exactly. The first term is the time derivative of $\tilde{f}$. The second term is the evolution of $\tilde{f}$ in the physical space. The third term is the evolution of $\tilde{f}$ in mixture fraction space due to spray evaporation. The term on the right-hand which represents evolution of $\tilde{f}$ in mixture fraction space by molecular fluxes has to be modeled.

2.2.1.2 Joint Scalar PDF Transport Equation

A joint scalar PDF for the turbulent spray flames is proposed. The scalars considered here are mixture fraction and enthalpy. The one-point one-time Eulerian mass weighted joint PDF of mixture fraction and total enthalpy is defined as

$$\tilde{f}(\zeta_C, \eta; \mathbf{x}, t) = \frac{\rho(\zeta_C)\langle\delta(\xi_C - \zeta_C)\delta(h-\eta)\rangle}{\bar{\rho}}. \tag{2.54}$$

Here η is the enthalpy in sample space. Following the similar way in Section (2.2.1.1), the transport equation of this joint PDF can be deduced from Eq. (2.27) and (2.16):

$$\begin{aligned}&\bar{\rho}\frac{\partial \tilde{f}}{\partial t} + \bar{\rho}V_i\frac{\partial \tilde{f}}{\partial x_i} + \frac{\partial(\bar{S}_{l,1}\tilde{f})}{\partial \zeta_C} + \frac{\partial \tilde{f}}{\partial \eta}\left(\bar{S}_{l,h} + \dot{Q} + \frac{\partial p}{\partial t}\right) = \\ -\ &\frac{\partial}{\partial \zeta_C}\left[\left\langle \frac{\partial}{\partial x_j}\left(\Gamma_M \frac{\partial \xi_C}{\partial x_j}\right)\middle|\zeta_c, \eta\right\rangle \tilde{f}\right] - \frac{\partial}{\partial \eta}\left[\left\langle \frac{\partial}{\partial x_j}\left(\Gamma_h \frac{\partial h}{\partial x_j}\right)\middle|\zeta_c, \eta\right\rangle \tilde{f}\right].\end{aligned} \tag{2.55}$$

The fourth to sixth terms on the left-hand side are the evolution of $\tilde{f}$ in enthalpy space due to spray evaporation, heat release from the chemical reaction, and pressure change, respectively. The term on the right-hand which represents evolution of $\tilde{f}$ in mixture fraction space and enthalpy space by molecular fluxes has to be modeled.

2.2.1.3 Joint Velocity-Scalar PDF Transport Equation

In the scalar PDFs, we postulate that the fluid particle velocity and scalar are statistically independent. The joint velocity-scalar PDF is decomposed into two marginal PDFs:

$$f_{\mathbf{U}\xi_C\chi}(\mathbf{V}, \zeta_C; \mathbf{x}, t) = f_{\mathbf{U}}(\mathbf{V}; \mathbf{x}, t) \cdot f_{\xi_C}(\zeta_C; \mathbf{x}, t). \tag{2.56}$$

PDF of the fluid particle velocity is usually assumed as a Gaussian distribution with the mean $\tilde{\mathbf{U}}$ and variance $\frac{2}{3}\tilde{k}$. However, such assumptions are not always true. The

conditional PDF should be considered. In this section, a joint velocity-mixture fraction PDF is proposed. Here we define a one-point one-time Eulerian mass-weighted joint velocity-scalar PDF $\tilde{f}$ of $\mathbf{U}(\mathbf{x},t)$ and $\xi_C(\mathbf{x},t)$ by

$$\tilde{f}(\mathbf{V},\zeta_C;\mathbf{x},t)=\frac{\rho(\zeta_C)\langle\delta(\mathbf{U}-\mathbf{V})\delta(\xi_C-\zeta_C)\rangle}{\bar{\rho}}. \tag{2.57}$$

According to the conservation equation of momentum and mixture fraction of turbulent spray flow (Eqs. (2.15) and (2.27)), the transport equation of $\tilde{f}(\mathbf{V},\zeta_C;\mathbf{x},t)$ can be deduced:

$$\begin{aligned}\bar{\rho}\frac{\partial\tilde{f}}{\partial t} &+ \bar{\rho}V_i\frac{\partial\tilde{f}}{\partial x_i}+\frac{\partial\tilde{f}}{\partial V_i}\left(\bar{\rho}g_i-\frac{\partial\bar{p}}{\partial x_i}+\bar{S}_{l,U_i}\right)+\frac{\partial}{\partial\zeta_C}\left(\bar{S}_{l,1}\tilde{f}\right) \\ &= \frac{\partial}{\partial V_i}\left[\left\langle-\frac{\partial\tau_{ij}}{\partial x_j}+\frac{\partial p'}{\partial x_i}\middle|\mathbf{V},\zeta_C\right\rangle\tilde{f}\right]+\frac{\partial}{\partial\zeta_C}\left[\left\langle\frac{\partial}{\partial x_j}\left(\Gamma_M\frac{\partial\xi_C}{\partial x_j}\right)\middle|\mathbf{V},\zeta_C\right\rangle\tilde{f}\right].\end{aligned} \tag{2.58}$$

The third to fifth terms on the left-hand side are the evolution of $\tilde{f}$ in velocity space due to body force, mean pressure gradient, and spray evaporation, respectively. The first and second terms on the right-hand side are the evolution of $\tilde{f}$ in velocity space due to viscous stress tensor and fluctuating pressure gradient, respectively.

2.2.1.4 Numerical Viewpoint of PDF Method

In the PDF transport equation (Eqs. (2.53, 2.55, 2.58)), the terms on the left-hand side are treated exactly. The terms on the right-hand side are unclosed. Appropriate physical models are needed to close these terms. The resulting modeled PDF transport equation is usually a high-dimensional equation. It is infeasible to solve it with a finite difference method or finite volume method. As an alternative, Monte-Carlo method is widely used to solve the high-dimensional problem since the computational costs increase only linearly with the number of dimensions. Therefore Monte-Carlo method (particle method) is feasible to solve the PDF transport equations.

There are two different type of particle method: Eulerian particle method and Lagrangian particle method. The latter is more frequently used, because it is easier to construct physical models in Lagrangian frame, and the history of the turbulence is fully included in the Lagrangian PDF.

In Lagrangian particle method, the flow is represented by a large number of fluid particles. Each particle has a set of properties. In the present work, it includes m^*, $\mathbf{x}^*$, $\mathbf{U}^*$, ξ_C^*, h^*, where m^* is the mass, $\mathbf{x}^*$ the position, $\mathbf{U}^*$ the velocity, ξ_C^* the mixture fraction, h^* the total enthalpy of the particle (the superscript '*' indicates the particle's property). These particles form a sample space. The PDF transport equations are converted into a set of stochastic differential equations (SDEs). The properties of the particles evolve in the sample space following the corresponding stochastic differential

equations. In the following sections, the models used in PDF method are described. The resulting SDEs are presented.

2.2.1.5 Velocity Model

In the PDF methods, the fluid particle velocity $\mathbf{U}^+(t)$ is represented by the stochastic particle velocity $\mathbf{U}^*(t)$. Various models are available to model the evolution of the particles in the velocity sample space. The Langevin equation remains the basis for stochastic model of turbulent dispersion [51]. Stochastic process generated by the Langevin equation is called "Ornstein-Uhlenbeck (OU) process". Its PDF evolves by the Fokker-Planck equation. The generalized Langevin model [199] can be written as

$$dU_i^*(t) = \frac{1}{\rho}\frac{\partial \langle p \rangle}{\partial x_i}dt + G_{ij}(U_j^*(t) - \langle U_j \rangle)dt + (C_0\epsilon)^{1/2}dW_i(t). \tag{2.59}$$

The first term on the right-hand side is for the acceleration due to the mean pressure gradient. The second term on the right-hand side is for the effects of viscous stress tensor. The last term is a Wiener process representing the effects of fluctuating pressure gradients. Coefficient $G_{ij}(\mathbf{x}, t)$ depends on the local values. When G_{ij} is given by

$$G_{ij} = -\left(\frac{1}{2} + \frac{3}{4}C_0\right)\frac{\epsilon}{k}\delta_{ij}, \tag{2.60}$$

it is the simplified Langevin model (SLM) [51]. Another model, the isotropization-of-production model, takes the G_{ij} as

$$G_{ij} = -\frac{1}{2}C_R\frac{\epsilon}{k}\delta_{ij} + C_2\frac{\partial \langle U_i \rangle}{\partial x_j}, \tag{2.61}$$

with

$$C_R = 1 + \frac{3}{2}C_0 - C_2\frac{\mathcal{P}}{\epsilon}. \tag{2.62}$$

Further study of this topic could refer to [199, 200, 201, 51].

In the present work we extend the simplified Langevin model to the turbulent multiphase flows. In SLM, the effect of the mean velocity gradient is neglected. The stochastic particle velocity advances with

$$\begin{aligned} dU_i^*(t) &= \frac{1}{\bar{\rho}}\left(\bar{\rho}g_i - \frac{\partial \bar{p}}{\partial x_i} + \bar{S}_{l,U_i}\right)dt \\ &- \left(\frac{1}{2} + \frac{3}{4}C_0\right)\frac{\tilde{\epsilon}}{\tilde{k}}\left(U_i^*(t) - \tilde{U}_i\right)dt + \left(C_0\tilde{\epsilon}\right)^{1/2}dW_i(t), \end{aligned} \tag{2.63}$$

where $C_0 = 2.1$ is the model constant [51]. The first term on the right hand side is for the acceleration due to the body force (gravitational force). The second term is for the acceleration due to the mean pressure gradient. The third term is the source term from

spray flows. The fourth term is the viscous stress tensor. The last term represents the diffusion process in which $\mathbf{W}(t)$ is a Wiener process. $dW_i(t) = W_i(t + dt) - W_i(t)$ is a normal distribution with the mean $\langle dW_i(t)\rangle = 0$ and the variance $\langle dW_i(t)dW_j(t)\rangle = dt\delta_{ij}$ [51].

2.2.1.6 Mixing Model

Effects of the molecular diffusion are taken into account through a mixing model. There are some models available, including the interaction-by-exchange-with-the-mean (IEM) [202], modified Curl's model [203], Euclidean minimum spanning tree (EMST) mixing model [87]. In the present thesis, the simplest model–the IEM model is employed. Good predictions with IEM model were reported [204]. With the IEM model, the mixture fraction and enthalpy of the particle evolve by

$$\frac{d\xi_C^*(t)}{dt} = -\frac{1}{2}C_\phi\frac{\tilde{\epsilon}}{\tilde{k}}(\xi_C^*(t) - \tilde{\xi}_C) + \frac{\bar{S}_{l,1}}{\bar{\rho}}; \tag{2.64}$$

$$\frac{dh_s^*(t)}{dt} = -\frac{1}{2}C_\phi\frac{\tilde{\epsilon}}{\tilde{k}}(h_s^*(t) - \tilde{h}_s) + \frac{\bar{S}_{l,h_s}}{\bar{\rho}}. \tag{2.65}$$

Here $C_\phi = 2.0$ is the standard model constant [51]. The first term on the right-hand side represents the mixing process. The last term is for the source term due to the spray evaporation.

2.2.2 Presumed PDF methods

Presumed PDF methods have been widely used in fluid dynamics. Most of the fluid processes are stochastic processes. The presumed PDF methods provide simple empirical mathematical tools to describe such complex processes. The presumed PDF methods enable us to describe a collection of data in a more concise and convenient way. The data becomes easier to be comprehended and be communicated. The presumed PDF methods provide some practical insights into the way that the variable seems to behave. It becomes easier to choose an appropriate theoretical model for the random variables.

Usually, the procedure of the presumed PDF method is:

1. to collect the samples from experiment, the numerical results of DNS or LES or transported PDF method, or other resources;
2. to present the samples in a distribution;
3. to calculate a few sample statistic(s), for instance, mean, variance;
4. to choose an appropriate PDF to represent the empirical data;

5. to estimate the parameter(s) of this PDF from the calculated sample statistic(s);

6. to assess the predictive ability by applying it to a particular test.

Valid samples should be independent and identically distributed.

In this section, the most frequently used presumed PDFs in fluid dynamics are presented, including the normal distribution (Gaussian distribution), log-normal distribution, Nukiyama-Tanasawa distribution, Rosin-Rammler distribution, β distribution, modified (four-parameter) β distribution. Their applications in the engineering simulation are analyzed.

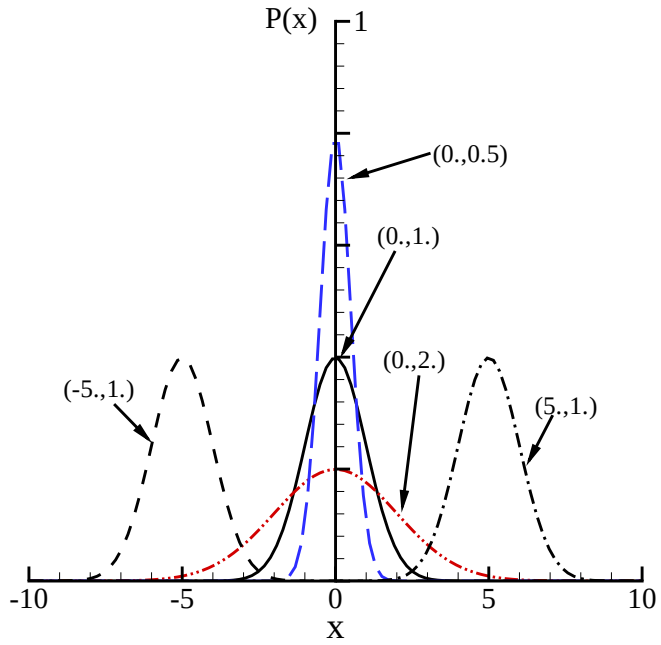

Fig. 2.1: Typical normal distributions with different parameters (μ, σ).

2.2.2.1 Normal Distribution

Normal distribution, sometimes referred as Gaussian distribution, is the best-known and the most frequently used presumed PDF in engineering simulation. Because of its curved flaring shape, the normal distribution is often referred as the "bell curve". It was used by Laplace in 1783 to study the experimental errors and by Gauß in 1809 in the analysis of the astronomical data.

Normal distributions have many convenient properties. They represent the distribution of the random errors in many kinds of measurements. Many sets of the

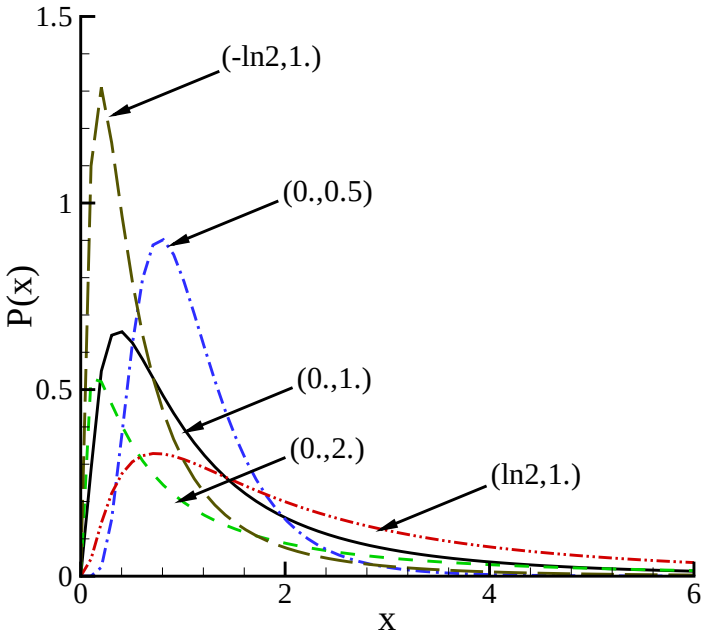

Fig. 2.2: Typical log-normal distributions with different parameters $(\mu_{\log}, \sigma_{\log})$.

experimental results in practice turn out to follow the normal distribution. The central limit theorem states that given a distribution with a mean μ and variance σ^2, the sampling distribution of the mean approaches a normal distribution with a mean μ and a variance σ^2/N as the sample size N increases, even if the parent population is not normal. Therefore, the random variables with unknown distributions are often assumed to be normal, especially in physics. Although this might be a dangerous assumption, it is often a good approximation due to a surprising result known as the central limit theorem. Many common attributes, such as test scores and height, follow roughly normal distributions. In fluid dynamics, the velocity follows roughly normal distribution [205]. Other physical variables, which are defined in $(-\infty, +\infty)$, could be approximated by normal distribution, too.

A normal distribution in a variable x with mean μ and variance σ^2 is a statistic distribution with probability function

$$P(x) = \frac{1}{\sigma\sqrt{2\pi}} \exp\left[-\frac{(x-\mu)^2}{2\sigma^2}\right], \tag{2.66}$$

on the domain $x \in (-\infty, +\infty)$. The normal distributions with different means and variances are illustrated in Fig. 2.1. The values in brackets are the mean μ and the root of the variance σ. The standard normal distribution is a special case of the general normal distribution by taking the mean $\mu = 0$ and variance $\sigma^2 = 1$.

Variables X_i with a normal distribution can be generated from variables Y_i having a uniform distribution in $(0, 1)$ via

$$X_i = \sigma\sqrt{2}\text{erfc}^{-1}(2Y_i - 1) + \mu. \tag{2.67}$$

A simpler way to obtain numbers with a normal distribution is to use the Box-Muller transformation [206]. In the present work, the fluctuating velocity in Eq. (3.31) is generated using Box-Muller transformation [207]. We take a random point $(x_1,\ x_2)$ inside the unit circle around the origin, $R = x_1^2 + x_2^2 < 1$. A pair of random numbers with zero mean and unit variance are generated:

$$v_1 = x_1\sqrt{-\frac{2\ln R}{R}}; \tag{2.68}$$

$$v_2 = x_2\sqrt{-\frac{2\ln R}{R}}. \tag{2.69}$$

2.2.2.2 Log-Normal Distribution

Log-normal distribution is a continuous distribution in which the logarithm of a variable has a normal distribution:

$$P(x) = \frac{1}{\sigma_{\log}\sqrt{2\pi}x}\exp\left[-\frac{(\ln x - \mu_{\log})^2}{2\sigma_{\log}^2}\right]. \tag{2.70}$$

It is defined on the domain $x \in (0, +\infty)$. The mean and variance are given by

$$\mu = \exp\left(\mu_{\log} + \frac{1}{2}\sigma_{\log}^2\right); \tag{2.71}$$

$$\sigma^2 = \left[\exp\left(\sigma_{\log}^2\right) - 1\right]\exp\left(2\mu_{\log} + \sigma_{\log}^2\right), \tag{2.72}$$

where $\ln\mu_{\log}$ represents the logarithmic mean value of the distribution. Typical log-normal distributions with different values of $\mu_{\log}$ and $\sigma_{\log}$ are illustrated in Fig. 2.2. Small values of $\sigma_{\log}$ are associated with broad distribution, and large values of $\sigma_{\log}$ are associated with narrow distributions. By taking $\mu_{\log} = 0$ and $\sigma_{\log} = 1$, it turns to a Gibrat's distribution:

$$P(x) = \frac{1}{\sqrt{2\pi}x}\exp\left[-\frac{(\ln x)^2}{2}\right]. \tag{2.73}$$

Examples of variables which have approximately log-normal distributions include the turbulent scalar dissipation rate, the size of small droplet in the spray flows, the size of silver particles in a photographic emulsion, acidity by pH, noise intensity, fatigue life of some materials, volume of air traffic, daily water flow, rainfall, flood discharge, survival time of bacteria in disinfectants, weight and blood pressure of humans, and number of words written in sentences by George Bernard Shaw [208].

Random numbers following log-normal distribution can be generated from a unit normal variable. The log-normal variable with mean μ and variance σ^2, denoted by $\mathrm{Logn}\left(\mu, \sigma^2\right)$, is related to unit normal variable $N(0,1)$ by

$$\mathrm{Logn}\left(\mu, \sigma^2\right) \sim \mu \cdot \exp\left[\sigma \cdot N(0,1)\right]. \tag{2.74}$$

This method is implemented into the code to generate the random number for the dissipation rate of the mixture fraction (see Eq. (2.148)).

2.2.2.3 Nukiyama-Tanasawa Distribution

Nukiyama-Tanasawa distribution was introduced by Nukiyama and Tanasawa in 1939 [209]. It has been used to describe the number distribution of drops in the sprays from a pneumatic atomizer. The function is

$$P(x) = ax^p \exp\left(-bx^q\right), \tag{2.75}$$

for $x \in [0, \infty)$, where b, p, q are adjustable parameters, and a is the normalizing constant. Sometimes p is fixed to 2 [210].

Obviously, a presumed PDF for droplet size distributions should be defined in $[0, \infty)$. It must be zero at the lower and upper end of the range:

$$P(0) = 0, \quad P(\infty) = 0. \tag{2.76}$$

The Nukiyama-Tanasawa distribution fulfills this condition.

In practice the maximum droplet size is not infinite. Thus, a more accurate restriction should be:

$$P(0) = 0, \quad P(x|x > r_{\max}) = 0. \tag{2.77}$$

Nukiyama-Tanasawa distribution is the generalized form of many popular distributions. Maxwell distribution, which describes the distribution of the molecule speeds in thermal equilibrium in statistical mechanics, is defined as

$$P(x) = \sqrt{\frac{2}{\pi}} a^{\frac{3}{2}} x^2 \exp\left(-\frac{ax^2}{2}\right), \tag{2.78}$$

for $x \in [0, \infty)$. It is a special form of the Nukiyama-Tanasawa distribution with $p = 2$, $q = 2$, and $b = a/2$. Rayleigh distribution, which is defined as

$$P(x) = a^{-2} x \exp\left(-\frac{x^2}{2a^2}\right), \tag{2.79}$$

for $x \in [0, \infty)$, is also a special form of the Nukiyama-Tanasawa distribution with $p = 1$, $q = 2$, and $b = 1/(2a^2)$. Rosin-Rammler (two-parameter Weibull) distribution described in the following section is a special form of the Nukiyama-Tanasawa distribution, too.

2.2.2.4 Rosin-Rammler (Two-Parameter Weibull) Distribution

Rosin-Rammler distribution is referred as "two-parameter Weibull distribution" in mathematical literature. The Weibull distribution was primarily derived as the third asymptotic distribution of extreme values [211]. The two-parameter Weibull distribution was originally proposed to analyze the breaking strengths [212, 213]. The distribution of the lifetimes of objects is often described using Weibull distribution. It has been widely used to analyze the systems with a weakest link, such as fatigue failure in structures, ball-bearing failure, failure of electronic components, breaking strengths of a ceramic, traffic flow [214]. In these cases, the problem becomes to find the weakest element. It is very interesting for the spray systems. The breakup processes of the liquid jets and droplets are of great interest. Such processes are similar to the problem of material strength, but much more complex. The properties of liquid jets and droplets change a lot during their lifetime. Additionally, the liquid jets and droplets undergo other processes such as evaporation and coalescence.

Rosin-Rammler distribution was introduced to describe the cumulative volume distribution of coal particles by Rosin and Rammler [215]. The function is

$$P(x) = qd^{-q}x^{q-1}\exp\left[-\left(\frac{x}{d}\right)^{q}\right], \tag{2.80}$$

for $x \in [0, \infty)$ and $q > 0$. The mean and variance of this distribution are

$$\mu = d\Gamma(1+\frac{1}{q}); \tag{2.81}$$

$$\sigma^2 = d^2[\Gamma(1+\frac{2}{q}) - \Gamma^2(1+\frac{1}{q})]. \tag{2.82}$$

Typical shapes of Rosin-Rammler distributions with different parameters of d and q are illustrated in Fig. 2.3. Actually, it is a special form of Nukiyama-Tanasawa distribution with $p = q - 1$ and $b = d^{-q}$.

The Rosin-Rammler distribution has been widely used in the spray literature. It is mainly due to its mathematical simplicity.

2.2.2.5 β Distribution

The β distribution is defined as

$$P(x) = \frac{\Gamma(\alpha+\beta)}{\Gamma(\alpha)\Gamma(\beta)}x^{\alpha-1}(1-x)^{\beta-1}, \tag{2.83}$$

for $x \in [0, 1]$. Γ is the Gamma function. The mean and variance are given by

$$\mu = \frac{\alpha}{\alpha+\beta}; \tag{2.84}$$

$$\sigma^2 = \frac{\mu(1-\mu)}{\alpha+\beta+1} = \frac{\alpha\beta}{(\alpha+\beta)^2(\alpha+\beta+1)}. \tag{2.85}$$

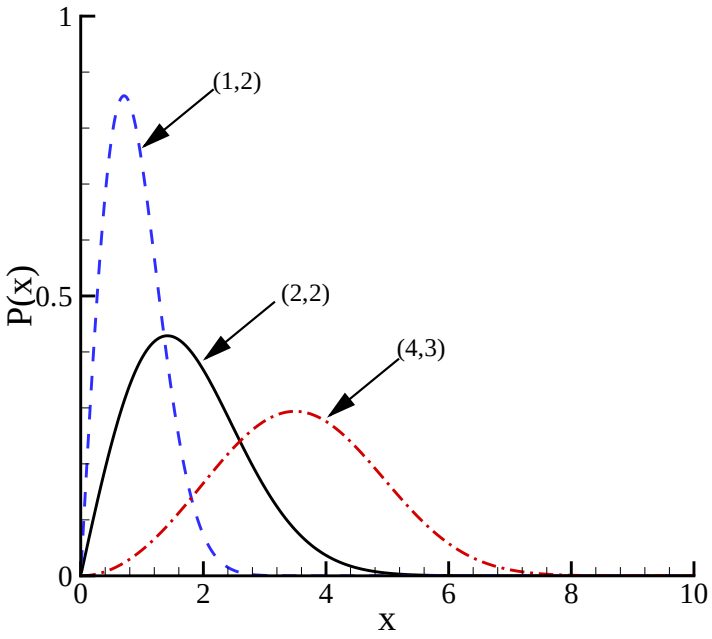

Fig. 2.3: Typical Rosin-Rammler distributions with different parameters (d, q).

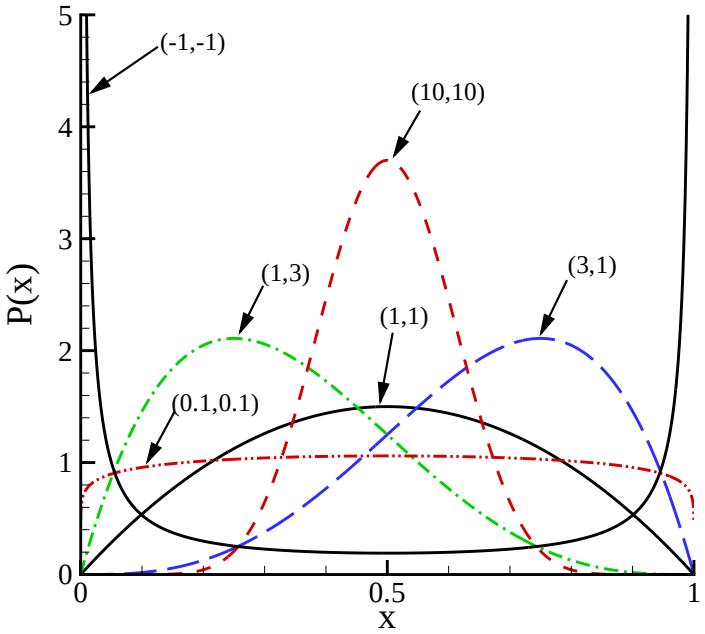

Fig. 2.4: Typical β distributions with different parameters (α, β).

Typical shapes of the β distributions with different α and β are illustrated in Fig. 2.4. When the variance is small, the β distribution shows unimodal shape. It shows bimodal shape when the variance is large (see the one with $\alpha = \beta = -1$). The β distribution is often used to describe the mixture fraction or mass fraction of species in turbulent single-phase flows [170].

2.2.2.6 Modified β Distribution

In the practical application, the properties are valid only in a certain range, $[x_{\min}, x_{\max}]$. For instance, the maximum value of the mixture fraction in turbulent spray flows is smaller than the unity. The distribution of mixture fraction in the turbulent spray flows cannot be reproduced using the standard β distribution (Eq. (2.83)). Modified β distribution, is a general form of the β distribution [140]. The definition range of the modified β distribution relaxes to $[x_{\min}, x_{\max}]$. Thus, many boundedness random properties defined in $[x_{\min}, x_{\max}]$ can be described using modified β distribution. It is a four-parameter function:

$$P(x) = \frac{\Gamma(\alpha+\beta)}{\Gamma(\alpha)\Gamma(\beta)}(x_{\max}-x_{\min})^{1-\alpha-\beta}(x-x_{\min})^{\alpha-1}(x_{\max}-x)^{\beta-1}. \tag{2.86}$$

for $x \in [x_{\min}, x_{\max}]$. The mean and variance are given by

$$\mu = x_{\min} + \frac{\alpha}{\alpha+\beta}(x_{\max}-x_{\min}); \tag{2.87}$$

$$\sigma^2 = \frac{(\mu-x_{\min})(x_{\max}-\mu)}{\alpha+\beta+1} = \frac{\alpha\beta}{(\alpha+\beta)^2(\alpha+\beta+1)}(x_{\max}-x_{\min})^2. \tag{2.88}$$

When $x_{\max} = 1$ and $x_{\min} = 0$, the modified β function is turned into the standard β function (Eq. (2.83)). If we define

$$x' = \frac{x-x_{\min}}{x_{\max}-x_{\min}}, \tag{2.89}$$

x' follows a standard β function. Thus, the modified β distribution has the same basic shapes as the ones of standard β distribution (see Fig. 2.4). When the variance is much smaller than the width of definition, say,

$$\sigma^2 << (\mu-x_{\min})(x_{\max}-\mu), \tag{2.90}$$

the modified β distribution is identical to a normal distribution. Fig. 2.5 shows the comparison of modified β function (indicated by "MBeta") and normal distribution with the same mean ($\mu = 1$) and variance ($\sigma = 1$). Here the parameters $x_{\max}$ and $x_{\min}$ of modified β function are set to 20 and -20, respectively. The solid line indicates the modified β distribution. The symbols indicate the normal distribution. Therefore, the

processes following normal distribution can be described by modified β distribution too. In such cases, the parameters $x_{\max}$ and $x_{\min}$ are set to the upper and lower limitation.

When the property is defined in $[0, \infty)$, the parameter $x_{\min}$ is zero, and $x_{\max}$ equals to $+\infty$. We have

$$\mu - x_{\min} \ll x_{\max} - \mu, \ \sigma^2 \ll (\mu - x_{\min})(x_{\max} - \mu), \tag{2.91}$$

which will lead to

$$\alpha \ll \beta, \ \alpha + \beta + 1 \gg 1. \tag{2.92}$$

In this case, the shape of the modified β distribution is close to the ones of log-normal distribution. Fig. 2.6 shows the comparison of modified β distribution with the log-normal distribution as well as the Rosin-Rammler distribution. All of them have the same mean ($\mu = 2$) and variance ($\sigma = 1$). Here the parameter $x_{\min}$ in the modified β distribution is set to zero. Squares indicate the log-normal distribution. The circles are the Rosin-Rammler distribution. The solid line indicates the modified β distribution with $x_{\max} = 10$. The dashed line indicates the modified β distribution with $x_{\max} = 100$. They are very close to each other. Therefore, the log-normal distribution and the Nukiyama-Tanasawa-class distribution can be reproduced or estimated by the modified β distribution.

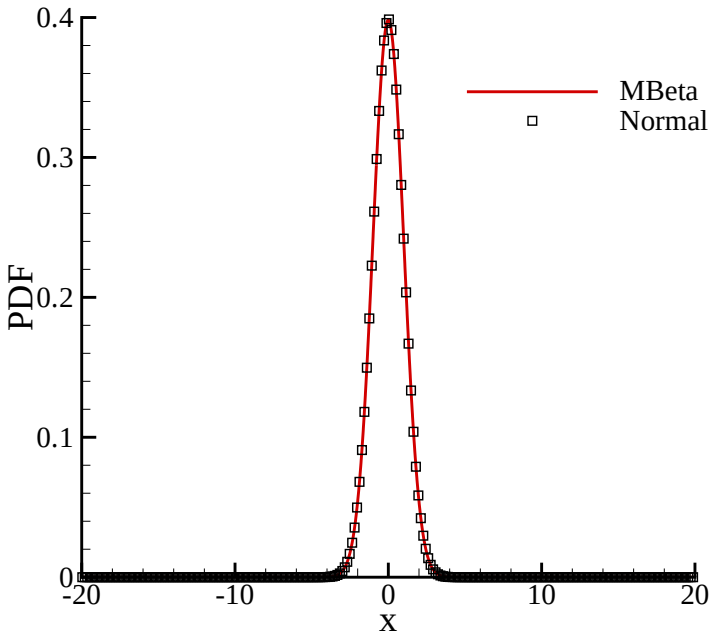

Fig. 2.5: Comparison of modified β distribution with the normal distribution.

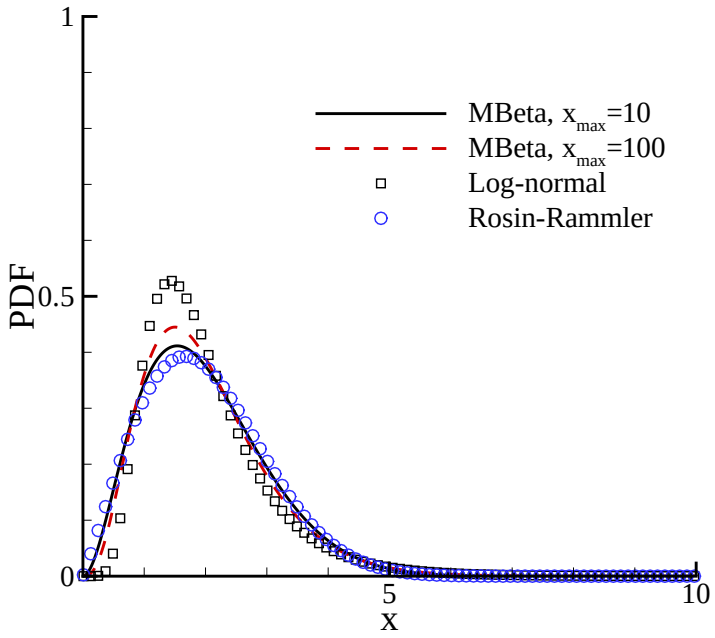

Fig. 2.6: Comparison of modified β distribution with the log-normal distribution and the Rosin-Rammler distribution.

2.3 Liquid Phase Flow

Spray flow is described by a droplet density function f_d which follows the famous Williams' spray equation [216]. Assuming dilute spray, both droplet-droplet interaction and coalescence are neglected. The droplet's position $\mathbf{x}_d$, velocity $\mathbf{U}_d$, equilibrium radius r_d, temperature T_d are considered in f_d. A droplet density function is defined as

$$f_d(\mathbf{V}_d, \iota_d, \theta_d; \mathbf{x}_d, t) = \langle \delta(\mathbf{U}_d - \mathbf{V}_d)\delta(r_d - \iota_d)\delta(T_d - \theta_d)\rangle, \tag{2.93}$$

where $\mathbf{V}_d, \iota_d, \theta_d$ are the sample space variables corresponding to $\mathbf{U}_d, r_d, T_d$. The transport equation of f_d is written as

$$\begin{aligned}\frac{\partial f_d}{\partial t} + U_{d,j}\frac{\partial f_d}{\partial x_j} &= -\frac{\partial}{\partial V_{d,j}}\left(f_d \left\langle F_j \middle| \mathbf{V}_d, \iota_d, \theta_d\right\rangle\right) - \frac{\partial}{\partial \iota_d}\left(f_d \left\langle \dot{r}_d \middle| \mathbf{V}_d, \iota_d, \theta_d\right\rangle\right) \\ &\quad -\frac{\partial}{\partial \theta_d}\left(f_d \left\langle \dot{T}_d \middle| \mathbf{V}_d, \iota_d, \theta_d\right\rangle\right).\end{aligned} \tag{2.94}$$

The first term is the time derivative of f_d. The second term represents the evolution of f_d in the physical space. The terms on the right-hand side are the evolution of f_d in the droplet velocity space, droplet radius space, and droplet temperature space, respectively. With this droplet density function, the mean value of an arbitrary function

Φ can be determined by

$$\langle \Phi \rangle = \int f_d \Phi d\mathbf{V}_d d\iota_d d\theta_d. \tag{2.95}$$

It is worthwhile to mention that Subramaniam [217] clarified the statistical information contained in the droplet distribution function (DDF). The connections between the physical phenomena and mathematical descriptions were pointed out. He derived the transport equation of DDF using an alternative way. The unclosed terms in the transport equation were precisely defined.

Droplets move in the physical space according to its instantaneous velocity:

$$\frac{d\mathbf{x}_d}{dt} = \mathbf{U}_d. \tag{2.96}$$

To determine the trajectories of individual droplets, $F_j, \dot{r}_d, \dot{T}_d$ should be evaluated. The effect of gas-phase turbulence on droplet velocities is modeled with SSF (Stochastic Separated Flow) model. The acceleration of a droplet is written as [8]

$$\begin{aligned} F_j = \frac{dU_{d,j}}{dt} &= \frac{3}{8}\frac{\bar{\rho}}{\rho_l} C_d(\mathrm{Re}_d)\frac{|U_{r,j}|}{r_d}U_{r,j} + F_{e,j} - \frac{1}{\rho_l}\frac{\partial p}{\partial r}n_r \\ &+ \frac{1}{2}\frac{\rho}{\rho_l}C_I\frac{dU_{r,j}}{dt} + \frac{9}{2\rho_l r_d}\sqrt{\frac{\rho\mu}{\pi}}C_B\int_{t_0}^{t}\frac{dU_{r,j}}{\sqrt{t-\tau}}d\tau, \end{aligned} \tag{2.97}$$

The first term on the right-hand-side is the drag force including skin friction and form drag. The second term is the external force (body force). The third term is due to the static pressure gradient. In the present work, only the spray jets in atmospheric air are considered. This term is negligible. The fourth term is the virtual-mass term being due to the inertia of adjacent fluid displaced by its motion. It is negligible when the gas density is much smaller than the liquid density which is usually the case. The last term is the Bassett force. It is also negligible when the gas density is much smaller than the liquid density. In the present work, only the drag force and the gravitational force are considered. Eq. (2.97) is simplified as

$$\frac{dU_{d,j}}{dt} = \frac{3}{8}\frac{\bar{\rho}}{\rho_l} C_d(\mathrm{Re}_d)\frac{|U_{r,j}|}{r_d}U_{r,j} + \frac{\rho_l - \rho}{\rho_l}g_j, \tag{2.98}$$

where ρ_l is the density of liquid phase. The relative velocity between the gas phase and liquid phase is

$$U_r = U - U_d. \tag{2.99}$$

The parameter C_d depends on the droplet Reynolds number Re_d [218]:

$$C_d = \begin{cases} \frac{24}{\mathrm{Re}_d}\left(1 + \frac{1}{6}\mathrm{Re}_d^{\frac{2}{3}}\right) & : \quad \mathrm{Re}_d < 1000 \\ 0.424 & : \quad \mathrm{Re}_d > 1000. \end{cases} . \tag{2.100}$$

The droplet Reynolds number Re_d is defined according to the droplet diameter, the relative velocity and the mean dynamic viscosity in the film surrounding the droplet:

$$\mathrm{Re}_d = 2\bar{\rho} r_d \frac{|U_r|}{\hat{\mu}(\hat{T})}. \tag{2.101}$$

The symbol "$\hat{}$" here indicates the properties of the film between the droplet surface and gas phase which are evaluated according to the "1/3 rule" [219]. The reference temperature $\hat{T}$ is calculated by:

$$\widehat{T} = \frac{\widetilde{T} + 2T_d}{3}. \tag{2.102}$$

Effects of turbulent dispersion is modeled using a Monte-Carlo method [6]. The instantaneous gas velocity U in Eq. (2.99) is the sum of the mean velocity and fluctuating velocity:

$$U = \tilde{U} + u''. \tag{2.103}$$

Here we assume the gas velocity follows a Gaussian distribution. The fluctuating velocity is sampled from a Gaussian distribution with the mean of zero and variance of $\frac{2}{3}k$ [2]. The droplet-eddy interaction time is established by taking the minimum of the characteristic lifetime of the eddy and the time for the droplet to traverse the eddy [220]

$$t_{\mathrm{corr}} = \min(t_\tau, t_{\mathrm{tr}}), \tag{2.104}$$

with

$$t_\tau = \frac{\tilde{k}}{\tilde{\epsilon}}; \tag{2.105}$$

$$t_{\mathrm{tr}} = c_{\mathrm{tr}} \frac{k^{\frac{3}{2}}}{\epsilon}. \tag{2.106}$$

c_{tr} is the empirical constant with the value of 0.16432 [195].

Two-film model in a convective surrounding (so-called "Abramzon-Sirignano model") [221] is used to calculate the evaporation rate of droplets:

$$\dot{m}_d = 2\pi \widehat{\rho D} r_d \mathrm{Sh}^* \ln(1 + \mathrm{B}_M), \tag{2.107}$$

and

$$\dot{m}_d = 2\pi \frac{\widehat{\lambda}}{\widehat{C_p}} r_d \mathrm{Nu}^* \ln(1 + \mathrm{B}_T), \tag{2.108}$$

[2] The turbulent kinetic energy is $k = \frac{1}{2}\left(u_1''^2 + u_2''^2 + u_3''^2\right)$. Assuming an isotropic turbulence, $k = \frac{3}{2}\left(u_1''^2\right) = \frac{3}{2}\left(u_2''^2\right) = \frac{3}{2}\left(u_3''^2\right)$. Therefore, the variance of the fluctuating velocity is $\frac{2}{3}k$.

where $\widehat{C_p}$ is the mean vapor specific heat in the film. Sh^* and Nu^* are the modified Sherwood number and modified Nusselt number which are written as

$$\mathrm{Sh}^* = 2 + \frac{\mathrm{Sh}_0 - 2}{F(\mathrm{B}_M)}; \tag{2.109}$$

$$\mathrm{Nu}^* = 2 + \frac{\mathrm{Nu}_0 - 2}{F(\mathrm{B}_T)}, \tag{2.110}$$

with

$$F(\mathrm{B}) = (1+\mathrm{B})^{0.7}\frac{\ln(1+\mathrm{B})}{\mathrm{B}}. \tag{2.111}$$

The Sherwood number and Nusselt number are evaluated following Clift's correlation [222]:

$$\mathrm{Sh}_0 = 1 + (1 + \mathrm{Re}_d\mathrm{Pr})^{1/3} f(\mathrm{Re}_d); \tag{2.112}$$

$$\mathrm{Nu}_0 = 1 + (1 + \mathrm{Re}_d\mathrm{Sc})^{1/3} f(\mathrm{Re}_d). \tag{2.113}$$

Function $f(\mathrm{Re}_d)$ depends on the droplet Reynolds number:

$$f(\mathrm{Re}_d) = \begin{cases} \mathrm{Re}_d^{0.077} & : \ 1 \leq \mathrm{Re}_d \leq 400 \\ 1 & : \ \mathrm{Re}_d < 1. \end{cases} \tag{2.114}$$

Prandtl number Pr and Schmidt number Sc of the film are calculated by

$$\mathrm{Pr} = \widehat{\mu}\frac{\widehat{C_p}}{\widehat{\lambda}} \tag{2.115}$$

$$\mathrm{Sc} = \frac{\widehat{\mu}}{\widehat{\rho D}}. \tag{2.116}$$

B_M is the Spalding mass transfer number [223] defined as:

$$\mathrm{B}_M = \frac{Y_{Fs} - Y_{F\infty}}{1 - Y_{Fs}}, \tag{2.117}$$

where Y_{Fs} and $Y_{F\infty}$ are the mass fractions of vapor at the droplet surface and outer boundary of the film, respectively. Y_{Fs} is calculated according to Clausius-Clapeyron equation:

$$Y_{Fs} = \frac{M_F}{M_F + \bar{M}(\bar{p}/p_F - 1)}, \tag{2.118}$$

where M_F is the molecular weight of the fuel and $\bar{M}$ is the mean molecular weight of the surrounding gas. $\bar{p}$ is the mean pressure of surrounding gas. p_F is the vapor pressure of the fuel which is calculated from the critical temperature, critical pressure and droplet temperature [224]:

$$p_F = p_{\mathrm{crit}} \exp\left(\frac{f(T_{d,\mathrm{ref}})}{1 - T_{d,\mathrm{ref}}}\right), \tag{2.119}$$

with

$$T_{d,\text{ref}} = 1 - \frac{T_d}{T_{\text{crit}}}; \tag{2.120}$$

$$f(T) = -8.54796T + 0.76982T^{1.5} - 3.1085T^3 + 1.54481T^6. \tag{2.121}$$

B_T is the Spalding heat transfer number [223]. Substituting Eq. (2.107) into Eq. (2.108), we obtain

$$\widehat{\rho D}\mathrm{Sh}^* \ln(1+\mathrm{B}_M) = \frac{\widehat{\lambda}}{\widehat{C_p}}\mathrm{Nu}^* \ln(1+\mathrm{B}_T). \tag{2.122}$$

Thus, B_T can be calculated from B_M using

$$\mathrm{B}_T = (1+\mathrm{B}_M)^{\Phi} - 1, \tag{2.123}$$

with

$$\Phi = \frac{\widehat{C_p}\widehat{\rho D}}{\widehat{\lambda}}\frac{\mathrm{Sh}^*}{\mathrm{Nu}^*}. \tag{2.124}$$

The change rate of the droplet radius is obtained from Eq. (2.107),

$$\dot{r}_d = \frac{\dot{m}_d}{4\pi\rho_l r_d^2} = \frac{\widehat{\rho D} r_d \mathrm{Sh}^* \ln(1+\mathrm{B}_M)}{2\rho_l r_d^2}. \tag{2.125}$$

With infinite-conductivity model [221], the evolution equation of droplet temperature is written as:

$$\dot{T}_d = \frac{dT_d}{dt} = \frac{\dot{m}_d\left(\hat{C}_p(T_\infty - T_d)/\mathrm{B}_T - L_v(T_d)\right)}{\frac{4}{3}\pi\rho_l C_{p,l} r_d^3}. \tag{2.126}$$

The latent heat of vaporization of the fuel with droplet temperature T_d is related to the latent heat of the fuel at the boiling point with the following relationship [224]:

$$L_v(T_d) = \left(\frac{1 - T_d/T_{\text{crit}}}{1 - T_b/T_{\text{crit}}}\right)^{\kappa} L_v(T_b), \tag{2.127}$$

where T_b is the boiling point of liquid; and

$$\kappa = \left(\frac{0.00264 L_v(T_b)}{RT_b} + 0.8794\right)^{10}. \tag{2.128}$$

The latent heat of the fuel at the boiling point is estimated using Riedel estimation method [224]:

$$L_v(T_b) = \frac{1.093 RT_b \log(p_{\text{crit}}/p_{\text{ref}} - 1.103)}{0.930 - T_b/T_{\text{crit}}}, \tag{2.129}$$

with $p_{\text{ref}} = 1.0$ bar.

The infinite-conductivity model is appropriate for small droplets and for the fuel with its relatively high volatility at atmospheric pressure.

2.4 Flamelet Model

Flamelet models are constructed from an asymptotic view of diffusive-reaction layers. The idea was proposed in 1970 in the field of chemical engineering [225] and in 1972 in the field of combustion [226]. The flamelet concept views the turbulent diffusion flame as an ensemble of stretched flamelets attached to the instantaneous position of the flame surface. By assuming the terms involving transients and gradients parallel to the instantaneous surface of the constant mixture fraction to be small, and assuming equal diffusibility of all species, the species conservation equations can locally and instantaneously be transformed into the stationary laminar flamelet equation [169]:

$$\rho\frac{\partial Y_i}{\partial t} = \frac{\rho\chi}{2}\frac{\partial^2 Y_i}{\partial \xi_C^2} + \dot{\omega}_i; \tag{2.130}$$

$$\rho\frac{\partial T}{\partial t} = \frac{\rho\chi}{2}\frac{\partial^2 T}{\partial \xi_C^2} + \frac{1}{C_p}\dot{Q}, \tag{2.131}$$

where the instantaneous scalar dissipation rate χ depends on the details of the characteristics of the turbulence. It is defined as

$$\chi = 2D\left(\frac{\partial \xi_C}{\partial x_i}\right)^2 = 2D\left[\left(\frac{\partial \xi_C}{\partial x_1}\right)^2 + \left(\frac{\partial \xi_C}{\partial x_2}\right)^2 + \left(\frac{\partial \xi_C}{\partial x_3}\right)^2\right]. \tag{2.132}$$

The underlying concept is that the flame reaction zones are very thin. The only two control parameters are the mixture fraction ξ_C and its dissipation rate χ. The mixture fraction indicates the progress of the chemical reaction, while its dissipation rate indicates the effects of the turbulence. With the scalar dissipation rate χ, the effects of finite rate chemistry are included. For a given state of the turbulent flow with certain value of ξ_C and χ, the flamelet models assume that the local balance between diffusion and reaction is similar to the one in a prototype laminar flame with the same value of ξ_C and χ. The balance equations of species are then replaced with the conservation equation of the mean and variance of the mixture fraction.

The solutions may be available either in form of steady state flamelet libraries or in form of unsteady flamelet libraries [227]. The results are stored in a structured table. The composition state space can be determined by looking up the table according to the mixture fraction and its dissipation rate. The mean values of the scalars are obtained usually through a presumed PDF approach. Eq. (1.6) is then changed to

$$\tilde{Y}_i = \int_{\xi_C}\int_{\chi} Y_i^{\mathrm{SFLM}}(\xi_C,\chi)\tilde{f}(\xi_C,\chi;\mathbf{x},t)d\xi_C d\chi, \tag{2.133}$$

where SFLM stands for "steady flamelet model". The flamelet structure is pre-calculated by solving the one-dimensional flamelet equations. Usually the counter-flow structure is used to build the flamelet library [67, 181]. $Y_i^{\mathrm{SFLM}}(\xi_C,\chi)$ is usually tabulated from

the flamelet library. Then the calculation of the turbulent flow and mixture fields is separated from the calculation of the chemistry. Detailed chemical reaction mechanisms and molecular diffusion processes can be included in these flamelet libraries.

Recently, unsteady laminar flamelet models (Lagrangian flamelet models) were developed to take into account the effects of the transients [228, 227, 229]. They incorporate a Lagrangian viewpoint associated with the treatment of the strong fluctuations that can occur in scalar dissipation. They accommodates the effects of the convection terms parallel to the surfaces of the constant mixture fraction. History effects were taken into account using a Lagrangian time measured along the stoichiometric line.

Mean scalar dissipation rate is defined as

$$\tilde{\chi} = 2D(\frac{\partial \widetilde{\xi_C}}{\partial x_j})^2, \tag{2.134}$$

and modeled as

$$\tilde{\chi} = c_\chi \frac{\tilde{\epsilon}}{\tilde{k}} \widetilde{\xi_C''^2}. \tag{2.135}$$

The scalar dissipation rate directly indicates the decaying speed of fluctuations via turbulent micro-mixing. Since the burning rate depends on the contact between the reactants, the scalar dissipation rate enters directly or indirectly the expression for the mean burning rate. It is a very important concept for turbulent combustion. The main stumbling block in turbulent combustion modeling and bridges between the various modeling concepts emerge through the scalar dissipation rate [68].

Another important quantity is the scalar dissipation rate $\tilde{\chi}_{st}$ at the stoichiometric conditions which should be modeled. However the CFD code cannot provide this conditional scalar dissipation rate. It only can determine the unconditional one through Eq. (2.135). For the counter-flow, assuming constant density and diffusivity, the scalar dissipation rate is approximated by

$$\chi = \frac{a}{\pi} \exp(-2[\mathrm{erfc}^{-1}(2\xi_C)]^2), \tag{2.136}$$

where erfc^{-1} is the inverse of the complementary error function. The above equation implies that the scalar dissipation rate depends on the mixture fraction. The conditional scalar dissipation rate can be related to the unconditional one by

$$\chi(\xi_C) = \chi(\xi_{C,st}) \frac{f(\xi_C)}{f(\xi_{C,st})}, \tag{2.137}$$

where f is the exponential term in Eq. (2.136). Taking an average of χ, we obtain

$$\tilde{\chi} = \int_0^1 \chi(\xi_C) P(\xi_C) d\xi_C = \chi(\xi_{C,st}) \int_0^1 \frac{f(\xi_C)}{f(\xi_{C,st})} P(\xi_C) d\xi_C. \tag{2.138}$$

Coupling with eq. (2.135), the stoichiometric scalar dissipation rate is determined by

$$\chi(\xi_{C,st}) = \frac{c_\chi \frac{\tilde{\epsilon}}{\tilde{k}} \widetilde{\xi_C''^2}}{\int_0^1 \frac{f(\xi_C)}{f(\xi_{C,st})} P(\xi_C) d\xi_C}. \tag{2.139}$$

Mixture fraction and dissipation rate are the two most important scalars. The dissipation rate χ can be related to the strain rate of the local flamelet. χ describes the deviations from chemical equilibrium. It is possible to add the effects of the strain into combustion models if the shape of the joint PDF of mixture fraction and the dissipation rate is known. Experimental study showed that the scalar dissipation rate follows log-normal distribution [230, 231, 232].

In the turbulent spray diffusion flame, the liquid phase affects the flame structure significantly even for dilute sprays [178]. Fluctuations of the equivalence ratio and temperature induced by the presence of fuel droplets may not be neglected, even when the flow is premixed on a large scale [181]. Additional parameters should be taken into account in the flamelet library, including initial droplet radius r_{l0}, initial spray velocity for fixed strain rate at the inlet v_{l0}, and the equivalence ratio at the spray inlet E_r [180]. Thus, Eq. (2.133) becomes

$$\begin{aligned} \tilde{Y}_i &= \int_{\xi_C} \int_\chi Y_i^{\mathrm{SFLM}}(\xi_C, \chi, r_{l0}, v_{l0}, E_r) \\ &\times \tilde{f}(\xi_C, \chi, r_{l0}, v_{l0}, E_r; \mathbf{x}, t) d\xi_C d\chi dr_{l0} dv_{l0} dE_r. \end{aligned} \tag{2.140}$$

New flamelet model includes the effects of the liquid phase through these additional parameters. Here all the parameters are assumed to be statistically independent:

$$\begin{aligned} f(\xi_C, \chi, r_{l0}, v_{l0}, E_r; \mathbf{x}, t) &= f_{\xi_C}(\xi_C; \mathbf{x}, t) f_\chi(\chi; \mathbf{x}, t) \\ &\times f_{r_{l0}}(r_{l0}; \mathbf{x}, t) f_{v_{l0}}(v_{l0}; \mathbf{x}, t) f_{E_r}(E_r; \mathbf{x}, t). \end{aligned} \tag{2.141}$$

Following the ideas of the flamelet model for gas phase combustion, the turbulent fluctuation of the mixture fraction is modeled using a presumed β distribution [178]:

$$f_{\xi_C}(\xi_C) = P_1(\xi_C) = \frac{\Gamma(\alpha+\beta)}{\Gamma(\alpha)\Gamma(\beta)} \xi_C^{\alpha-1} (1-\xi_C)^{\beta-1}. \tag{2.142}$$

The parameters α and β are determined from the mean and the variance of the local mixture fraction:

$$\alpha = \widetilde{\xi_C} \left[\frac{\widetilde{\xi_C}(1-\widetilde{\xi_C})}{\widetilde{\xi_C''^2}} - 1 \right]; \tag{2.143}$$

$$\beta = (1-\widetilde{\xi_C}) \left[\frac{\widetilde{\xi_C}(1-\widetilde{\xi_C})}{\widetilde{\xi_C''^2}} - 1 \right]. \tag{2.144}$$

It has been proven that this presumed β function is questionable in the presence of a spray [45, 233, 140]. A modified β function is a better choice [140]. It is defined as

$$P_2(\xi_C) = \frac{\Gamma(\alpha+\beta)}{\Gamma(\alpha)\Gamma(\beta)}(\xi_{C,\max}-\xi_{C,\min})^{1-\alpha-\beta}(\xi_C-\xi_{C,\min})^{\alpha-1}(\xi_{C,\max}-\xi_C)^{\beta-1}. \quad (2.145)$$

The parameters $\xi_{C,\min}$ and $\xi_{C,\max}$ represent the minimum and maximum value of mixture fraction. Their values depend on the local conditions. The parameters α and β are determined from the mean and variance of the local mixture fraction, and $\xi_{C,\min}$, $\xi_{C,\max}$:

$$\alpha = \frac{\widetilde{\xi_C}-\xi_{C,\min}}{\xi_{C,\max}-\xi_{C,\min}}\left[\frac{(\widetilde{\xi_C}-\xi_{C,\min})(\xi_{C,\max}-\widetilde{\xi_C})}{\widetilde{\xi_C''^2}}-1\right]; \quad (2.146)$$

$$\beta = \frac{\xi_{C,\max}-\widetilde{\xi_C}}{\xi_{C,\max}-\xi_{C,\min}}\left[\frac{(\widetilde{\xi_C}-\xi_{C,\min})(\xi_{C,\max}-\widetilde{\xi_C})}{\widetilde{\xi_C''^2}}-1\right]. \quad (2.147)$$

Another alternative is to replace the presumed PDF with the marginal PDF computed using a transported PDF method [142].

Scalar dissipation rate is modeled using a log-normal distribution:

$$f_\chi(\chi) = P_3(\chi) = \frac{1}{\sigma_{\log}\sqrt{2\pi}x}\exp\left[-\frac{(\ln x-\mu_{\log})^2}{2\sigma_{\log}^2}\right]. \quad (2.148)$$

The parameter $\sigma_{\log}$ is set to 2 [194]. The parameter $\mu_{\log}$ is computed from the mean dissipation rate:

$$\mu_{\log} = \ln(\tilde{\chi}) - 1. \quad (2.149)$$

Since there are no guidelines from experiments or from DNS for the evaluation of the PDFs for r_{l0}, v_{l0}, and E_r, simple approaches are used. Dirac delta functions are used for the initial spray velocity, equivalence ratio at the spray inlet, and the initial droplet size.

3. Numerical Methods

In the numerical simulation, the governing equations are discretized and solved by computer programs. Appropriate numerical algorithms are required. An ideal numerical algorithm should

- be linearly stable for all cases of interest;
- mirror the conservation properties of the physics;
- ensure the positivity property when appropriate;
- be reasonably accurate;
- be computationally efficient;
- be independent of specific properties of one particular application.

Stability, conservation, and positivity generally relate to the accuracy. None of them can guarantee any of the others.

There are several numerical methods available for the fluid mechanics. The methods ranging from the most discrete (or particulate) in nature to the most continuous (or global) include:

- particle methods
- characteristic methods
- Lagrangian finite difference/finite volume method
- Eulerian finite difference/finite volume method
- finite element method
- spectral methods

Each method has advantages and disadvantages, consequently has the preferable application fields. Usually, it is difficult or inefficient for a stand-alone method to simulate a complex system. Hybrid method, which is like a bootstrapping process, combines

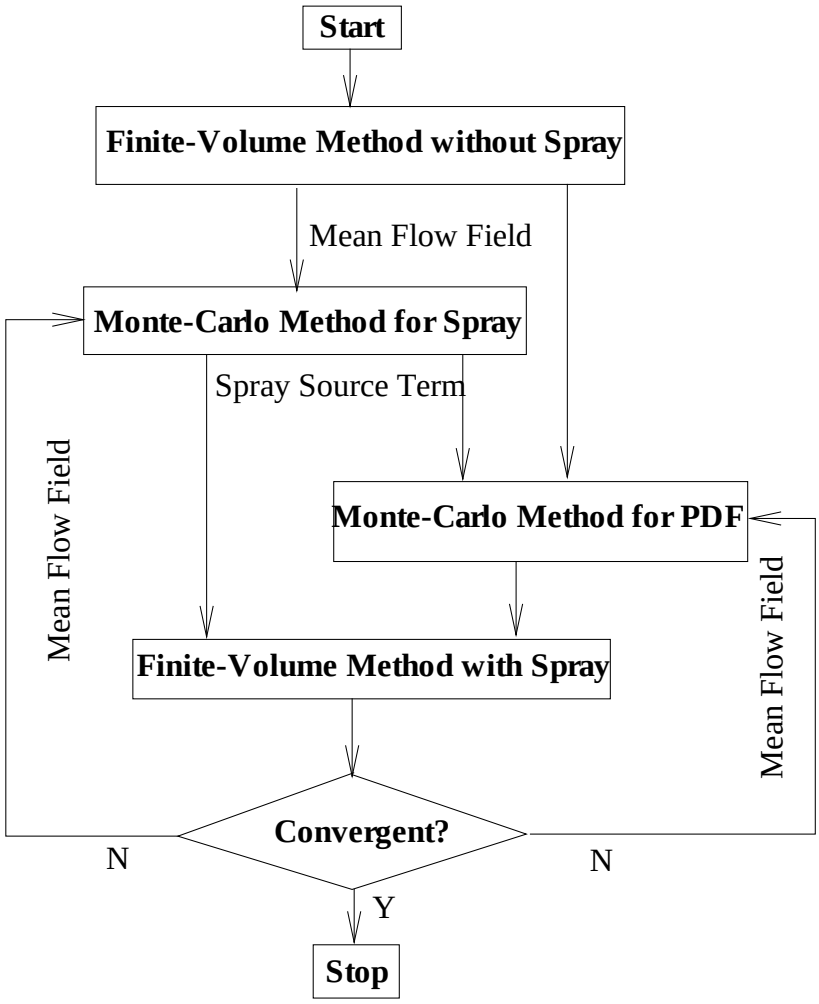

Fig. 3.1: Flowchart of the computation code.

the advantages of the multiple methods and minimizes their disadvantages. The disadvantage of hybrid method is that the consistency problem is more serious. Special strategies are needed to keep consistent between the multiple methods.

In the present work, a finite volume method based on the SIMPLE-algorithm is used to solve the mean conservation equation of the gas flow; a Lagrangian Monte-Carlo/particle method is used for the PDF transport equation of the gas flow; a Lagrangian stochastic droplet parcel method is used for the spray flow. The flowchart of the computational code is illustrated in Fig. 3.1. In this chapter, the detailed descriptions of these three methods are presented as well as the information exchange between the different numerical methods.

3.1 Finite Volume Method

Basic laws of the fluid mechanics are the conservation laws. They are the statements that express the conservation of mass, momentum, and energy in a volume enclosed by a surface. To represent the conservation laws, the most natural way is to solve the weak forms of the governing equations, i.e., the integral forms of the equations. The integral forms can be discretized by the finite volume method. The whole computational domain is subdivided into a set of non-overlapping cells (control volume). The conservation laws are applied on each cell to determine the flow field variables stored in the nodes. If we write the Navier-Stokes Equations as

$$\frac{\partial \mathbf{W}}{\partial t} + \nabla \cdot (\mathbf{F}(\mathbf{W}) - \mathbf{N}(\mathbf{W})) = \mathbf{S}(\mathbf{W}), \tag{3.1}$$

where $\mathbf{W} = (\rho, \rho\mathbf{U}, \rho h)^T$ is the vector of the conserved variables; $\mathbf{F}$, $\mathbf{N}$ and $\mathbf{S}$ are the convective, viscous, and source terms, respectively. Let Ω be the control volume, and its surface area is A. Integrating Eq. (3.1) in the control volume, we obtain

$$\int_\Omega \frac{\partial \mathbf{W}}{\partial t} d\Omega + \oint_{\partial\Omega} (\mathbf{F}(\mathbf{W}) - \mathbf{N}(\mathbf{W})) \cdot \mathbf{n} dA = \int_\Omega \mathbf{S}(\mathbf{W}) d\Omega. \tag{3.2}$$

Using an explicit time integration, Eq. (3.2) leads to the form of

$$\mathbf{W}^{n+1} = \mathbf{W}^n - \frac{\Delta t}{\Omega} \oint_{\partial\Omega} (\mathbf{F}(\mathbf{W}^n) - \mathbf{N}(\mathbf{W}^n)) \cdot \mathbf{n} dA + \Delta t \cdot \mathbf{S}(\mathbf{W}^n), \tag{3.3}$$

where n indicates the time step. Substituting the formula of $\mathbf{F}$, $\mathbf{N}$ and $\mathbf{S}$ into Eq. (3.3), we get a large number of equations with independent variables $\mathbf{W}$. Solutions of the flows are obtained by solving these equations.

Finite volume method combines advantages of the finite element method (geometric flexibility) and of the finite difference method (flexibility in defining the discrete flow field). The finite volume method automatically fulfills the conservation laws. The numerical results of the finite volume method are relatively smooth. It can be adapted to complex geometries. The numerical solution is relatively simple with low computational cost comparing to other numerical methods. It is easy to construct high-order discretized formulation and to treat the boundary conditions.

In the present work, the mean conservation equations of gas flows are solved by a finite volume method which is based on the SIMPLE algorithm. For a steady, axisymmetry problem, all the conservation equations can be written in a uniform equation as the following [194]:

$$L(\tilde{\Phi}) \equiv \frac{\partial(\bar{\rho}\tilde{U}_i\tilde{\Phi})}{\partial x_i} - \frac{\partial}{\partial x_i}\left(\Gamma_{\Phi,\text{eff}} \frac{\partial \tilde{\Phi}}{\partial x_i}\right) = \bar{S}_{g,\Phi} + \bar{S}_{l,\Phi}. \tag{3.4}$$

The corresponding description for each term is listed in Table 3.1 [194]. The evaluation of the mean spray source terms $S_{l,\Phi}$ will be discussed in the Section 3.3.

$\tilde{\Phi}$	$\bar{S}_{g,\Phi}$	$\bar{S}_{l,\Phi}$
1	0	$\sum_{k=1}^{N_p}(n\dot{m}_d)_{p,k}$
$\tilde{U}_x$	$-\frac{\partial\bar{p}}{\partial x} - \frac{2}{3}\frac{\partial}{\partial x}\left[\mu_{\text{eff}}\left(\frac{\partial\tilde{U}_x}{\partial x} + \frac{1}{r}\frac{\partial\left(r\tilde{U}_r\right)}{\partial r}\right)\right] + \bar{\rho}g$	$\sum_{k=1}^{N_p}(n\dot{m}_d U_{d,x})_{p,k}$
$\tilde{U}_r$	$-\frac{\partial\bar{p}}{\partial r} - \frac{2}{3}\frac{\partial}{\partial r}\left[\mu_{\text{eff}}\left(\frac{\partial\tilde{U}_x}{\partial x} + \frac{1}{r}\frac{\partial\left(r\tilde{U}_r\right)}{\partial r}\right)\right] - 2\frac{\mu_{\text{eff}}\tilde{U}_r}{r^2}$	$\sum_{k=1}^{N_p}(n\dot{m}_d U_{d,r})_{p,k}$
$\tilde{h}$	0	$\sum_{k=1}^{N_p}(n\dot{m}_d h_d)_{p,k}$
$\tilde{k}$	$G_{\text{k}} - \bar{\rho}\tilde{\epsilon}$	$\sum_{k=1}^{N_p}\overrightarrow{u''}(n\dot{m}_d\mathbf{U}_d)_{p,k}$
$\tilde{\epsilon}$	$(C_1 G_{\text{k}} - C_2\bar{\rho}\tilde{\epsilon})\tilde{\epsilon}\,/\,\tilde{k}$	$C_s\tilde{\epsilon}/\tilde{k}\;\bar{S}_{l,k}$
$\widetilde{\xi_C}$	0	$\bar{S}_{l,1}$
$\widetilde{\xi_C''^2}$	$2\Gamma_{\widetilde{\xi_C''^2}_{\text{t}}}\,\text{div}^2\tilde{\xi_C} - 2\bar{\rho}\tilde{\epsilon}\,/\,\tilde{k}\,\widetilde{\xi_C''^2}$	$\bar{S}_{l,k}\,\widetilde{\xi_C''^2}\left(1 - 2\widetilde{\xi_C}\right)/\widetilde{\xi_C}$

Tab. 3.1: Governing equations of the gas phase flow with a dilute spray.

3.1.1 Staggered Grid

In the present work, a staggered grid technique is employed. Staggered grids for dependent variables in a flow field were first used in 1965 [234]. They are illustrated in Fig. 3.2 [235]. The control volume of the node (i, j) is indicated by the dashed line. All the information is stored in the node, except the velocity. The location of the velocity components are at the center of the cell faces to which they are normal. The pressure difference between two adjacent cells is the driving force for the velocity component located between the interfaces of these cells. This prevents the appearance of oscillatory solutions, particularly for the pressure, p, that can occur if centered difference scheme are used to discretize all derivatives on a non-staggered grid. The convective fluxes across the faces of the control volumes can be computed without interpolation of velocity components. With the staggered grid, the Poisson equation for the pressure (Eq. (3.20)) automatically satisfies the discrete form of the integral boundary condition [236]. This avoids additional adjustments to the right-hand side of the Poisson equation.

The use of staggered grid has some disadvantages [236]. The structure of computer program using a staggered grid is more complex than the one using a non-staggered grid, because the velocity U and V cannot be stored in the same array as other variables. Generally boundary conditions are more difficult to impose consistently with a stagger grid, since at least one dependent variable, U or V, will not be defined on a particular boundary. If non-rectangular grid and generalized coordinates are used, the incorporation of a staggered grid is more complicated.

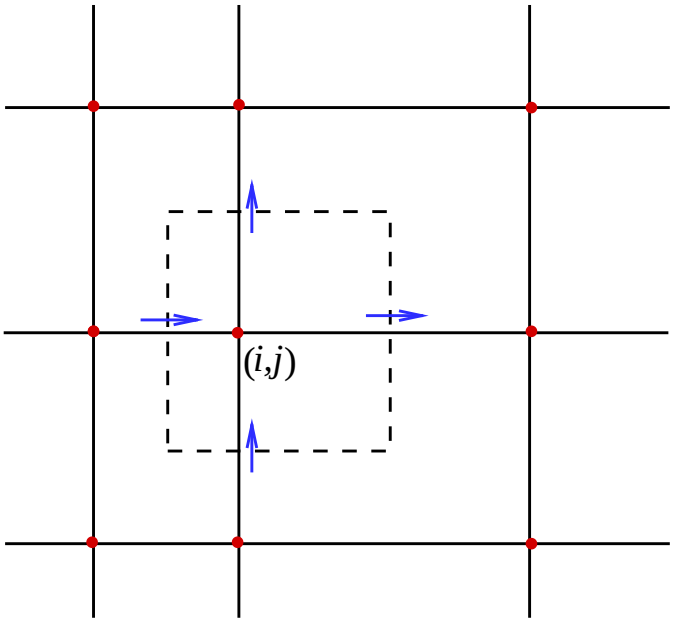

Fig. 3.2: Staggered grids in two dimensions: $\rightarrow = \tilde{U}$; $\uparrow = \tilde{V}$; $\bullet$ = other variables.

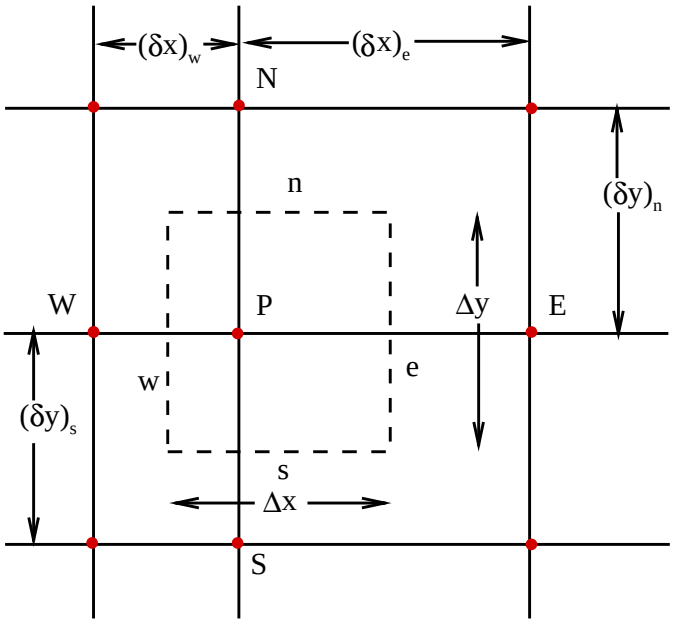

Fig. 3.3: Control volume of the grid nodes.

3.1.2 Discretized Formulation

A five-node formula is employed to solve the energy equation and the transport equations for the mixture fraction, variance of mixture fraction, turbulent kinetic energy, and dissipation rate. The value of one independent variable ϕ_p at a node p is connected with those of its two neighbors in x-direction, ϕ_e and ϕ_w, and its two neighbors in y-direction, ϕ_s and ϕ_n. Eq. (3.3) can be written as

$$a_p\phi_p = \sum_{l=e,w,n,s} a_l\phi_l + b, \tag{3.5}$$

where b is the source term. $l = e, w, n, s$ indicate the directions. The neighbor coefficients a_l represent the convection and diffusion influence of four faces of the control volume in terms of flow rate F_l and conductance D_l. The expression of a_l and b are derived by integrating the differential equation (3.4) over a control volume surrounding the node p (see Fig. 3.3 [235]).

$$a_l = D_l A(|\mathrm{P}_l|) + \frac{1}{2}\left(|F_l| - F_l\right),\ l = e, n; \tag{3.6}$$

$$a_l = D_l A(|\mathrm{P}_l|) + \frac{1}{2}\left(|F_l| + F_l\right),\ l = w, s; \tag{3.7}$$

$$a_p = \sum_I a_l; \tag{3.8}$$

$$b = S_c\Delta x\Delta y. \tag{3.9}$$

P is the cell Peclet number which is the square of the ratio between the cell size and the diffusion length:

$$\mathrm{P}_l = \frac{F_l}{D_l}. \tag{3.10}$$

Function $A(|\mathrm{P}|)$ depends on discretization schemes. In the present work, an upwind scheme is employed. A is set to unity:

$$A(|\mathrm{P}_l|) = 1. \tag{3.11}$$

F_l are expressed as

$$F_l = (\bar{\rho}\tilde{U})_l\Delta y,\ l = e, w; \tag{3.12}$$

$$F_l = (\bar{\rho}\tilde{V})_l\Delta x,\ l = n, s. \tag{3.13}$$

The upwind scheme is the only approximation that unconditionally satisfies the boundedness criterion. With upwind scheme, oscillations in the solutions are avoided, i.e. the the computation is more stable. However, the upwind scheme introduces numerical diffusion as a result of the first-order truncation.

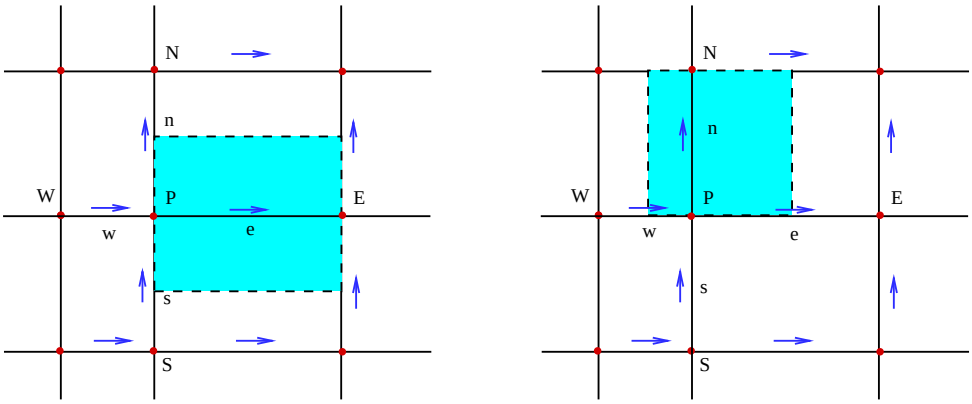

Fig. 3.4: Control volume of axial velocity (left) and radial velocity (right).

A central-difference scheme is used to calculate the diffusion flux. D_l are expressed as

$$D_l = \Gamma_l \frac{\Delta y}{(\delta x)_l}, \; l = e, w; \tag{3.14}$$

$$D_l = \Gamma_l \frac{\Delta x}{(\delta y)_l}, \; l = n, s. \tag{3.15}$$

The discretized momentum equation is different from the ones for other variables because of the usage of staggered grid technique. The staggered control volume for velocity U is shown in Fig. 3.4 [235]. The control volume is staggered in relation to the normal control volume around the grid point P and E. The difference $p_p - p_e$ is the pressure force acting on the control volume for the velocity U. The calculation of the diffusion coefficient and the mass flow rate at the faces of the control volume requires a calculation similar to Eq. (3.5). The resulting discretization equation can be written as

$$a_e U_e = \sum a_{lb} U_{lb} + b + (p_p - p_e) A_e; \tag{3.16}$$

$$a_n V_n = \sum a_{lb} V_{lb} + b + (p_p - p_n) A_n. \tag{3.17}$$

The neighbor coefficients a_{lb} account for the combined convection-diffusion influences at the control volume faces. The source term b is defined in the same manner as the one in Eq. (3.5).

3.1.3 SIMPLE Algorithm

SIMPLE algorithm is used to calculate the pressure and to ensure the satisfaction of the continuity equation. The acronym "SIMPLE" stands for "Semi-Implicit Method

for Pressure-linked Equations". The SIMPLE-type algorithm dominated the entire field of numerical simulation of fluid flows in the last century. Some modifications to the SIMPLE algorithm have been suggested in [237].

SIMPLE algorithm is based on the finite volume discretization on the staggered grids which the present work employed. It describes the iterative procedure by which the solutions of the discretized equations are obtained. The iterative procedure can be interpreted as a pseudo-transient treatment of the unsteady momentum conservation equations in discrete form to obtain the steady-state solution. The momentum equation (2.15) can be transformed to a Poisson equation:

$$\frac{\partial^2 \bar{p}}{\partial x_i^2} = -\frac{\partial}{\partial x_i}\left(\frac{\partial}{\partial x_j}\left(\bar{\rho}\tilde{U}_i\tilde{U}_j - \tau_{ij}\right) + \frac{\rho U_i}{\partial t} - \rho g_i - S_{l,U_i}\right). \tag{3.18}$$

Substituting the continuity equation (2.14) into the above equation, we obtain:

$$\frac{\partial^2 \bar{p}}{\partial x_i^2} = -\frac{\partial}{\partial x_i}\left(\frac{\partial}{\partial x_j}\left(\bar{\rho}\tilde{U}_i\tilde{U}_j - \tau_{ij}\right) - \rho g_i - S_{l,U_i}\right) + \frac{\partial^2 \bar{\rho}}{\partial t^2} + \frac{\partial \bar{S}_{l,1}}{\partial t}. \tag{3.19}$$

For the steady case, the viscous and unsteady terms disappear leaving:

$$\frac{\partial^2 \bar{p}}{\partial x_i^2} = -\frac{\partial}{\partial x_i}\left(\frac{\partial}{\partial x_j}\left(\bar{\rho}\tilde{U}_i\tilde{U}_j\right) - \rho g_i - S_{l,U_i}\right). \tag{3.20}$$

Its discretized form is

$$a_p \delta p_p = \sum_I (a\delta p)_I + b, \tag{3.21}$$

with the coefficients and source term:

$$\begin{aligned}
a_l &= \bar{\rho}_l d_l A_l, l = e, w, n, s, \\
a_p &= \sum_l a_l, \\
b &= \left[\left(\bar{\rho}\widetilde{U^*}\right)_w - \left(\bar{\rho}\widetilde{U^*}\right)_e\right] A_e + \left[\left(\bar{\rho}\widetilde{V^*}\right)_s - \left(\bar{\rho}\widetilde{V^*}\right)_n\right] A_s + (\rho g_i + \bar{S}_{l,U_i})\Delta V, \\
d_l &= A_l / a_l.
\end{aligned}$$

The procedure can be summarized as the follows:

1. a pressure field p^* is estimated at first;

2. the velocity U^* and V^* are calculated using

$$a_e U_e^* = \sum a_{nb} U_{nb}^* + b + (p_p^* - p_e^*) A_e, \tag{3.22}$$

$$a_n V_n^* = \sum a_{nb} V_{nb}^* + b + (p_p^* - p_n^*) A_n; \tag{3.23}$$

3. δp is obtained from Eq. (3.21);

4. the corrected velocity U^c and V^c is calculated from

$$U_e^c = U_e^* + \frac{A_e}{a_e}(\delta p_p - \delta p_e), \tag{3.24}$$

$$V_n^c = V_n^* + \frac{A_n}{a_n}(\delta p_p - \delta p_n); \tag{3.25}$$

5. p^{n+1} is obtained from $p^{n+1} = p^n + \delta p$;

6. check whether the source term b in Eq. (3.21) is zero. If not, return to the step 2 and repeat until convergence is achieved.

The resulting nonlinear algebraic equations are solved by the line-by-line tri-diagonal-matrix algorithm (TDMA). A relaxation method is used to accelerate the convergence. Large change in the variables could cause numerical instability. Therefore, we allow $\Phi^{n+1,r}$ to change only a fraction α_Φ of the would-be difference:

$$\Phi^{n+1,r} = (1 - \alpha_\Phi)\Phi^n + \alpha_\Phi \Phi^{n+1}. \tag{3.26}$$

For the pressure, only a fraction of the pressure-correction is added to the guessed pressure field:

$$p^{n+1,r} = p^n + \alpha_p \delta p. \tag{3.27}$$

The relaxation parameters α_Φ and α_p are a constant lying between 0 and 1. The relaxation method can improve the stability of the computation.

3.1.4 Boundary Conditions

Precision and potential applications of the numerical schemes are constrained by the boundary conditions.

In the present finite volume method, the velocity, enthalpy, composition, and turbulent properties of gas flow are fixed to the initial values at the inlet plane.

At the symmetry axis and outside boundary, the convection and diffusion fluxes in the normal direction are zero. The velocity components normal to the boundary are set to zero. Other properties at the boundary nodes are set to their values at the node next to boundary.

At the exit plane, the gradients of fluid properties in the normal direction are zero. The values at the exit plane are set to their values at the internal nodes which are the node next to boundary.

3.2 Lagrangian Monte-Carlo Particle Method for the Gas Flow

Particle method provides a suitable discrete form wherever the system is by nature particle or is described by a Lagrangian formulation. It is widely used in physics, chemistry, and engineering. Successful examples include electronics, condensed matter study, dynamics of the large biological molecules, evolution of the spiral structure in galaxies, plasma, hot gas plasmas in the fusion machines, molten salts, aqueous solutions, phase change, and flows of electrons in semiconductor devices. In fluid mechanics, the particle methods are very helpful. The PDF transport equations are usually solved by particle methods, where the particles represent "fluid elements". The dispersed phase in the multiphase flow is often solved by particle methods too, where the particles represent droplets, bubbles, or solid particles.

In the present work, the PDF transport equation is solved by a Lagrangian Monte-Carlo particle method. The one point PDF is represented by a finite number of gas particles. Each gas particle has a set of properties. The properties may be mass m^*, position $\mathbf{x}^*$, velocity $\mathbf{U}^*$, mixture fraction ξ_C^*, enthalpy h^* in different PDF formulations. The gas particle with the position $\mathbf{x}^*$ evolves according to

$$\frac{d\mathbf{x}^*}{dt} = \mathbf{U}^*(\mathbf{x}^*), \tag{3.28}$$

where $\mathbf{U}^*(\mathbf{x}^*)$ is the instantaneous velocity of the particle. For the scalar PDFs, the instantaneous velocity of the particle is written as

$$\mathbf{U}^*(\mathbf{x}^*) = \tilde{\mathbf{U}}(\mathbf{x}^*) + \mathbf{u}(\mathbf{x}^*, t), \tag{3.29}$$

where $\tilde{\mathbf{U}}$ is computed by the finite volume method and is interpolated into the particle's position $\mathbf{x}^*$. In the present work, first-order interpolation is used. If the particle locates in the cell e whose four nodes are $(i,\, j)$,$(i{+}1,\, j)$,$(i,\, j{+}1)$, and $(i{+}1,\, j{+}1)$, then the value of function ϕ at the particle position $(x,\, y)$ is interpolated from the values stored at the nodes:

$$\begin{aligned} \phi^*(x,y) &= g_{i,j}(x,y)\phi_{i,j} + g_{i+1,j}(x,y)\phi_{i+1,j} \\ &+ g_{i,j+1}(x,y)\phi_{i,j+1} + g_{i+1,j+1}(x,y)\phi_{i+1,j+1}, \end{aligned} \tag{3.30}$$

where $g_{i,j}(x,y)$ is the linear basis function coefficient of node $(i,\, j)$ to the particle position $(x,\, y)$ in the cell e. The linear basis function coefficient is defined as

$$g_{i,j}(x,y) = \frac{(x_{i+1}-x)(y_{i+1}-y)}{(x_{i+1}-x_i)(y_{i+1}-y_i)}$$

$$g_{i+1,j}(x,y) = \frac{(x-x_i)(y_{i+1}-y)}{(x_{i+1}-x_i)(y_{i+1}-y_i)}$$

$$g_{i,j+1}(x,y) = \frac{(x_{i+1}-x)(y-y_i)}{(x_{i+1}-x_i)(y_{i+1}-y_i)}$$
$$g_{i+1,j+1}(x,y) = \frac{(x-x_i)(y-y_i)}{(x_{i+1}-x_i)(y_{i+1}-y_i)}$$

The sum of these four coefficients equals to unity:

$$\sum_{\alpha=1}^{4} g_\alpha(x,y) = 1.$$

If the gas particle is not in the cell e, then the linear basis function coefficients equal zero:

$$g_\alpha(x,y) = 0.$$

The fluctuating velocity $\mathbf{u}$ is assumed to follow a Gaussian distribution with the mean of zero and the variance of $2k/3$:

$$f(u) = \left(\frac{4}{3}\pi\tilde{k}\right)^{-\frac{1}{2}} \exp\left(-\frac{3}{4\tilde{k}}u^2\right). \tag{3.31}$$

The value of the fluctuating velocity is determined through a Monte-Carlo method. The turbulent kinetic energy is interpolated from grids into the gas particle's position using Eq. (3.30). For the joint velocity-scalar PDF, the velocity of the gas particle is calculated from the Eq. (2.63).

A second-order algorithm is used to solve Eq.(3.28) [91]. The mid-point $\mathbf{x}^{*^{n+\frac{1}{2}}}$ is computed by

$$\mathbf{x}^{*^{n+\frac{1}{2}}} = \mathbf{x}^{*^n} + \frac{\Delta t}{2}\left(\tilde{\mathbf{U}}^n(\mathbf{x}^{*^n}) + \mathbf{u}^n\right). \tag{3.32}$$

The superscript n denotes the nth time step. Then the new mean velocity $\mathbf{U}^n(\mathbf{x}^{*^{n+\frac{1}{2}}})$ and fluctuating velocity $\mathbf{u}^{n+1}$ at position $\mathbf{x}^{*^{n+\frac{1}{2}}}$ are computed. The particle's position at $(n+1)$th time step is calculated by

$$\mathbf{x}^{*^{n+1}} = \mathbf{x}^{*^n} + \Delta t\left(\tilde{\mathbf{U}}^n(\mathbf{x}^{*^{n+\frac{1}{2}}}) + \frac{1}{2}(\mathbf{u}^n + \mathbf{u}^{n+1})\right). \tag{3.33}$$

To solve Eq. (2.63) numerically, we define

$$\begin{aligned} a_i &= g - \frac{1}{\bar{\rho}}\left(\frac{\partial \bar{p}}{\partial x_i} - \bar{S}_{l,U_i}\right); \\ b &= -\left(\frac{1}{2} + \frac{3}{4}C_0\right)\frac{\tilde{\epsilon}}{\tilde{k}}; \\ c &= C_0\tilde{\epsilon}. \end{aligned} \tag{3.34}$$

Then Eq. (2.63) becomes

$$dU_i^*(t) = a_i dt + bU_i^* dt + c^{1/2} dW_i. \tag{3.35}$$

The second-order scheme is applied to solve Eq. (3.35) [199, 91]:

$$\begin{aligned} \Delta U_i^* &= (a_i + bU_i^*)\,\Delta t + (c\Delta t)^{1/2}\xi_i; \\ U_i^{*^{n+1}} &= U_i^{*^n} + \Delta U_i^* + \frac{1}{2} b \Delta U_i^* \Delta t. \end{aligned} \tag{3.36}$$

For the k-th particle, the IEM model is expressed as

$$d\phi_k^* = -\frac{1}{2}\frac{C_\phi}{t_\tau(\mathbf{x}_k^*)}(\phi_k^* - \tilde{\phi}(\mathbf{x}_k^*))dt, \tag{3.37}$$

which is the first term on the right-hand side of Eqs. (2.64) and (2.65). The local turbulent fluctuating time scale $t_\tau(\mathbf{x}_k^*)$ is interpolated from the grid nodes. Frozen t_τ and $\tilde{\phi}$, the exact increment in ϕ_k^* over time Δt is

$$\Delta\phi_k^* = -d_k(\phi_k^* - \tilde{\phi}(\mathbf{x}_k^*)) \tag{3.38}$$

with

$$d_k = 1 - e^{-\frac{1}{2}C_\phi \Delta t/t_\tau}. \tag{3.39}$$

$\tilde{\phi}(\mathbf{x}_k^*)$ is interpolated from the grid node by

$$\tilde{\phi}(\mathbf{x}_k^*) = \sum_\alpha g_\alpha(\mathbf{x}_k^*)\hat{\phi}_\alpha, \tag{3.40}$$

where $g_\alpha(\mathbf{x}_k^*)$ is the linear basis function coefficient of node α to the particle position $\mathbf{x}_k^*$ with

$$\sum_\alpha g_\alpha(\mathbf{x}_k^*) = 1. \tag{3.41}$$

Thus

$$\Delta\phi_k^* = -d_k(\phi_k^* - \sum_\alpha g_\alpha(\mathbf{x}_k^*)\hat{\phi}_\alpha). \tag{3.42}$$

The global change in ϕ must be zero during the whole mixing process. However, if the value of $\hat{\phi}$ is directly taken from $\tilde{\phi}$ which is stored in the grid nodes, the global change may not be zero. Thus, the value of $\hat{\phi}$ must be estimated by setting the global change to zero,

$$\begin{aligned} 0 = \Delta G &\equiv \sum_k m_k^* \Delta\phi_k^* = -\sum_k m_k^* d_k \left(\phi_k^* - \sum_\alpha g_\alpha(\mathbf{x}_k^*)\hat{\phi}_\alpha\right) \\ &= -\sum_k m_k^* d_k \left(\sum_\alpha g_\alpha(\mathbf{x}_k^*)\phi_k^* - \sum_\alpha g_\alpha(\mathbf{x}_k^*)\hat{\phi}_\alpha\right) \\ &= -\sum_k \sum_\alpha \left(g_\alpha(\mathbf{x}_k^*) m_k^* d_k \left(\phi_k^* - \hat{\phi}_\alpha\right)\right) \\ &= \sum_\alpha \left(-\left(\sum_k g_\alpha(\mathbf{x}_k^*) m_k^* d_k \phi_k^*\right) + \hat{\phi}_\alpha \left(\sum_k g_\alpha(\mathbf{x}_k^*) m_k^* d_k\right)\right). \end{aligned} \tag{3.43}$$

Therefore, $\hat{\phi}_\alpha$ is determined by :

$$\hat{\phi}_\alpha = \frac{\sum_k g_\alpha(\mathbf{x}_k^*) m_k^* d_k \phi_k^*}{\sum_k g_\alpha(\mathbf{x}_k^*) m_k^* d_k}, \tag{3.44}$$

which is the CIC (Cloud-In-Cell) mean with particle weighting $m_k^* d_k$.

The mean values are evaluated from the results of the transported PDF method at each node. The computation is via the linear basis function coefficient. For an arbitrary function Φ, its mean value at the node α is calculated from its value of the gas particles:

$$\tilde{\Phi} = \frac{\sum_e \sum_k g_\alpha(\mathbf{x}_k^*) \Phi_k^*}{\sum_e \sum_k g_\alpha(\mathbf{x}_k^*) m_k^*}. \tag{3.45}$$

The first sum is over the cells e one of whose nodes is α.

Time step is restricted by Courant-Friedrichs-Lewy (CFL) condition [93]. Physically, the CFL condition indicates that a fluid particle should not travel more than one control volume in one time step. The global time step is computed by the following formula:

$$\Delta t = C_{\mathrm{CFL}} \cdot \min \left\{ \frac{\Delta x_i}{|\tilde{U}_i|}, \frac{\Delta y_i}{|\tilde{V}_i|}, \frac{\tilde{k}_i}{\tilde{\epsilon}_i}, \ldots \right\}, \quad i = 1, \ldots, N_g, \tag{3.46}$$

where N_g is the total number of the grids; Δx_i and Δy_i are the length of the control volume of node i in axial and radial direction, respectively; U and V are the axial and radial gas velocity, respectively; k and ϵ are the turbulent kinetic energy and its dissipation rate. The constant C_{CFL} should not be larger than 1 to satisfy the von Neumann stability condition. Here, C_{CFL} is set to 0.5. The resulting time step is used both in the finite volume method and the particle method.

In the particle method, the boundary conditions are necessary, too. Figure 3.5 shows the sketch of the computational domain. At the inlet plane, the Monte-Carlo gas particles are created and activated according to the local flow properties. The total mass of the new gas particles of one control cell is set to be the mass flux during the current time step:

$$M_{\mathrm{tot}}^* = \rho_0 U_{x,0} S_0 \Delta t, \tag{3.47}$$

where S_0 is the area of the control cell at inlet profile; $\rho_0, U_{x,0}$ are from experimental data.

When the gas particle moves across the axis of symmetry, the particle is reflected from the boundary without change in their properties except for the velocity and position in the direction normal to the boundary.

When the gas particle moves across the exit plane or outside boundary, the particle is discarded.

It is well-known that the statistical error is proportional to $N^{-1/2}$, where N is the sample number. In transported PDF method, the statistics of the flow field are

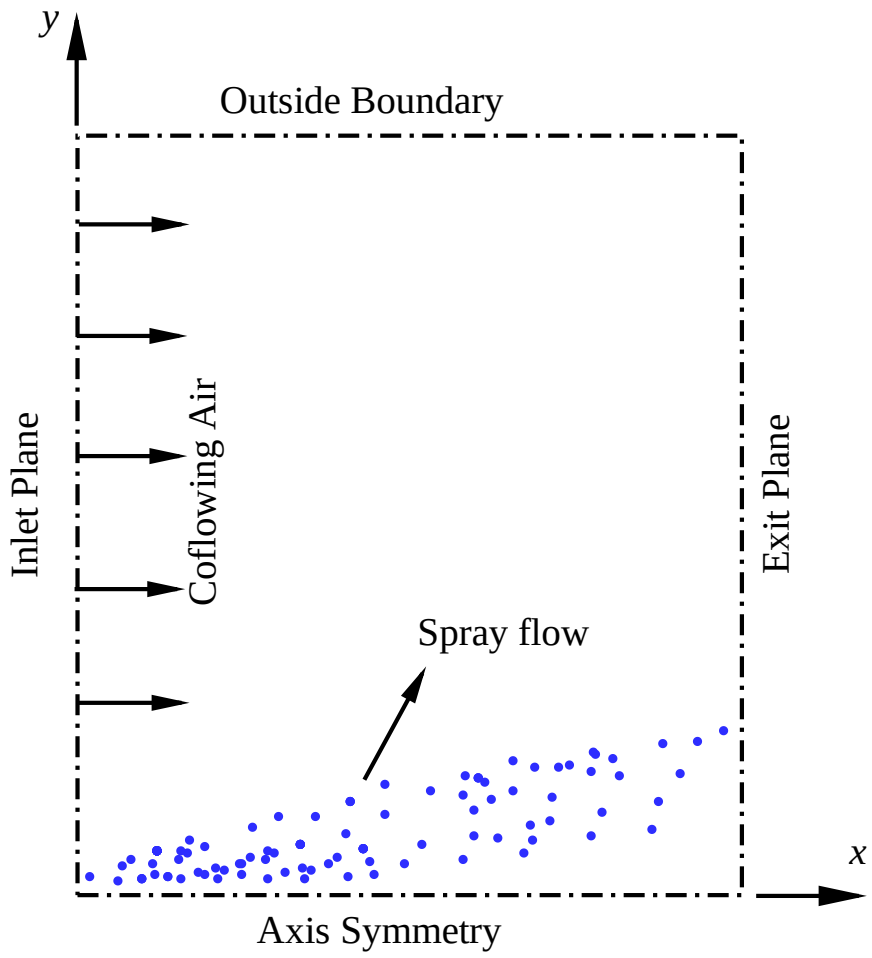

Fig. 3.5: Sketch of the computational domain

evaluated at each cell. When the total number of gas particles in one cell is too low, the corresponding statistical errors will be very large, and may prevent the code from convergence. Contrarily, if the total number of gas particles in one cell is too large, it may exceed the limitation of the array storing the properties of gas particles. To avoid such cases, special strategy [238] is needed to keep the gas particle number of every cell in a certain range, $[N_{\min}, N_{\max}]$. In the present work, a split/discard algorithm is used [94]. When the total particle number in one cell is smaller than $N_{\min}$, the largest gas particle in this cell is split into two identical gas particles. Both of them have the same properties as the original one, except half of the mass. This split operation is repeated until the total particle number in this cell equal to $N_{\min}$. Though the new "twin" gas particles have exactly all the same properties, the random terms in the governing equations will lead them to different futures. They will become valid samples after one time step. When the total particle number in one cell is larger than $N_{\max}$, the smallest

gas particle is discarded. This discard operation is repeated until the total particle number in this cell equal to $N_{\max}$. In the present work, $N_{\min}$ and $N_{\max}$ are set to 60 and 100, respectively.

3.3 Lagrangian Stochastic Parcel Method for the Droplets

Continuous distribution of droplets is represented by a finite number of the droplet parcels. Each parcel contains a number of droplets with identical position in physical space and size, velocity, and temperature in state space. Therefore, one parcel can be described as $(\dot{M}_p, \mathbf{x}_d, r_d, \mathbf{U}_d, T_d)$. $\dot{M}_p$ indicates the liquid flux represented by this droplet parcel. It evolves linearly with the droplet volume:

$$\dot{M}_p(t) = \dot{M}_{p,0}\frac{r_d^3(t)}{r_{d,0}^3}. \tag{3.48}$$

Droplet position is determined by Eq. (2.96), which is discretized as

$$\mathbf{x}_d^{n+1} = \mathbf{x}_d^n + \mathbf{U}_d^n \Delta t. \tag{3.49}$$

Eq. (2.98) is solved by a new implicit scheme described in Section 3.3.1. The instantaneous velocity of gas flow $\mathbf{U}$ in Eq. (2.99) is deformed into two parts: mean velocity $\widetilde{\mathbf{U}}$ and fluctuating velocity $\mathbf{u}$. The Favre-averaged velocity is computed by the finite volume method, and is linearly interpolated into the droplet's position using Eq. (3.30). Assuming that the fluctuating velocity follows an isotropic Gaussian distribution (see Eq. (3.31)), the fluctuating velocity is determined from the local turbulent kinetic energy using the same method described in the Section 3.2.

A second-order Runge-Kutta method is used to solve the Eq. (2.125) and (2.126):

$$r_d^{n+1} = r_d^{n+1} + \Delta t \frac{dr_d}{dt}\Big|_{n+\frac{1}{2}}, \tag{3.50}$$

$$T_d^{n+1} = T_d^{n+1} + \Delta t \frac{dT_d}{dt}\Big|_{n+\frac{1}{2}}. \tag{3.51}$$

When the droplet radius is small enough, say,

$$r_d < \max\{0.1 r_d, 1\mu m\}, \tag{3.52}$$

the droplet is assumed to have evaporated completely.

Spray source terms are evaluated according to the Particle-Source-In-Cell (PSI-Cell) model [239] (see Fig. 3.6 [194]). According to Eq. (2.95), the mean of function Φ can be approximated by

$$\langle \Phi \rangle = \int f_d \Phi d\mathbf{V}_d d\iota_d d\theta_d = \sum_{k=1}^{N_p} n_{p,k} \Phi, \tag{3.53}$$

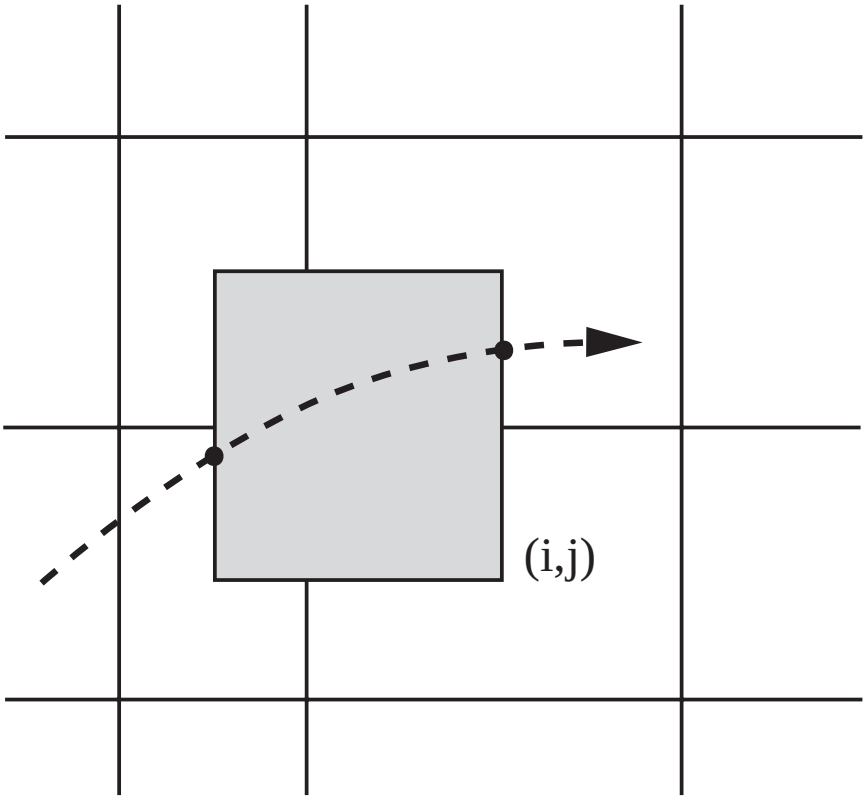

Fig. 3.6: Particle-Source-in-Cell (PSI-Cell) model

where $n_{p,k}$ is the droplet number of kth parcel. Therefore, for one certain control volume $\mathcal{V}$, the spray source term can be written as

$$\begin{aligned} \bar{S}_{l,\Phi} &= \frac{\overline{\dot{M}_d \Phi}}{\mathcal{V}} \\ &= \frac{1}{\mathcal{V}} \sum_{k=1}^{N_p} [(\dot{M}_{d,k}\Phi_k)_{in} - (\dot{M}_{d,k}\Phi_k)_{out}]. \end{aligned} \tag{3.54}$$

3.3.1 Implicit Scheme for the Computation of the Droplet Velocity

Eq. (2.98) is usually solved by explicit integration [195]:

$$U_d^{n+1} = U_d^n + RHS \cdot \Delta t. \tag{3.55}$$

In this section, this explicit scheme will be assessed. A new implicit scheme to compute the droplet velocity is proposed. This scheme can be applied to other types of multiphase flows, for instance, bubble flows, and gas/solid flows.

Without loss of generality, we take the direction of the acceleration of gravity as the positive x-axis. The droplet velocity in the z-direction is zero. The droplet velocities in the x- and y-directions are

$$U_d = U_{d,0},\ V_d = V_{d,0} \tag{3.56}$$

at the time $t = t_0$. We take

$$C = \frac{3}{8}\frac{\bar{\rho}}{\rho_l}\frac{C_d}{r_d},$$
$$a = \sqrt{\frac{g}{C}},$$

which are positive constants.

On the x-axis (parallel to the direction of gravity), the Eq. (2.98) can be written as

$$\frac{dU_d}{dt} = -C|U_d - U|(U_d - U) + Ca^2. \tag{3.57}$$

There are two possible cases. First, the drag force is in the same direction as the acceleration of gravity. In this case, the droplet velocity must be smaller than the gas velocity, $U_d < U$. Eq. (3.57) turns to be

$$\frac{dU_d}{dt} = C(U_d - U)^2 + Ca^2. \tag{3.58}$$

Integrating the above equation, the droplet velocity at the time $t = t_0 + \Delta t$ can be determined with the initial condition:

$$U_d = U + a \cdot \tan\left(\arctan\left(\frac{U_{d,0} - U}{a}\right) + aC\Delta t\right). \tag{3.59}$$

Eqs. (3.58, 3.59) hold only when $U_d < U$. Therefore, Δt should be smaller than the "lifetime" of this case:

$$t_l = -\frac{1}{aC}\arctan\left(\frac{U_{d,0} - U}{a}\right). \tag{3.60}$$

When $t = t_0 + t_l$, the droplet velocity equals to the gas velocity, $U_d = U$, and the drag force is zero. Because of gravitational force, the droplet velocity keeps increasing, which leads to the second case. In this case, the drag force is in the opposite direction of the acceleration of gravity ($U_d > U$). Eq. (3.57) turns to be

$$\frac{dU_d}{dt} = -C(U_d - U)^2 + Ca^2. \tag{3.61}$$

Integrating the above equation, the droplet velocity at the time $t = t_0 + \Delta t$ can be determined from the initial condition:

$$U_d = U + a + \frac{2a}{\frac{U_{d,0}-U+a}{U_{d,0}-U-a}\exp(2aC\Delta t) - 1}. \tag{3.62}$$

When $\Delta t \to \infty$, the droplet velocity U_d approaches to $U + a$. When $U_d = U + a$, the gravitational force is balanced by the drag force. Obviously, the direction of the drag force will not change. The variable $U_d - U - a$ has the same sign during the whole procedure:

$$(U_d - U - a)(U_{d,0} - U - a) \geq 0. \tag{3.63}$$

In the y-direction (perpendicular to the direction of gravity), the Eq. (2.98) can be written as

$$\frac{dV_d}{dt} = -C|V_d - V|(V_d - V). \tag{3.64}$$

Integrating the above equation, the droplet velocity at the time $t = t_0 + \Delta t$ can be determined from the initial condition:

$$V_d = \frac{V_{d,0} + C\Delta t|V_{d,0} - V|V}{1 + C\Delta t|V_{d,0} - V|}. \tag{3.65}$$

When $\Delta t \to \infty$, the droplet velocity V_d approaches to the gas velocity V. The direction of the drag force will not change in this case, too. The variable $V_d - V$ has the same sign during the whole procedure:

$$(V_d - V)(V_{d,0} - V) \geq 0. \tag{3.66}$$

Comparing to the explicit scheme, the computational complexity of the present implicit scheme is only slightly increased.

To assess the proposed implicit scheme, a numerical test is conducted in a simplified case. The droplets move in a steady and homogeneous 2D flow field. The velocities of gas-phase flow are set to $U = V = 1.0$ m/s. Without loss of generality, C is taken as a constant, 4.5 m^{-1}. The evaluation of the droplet velocity is calculated by the present implicit scheme and the explicit scheme (Eq. (3.55)). In Case I, the initial velocities of the droplet are $U_{d,0} = V_{d,0} = 10.0$ m/s. In Case II, the initial velocities are $U_{d,0} = V_{d,0}$ = -10.0 m/s. The time step is set to be a constant in each computation. Time steps chosen are $\Delta t = 0.001$ s, 0.01 s, 0.02 s, 0.025 s, 0.1 s.

As mentioned previously, the Eqs. (3.58, 3.59) are valid only when $U_d < U$. If the time step Δt is larger than the lifetime t_l, the droplet velocity is calculated by the Eq. (3.62) with the initial droplet velocity U and the time step $(\Delta t - t_l)$,

$$U_d = U + a - \frac{2a}{\exp[2aC(\Delta t - t_l)] + 1}. \tag{3.67}$$

Figures 3.7 show the comparisons of the results of the implicit scheme and explicit scheme with the time steps $\Delta t = 0.001$ s. Lines indicate the results from the implicit scheme; symbols indicate the results from the explicit scheme. Both cases show that the results of implicit scheme and explicit scheme are identical. Since the time step

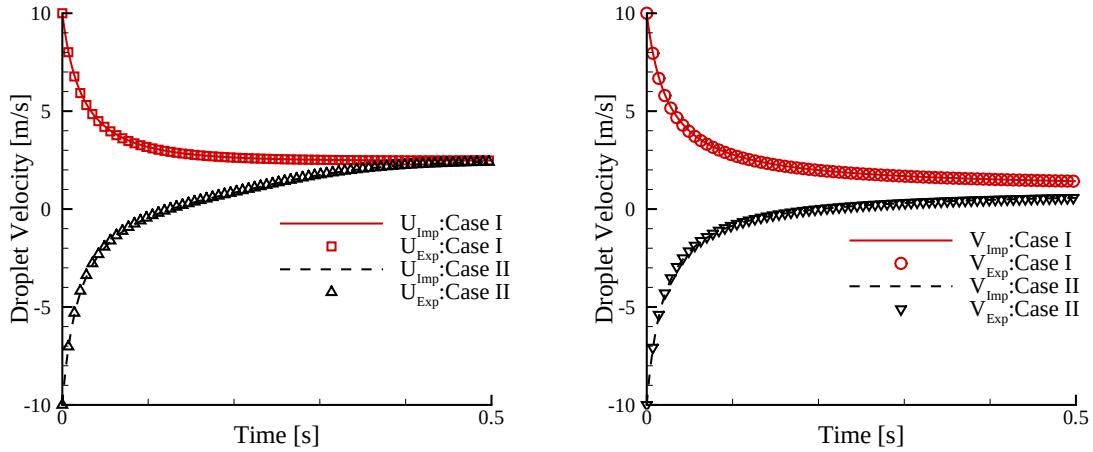

Fig. 3.7: Comparison of the results from the implicit and explicit scheme with time step $\Delta t = 0.001$ s. Left: U; Right: V

is very small, and both schemes give the identical results, these results can be taken as the "exact solution". The effects of the time step on the numerical results can be investigated by comparing with these exact solutions.

Figures 3.8–3.9 show the effects of the time steps on the results of the implicit scheme. The solid lines indicate the results with time step $\Delta t = 0.001$ s. The symbols indicate the results of other time steps, 0.01 s, 0.02 s, 0.025 s, and 0.1 s, respectively. All the results of other time steps coincide with the exact solutions (the results of time step $\Delta t = 0.001$ s). It implies that the present implicit scheme is very stable and robust. The size of time step does not affect the accuracy of the results.

Figures 3.10–3.11 show the effects of time steps on the results of explicit scheme. The solid lines indicate the results with time step $\Delta t = 0.001$ s. The symbols indicate the results of other time steps, 0.01 s, 0.02 s, and 0.025 s, respectively. The numerical results from the explicit scheme strongly depend on the size of time step. The explicit scheme gives accurate results only when the time step is small enough. Increasing the time step, discrepancy shows up between the exact solutions and the results of larger time steps. Here we define a time scale for the drag force:

$$t_{\text{drag}} = \frac{1}{C|U_d - U|}. \tag{3.68}$$

According to the initial condition, the characteristic time of drag force is about 0.0247 s for Case I and 0.0202 s for Case II. When the time step is set to 0.025 s, the explicit scheme gives non-physical results because the numerical results do not satisfy the Eqs. (3.63) and (3.66). Keep increasing the time step (0.1 s), the explicit scheme gives a divergent result, while the implicit scheme still produces stable results. Therefore, the

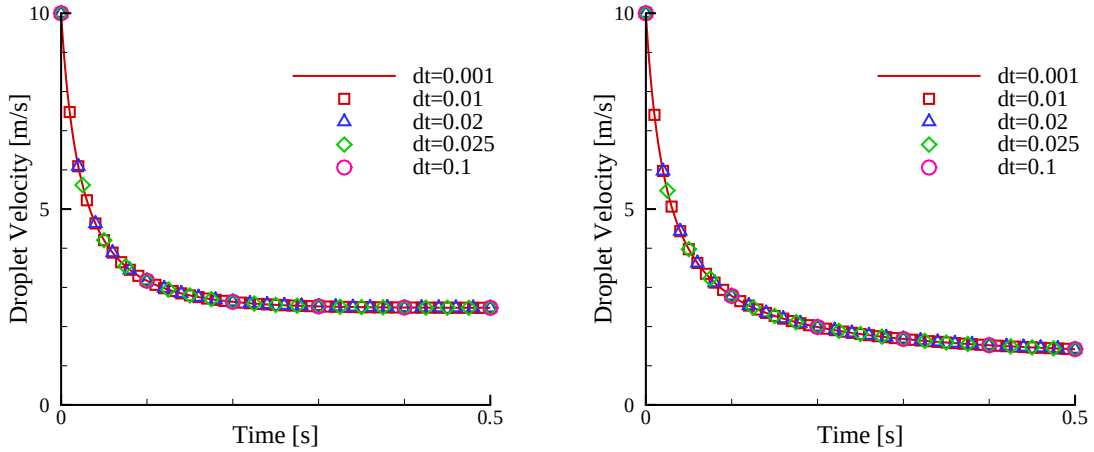

Fig. 3.8: Effects of the time steps on the results from implicit scheme: Case I. Left: U; Right: V

explicit scheme is unstable.

To sum up, the numerical tests show that the proposed implicit scheme for the computation of droplet velocity is very robust and accurate. In this scheme, the errors induced by the time discretization are minimized. The accuracy of the implicit scheme does not depend on the size of time step. The implicit scheme still gives reliable results when the time step is larger than the drag force time scale ($\Delta t >> t_{\text{drag}}$).

3.3.2 Boundary Conditions for Droplet Parcel Method

Boundary conditions of the stochastic parcel method [194] is similar to the Lagrangian Monte-Carlo particle method. When the droplets move across the axis of symmetry, the droplets are reflected from the boundary without change in their properties except for the velocity and position in the direction normal to the boundary. When the droplets move across the outlet plane or the outside boundary, they are discarded.

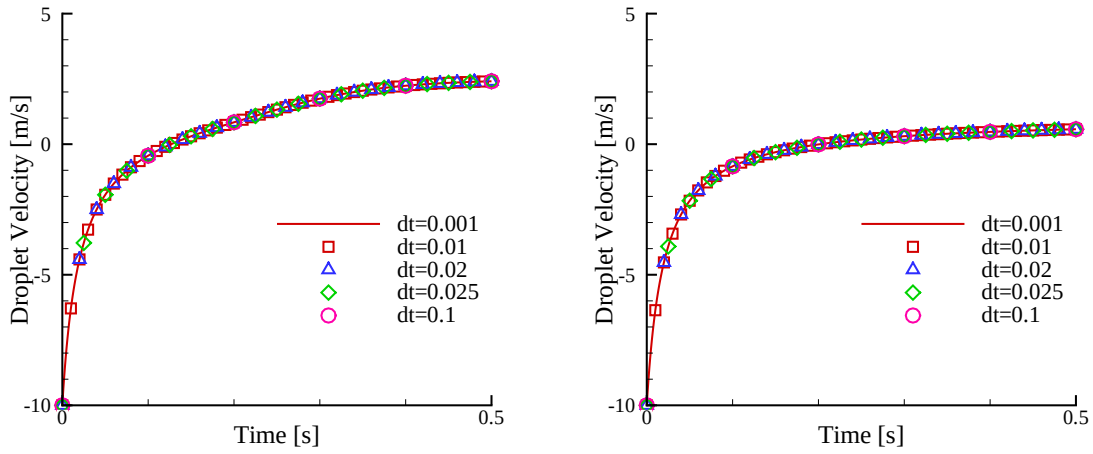

Fig. 3.9: Effects of the time steps on the results from implicit scheme: Case II. Left: U; Right: V

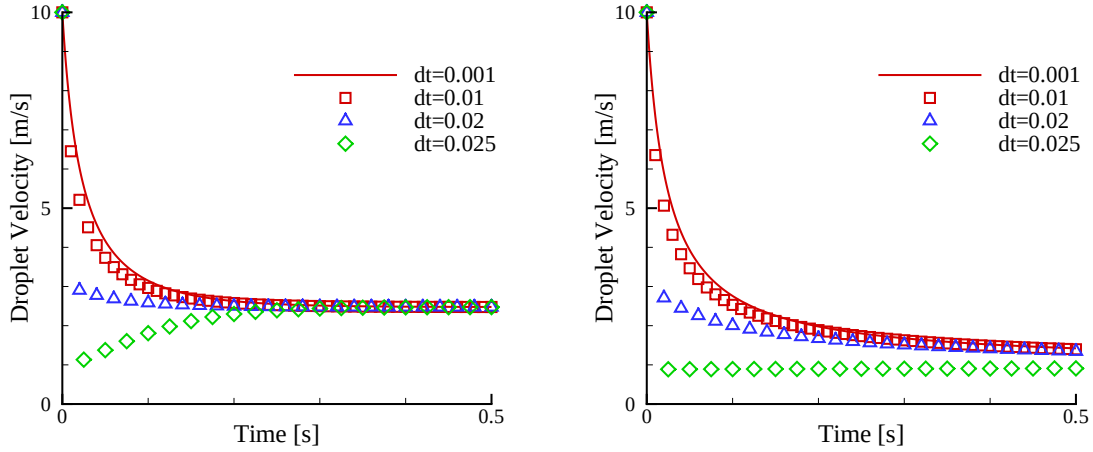

Fig. 3.10: Effects of the time steps on the results from explicit scheme: Case I. Left: U; Right: V

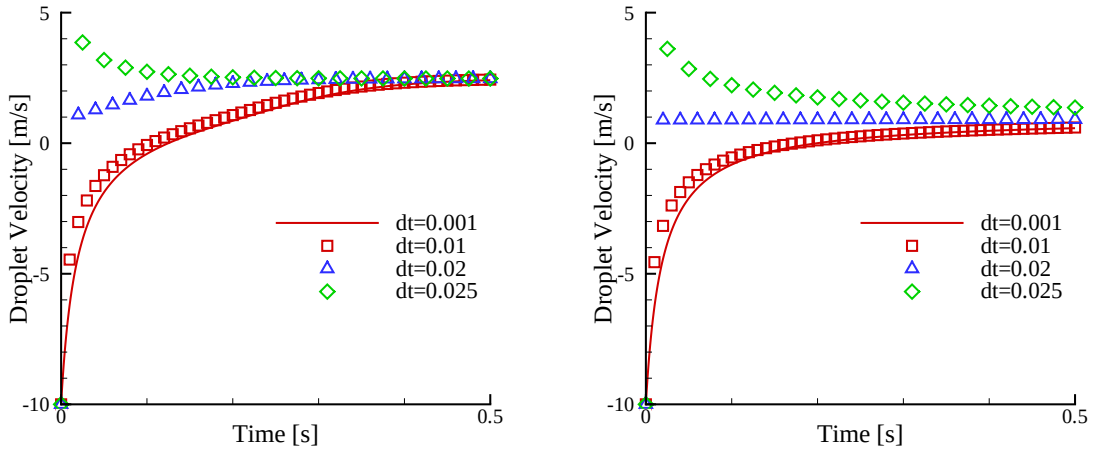

Fig. 3.11: Effects of the time steps on the results from explicit scheme: Case II. Left: U; Right: V

4. Results and Discussion

4.1 Turbulent Methanol/Air Spray Flows

4.1.1 Experimental Setup

Steady, two-dimensional, axi-symmetric, both non-reactive and reactive turbulent liquid jets are modeled. A dilute methanol spray is injected into a turbulent air flow. Experiments were conducted by McDonell and Samuelsen [240, 241]. Figure 4.1 illustrates the overall geometry of the methanol/air spray burner [241]. Figure 4.2shows the outline of the fuel injector [241]. We mark the section of the fuel injector's exit as $x = 0$ mm. The gas and droplet velocities, droplet size distribution, liquid flux, and concentration of methanol vapor are measured at the axial location $x = 7.5$ mm, 25 mm, 50 mm, 100 mm, and 150 mm. The gas velocity, droplet velocity and droplet size are measured using phase Doppler interferometry (PDI). The concentration of the methanol vapor is measured using infrared extinction/scattering (IRES). In the reactive case, the gas temperature is measured. The experimental data at $x = 7.5$ mm are taken as the inlet profiles for numerical computations. Mass flow rate of the liquid fuel is 1.32 g/s. The air flow results in a pressure drop of 3.73 kPa. In the PDF simulation, the Dirac delta profile is prescribed for the particles' mixture fraction at the inlet. Liu's [242] study of numerical accuracy in transported PDF methods shows that the number of particle per cell, *Npc*, should not be smaller than 50 to keep the bias error below 5% . In the present transported PDF method, *Npc* is set to 80, so that the bias error is kept below 4%.

Calculations of the spray and gas flow are sensitive to the initial conditions. In the present work, the inlet for computation locates near the nozzle ($x = 7.5$ mm), where the flow structure is very complex. Little disturbance of the initial conditions in spray or gas flow may result in a quite different field. The interaction between spray and gas flow is very strong. The coarse measurements of the droplet size distribution at the inlet profile cause uncertainties in the results of spray and consequently in the results of gas flow. In the non-reactive case, the lack of information about the initial gas temperature causes some uncertainties both in gas flow and spray, too.

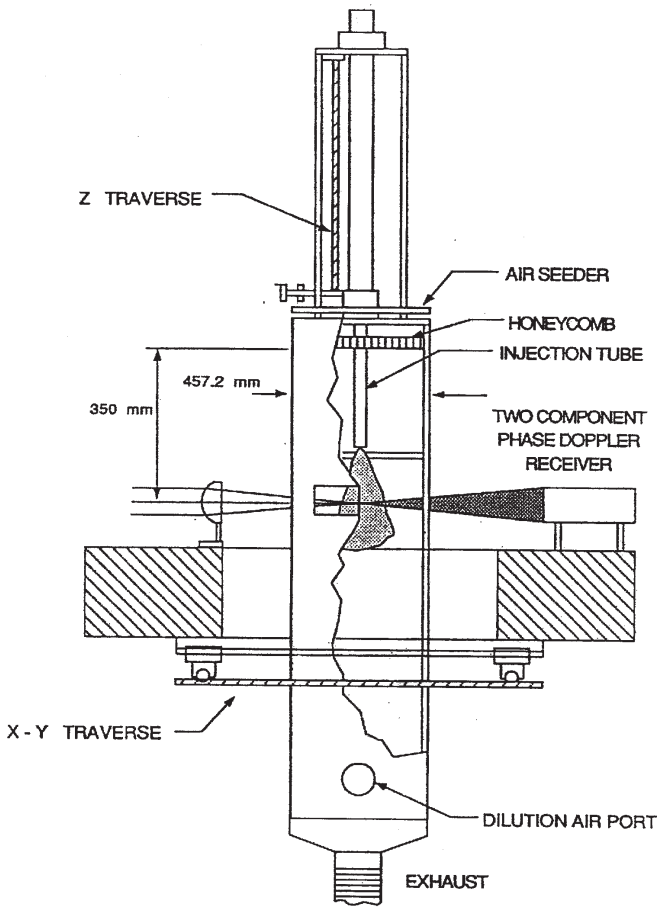

Fig. 4.1: Schematic of the methanol/air spray burner.

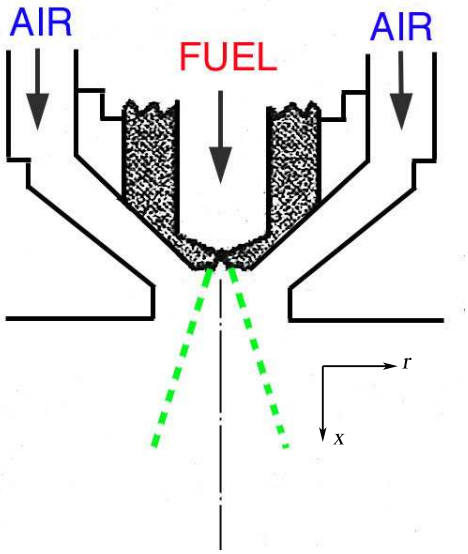

Fig. 4.2: Outline of the fuel injector.

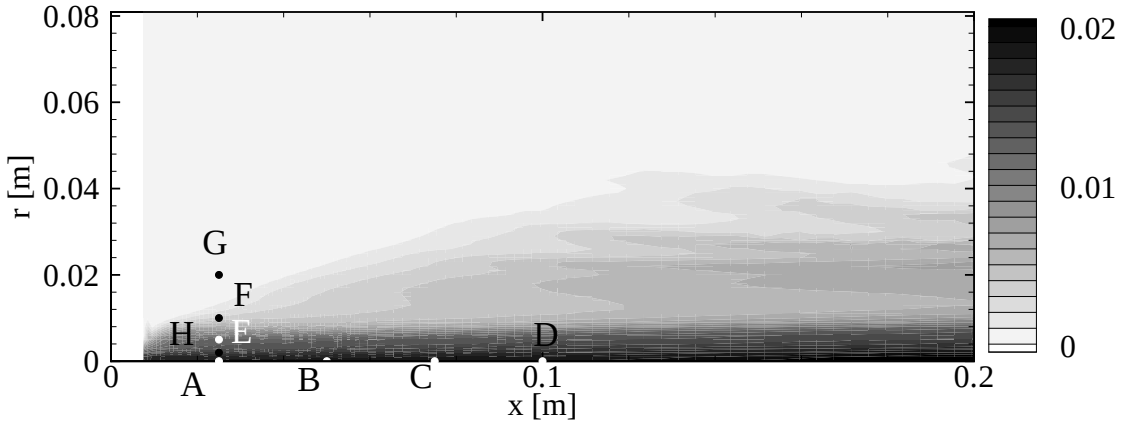

Fig. 4.3: Contour plot of the mean methanol vapor mass fraction computed by the transported PDF method. PDFs of single point are studied at marked positions.

4.1.2 Single-Scalar PDF for the Turbulent Non-Reactive Methanol/Air Spray Flows

The statistical distribution of the mixture fraction in a single-phase mixing layer is usually described by a standard (two-parameter) β function [170]. The β function gives good numerical results for the gas-phase flows [67, 169]. However, results from direct numerical simulations (DNS) [45] show that it fails in the evaporation region of the gas-liquid flow. The distribution of the mixture fraction does not follow the β function in regions where vaporization exists. Therefore, the presumed β function should be assessed before being used in the turbulent spray flows. On this purpose, a turbulent non-reactive methanol/air spray flow is simulated using a PDF of the mixture fraction. Details about the PDF transport equation and models are found in Section 2.2.1. The numerical algorithms being used to solve the PDF transport equation are found in Section 3.2.

Figure 4.3 shows the contour plot of the mean fuel vapor mass fraction computed by the transported PDF method. The positions A-H marked in the figure are used to evaluate the PDFs of the mixture fraction discussed in Figs. 4.7–4.11. The major vaporization occurs near the nozzle where the temperature and velocity differences between droplets and gas flow are relatively large. The vaporization becomes weak downstream. The highest concentration of the mass fraction of fuel vapor occurs near the centerline, It implies that most of the methanol vapor is transported along the axis of symmetry by the jet while the rest develops into radial direction.

Figures. 4.4–4.6 show the radial profiles of the gas velocity and mass fraction of the methanol vapor at the first three positions where the experiments [240, 241] are compared to the results from the moment closure method [180] and the results from the present transported PDF method. Triangles indicate the experimental data of the axial gas velocity; squares indicate the experimental data of mass fraction of methanol vapor; dashed lines indicate the axial gas velocity computed with the present method; dash-dotted lines indicate the mass fraction of methanol vapor computed using moment closure method; solid lines indicate the mass fraction of methanol vapor computed using the transported PDF method. The results of the transported PDF method are in good agreement with the experimental data, and they improve the results obtained by moment closure method in the initial region, c.f. Figs. 4.4–4.5. In the moment closure method, the mixture fraction is calculated by solving the Favre-averaged conservation equation (see Eq. (3.4) and Tab. 3.1). The effects of the turbulent transportation are modeled using a gradient-diffusion hypothesis (see Eq. (2.50)). In the PDF transport equation, the effects of turbulent transportation are taken into account through the Monte-Carlo method, which represents the physical mechanism better. It is well-known that the $k-\epsilon$ model always over-predicted the spreading rate of the jet. As a result in

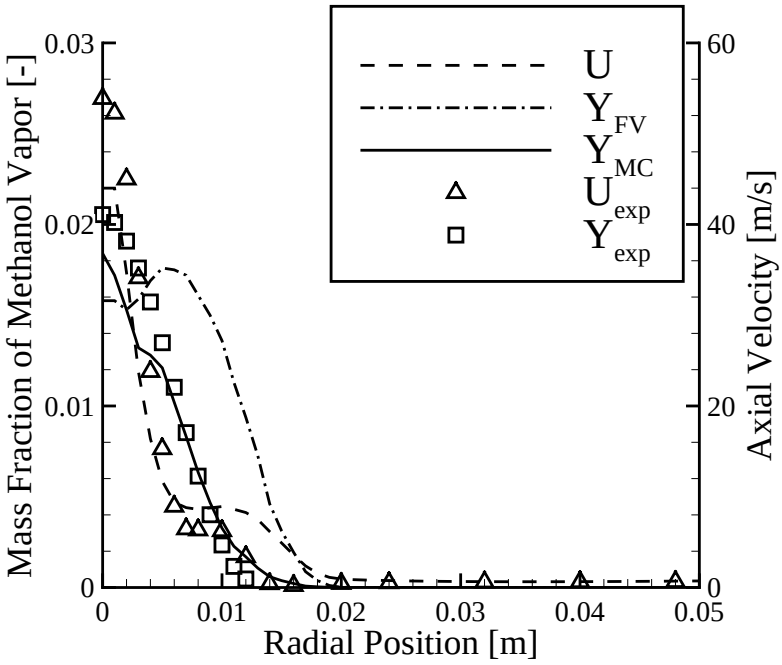

Fig. 4.4: Radial profiles of the gas velocity and mass fraction of the methanol vapor at the section $x = 25$ mm.

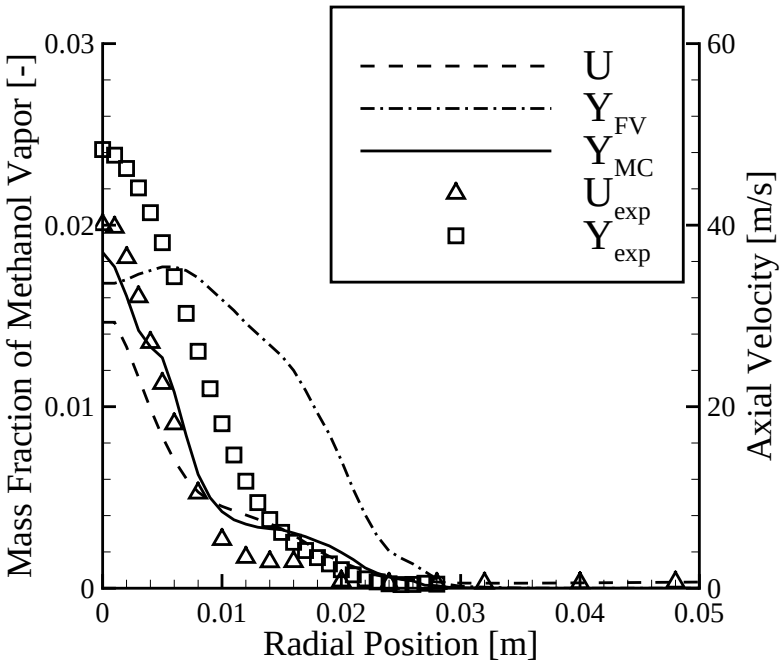

Fig. 4.5: Radial profiles of the gas velocity and mass fraction of the methanol vapor at the section $x = 50$ mm.

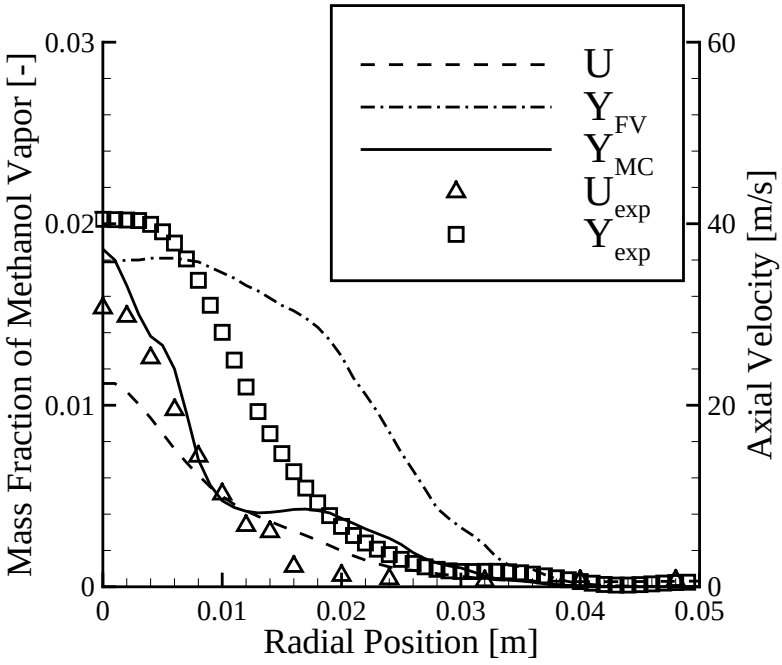

Fig. 4.6: Radial profiles of the gas velocity and mass fraction of the methanol vapor at the section $x = 75$ mm.

velocity field, the axial velocity at the axis of symmetry is under-predicted (see Figs. 4.4–4.6), especially in the region close to nozzle (see Fig. 4.4). This implies that the methanol vapor transported to the axis of symmetry is under-predicted. The droplets occurring near the axis of symmetry are also under-predicted. These effects result in the under-prediction of the mass fraction of methanol vapor near the axis of symmetry. This phenomenon becomes stronger downstream as seen in Fig. 4.6 because of the cumulation of these effects. Therefore, the results of the transported PDF method can be improved if the velocity field is more accurate.

Figures 4.7–4.8 show the PDFs of the mixture fraction at different positions, which are marked in Fig. 4.3. Along the axial line, all of the PDFs show a bimodal shape (see Fig. 4.7). The PDFs get narrow along the axial line, which means that the variance of the mixture fraction becomes smaller. The fluctuation of the scalar is larger upstream because of the stronger turbulent fluctuation there. As a result, the left peak gets weaker downstream (see Fig. 4.7 positions C and D). When the local fluctuation is small enough, the PDF will have a Gaussian-like shape. It will become a Dirac delta function when the variance is close to zero. Along the radial line (see Fig. 4.8), the positions A, F, G locate in the region of the main vaporization zone, weak vaporization and pure air. The fluctuation of the mixture fraction is weaker in the outer region than in the inner region. The variance of the mixture fraction along the radial line decreases

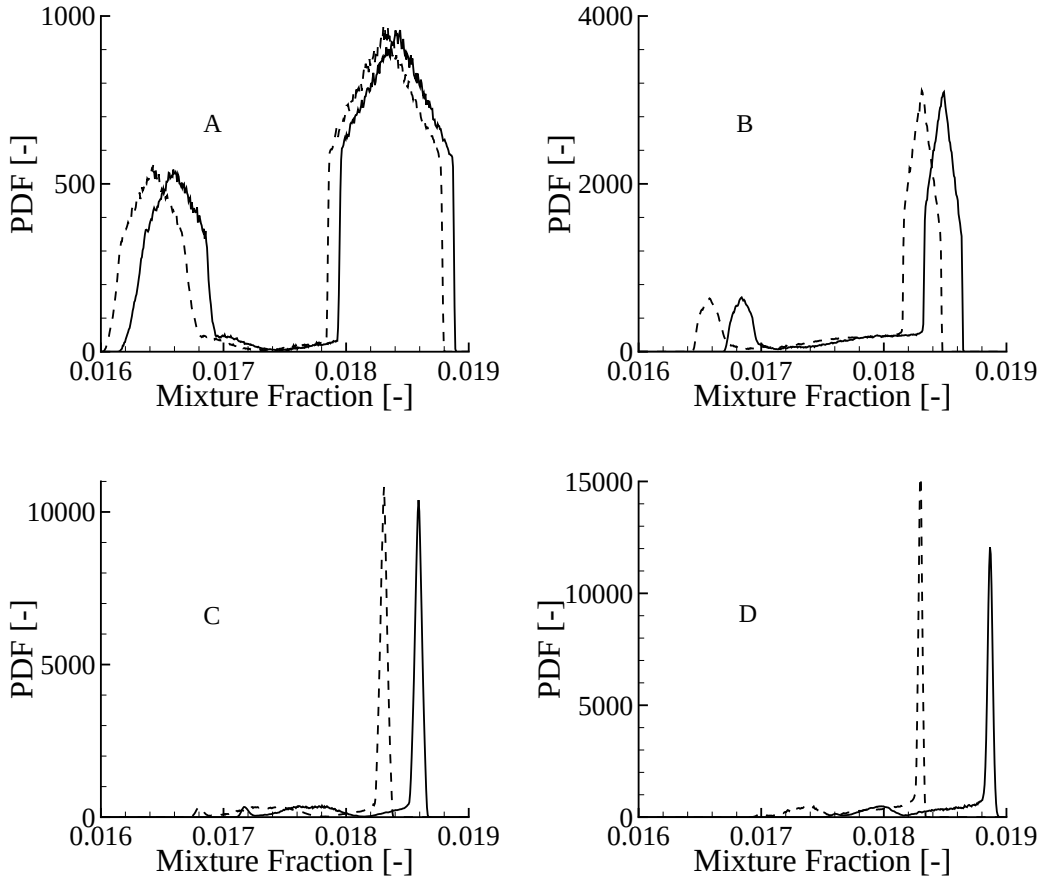

Fig. 4.7: PDFs of the mixture fraction, positions at the central line; dashed lines indicate the case when the spray source terms are set to zero.

with increasing the radial distance r. As a consequence, the PDF of the mixture fraction evolves from bimodal to unimodal shape, and to a Dirac delta function in the region of pure air (position G). The value of the PDF at the position G extends to a very high value (about 1.6×10^6) to satisfy the normalization condition of the PDF, and it is cut off in the figure. Similar results were obtained by LES of solid-fuel ramjet combustors [243]. The PDF of passive scalars in the turbulent gas-phase flows shows similar statistical behavior [244].

4.1.2.1 Effects of the Spray Source

The effects of the spray source on the PDF of the mixture fraction are studied. The same calculation is conducted where the spray source terms are set to zero. All other flow characteristics including density, velocity, turbulent kinetic energy and its dissipation rate are retained. The PDFs along the central line indicated by the dash-line is presented in Fig. 4.7. Compared to the case with spray source (solid line in Fig. 4.7),

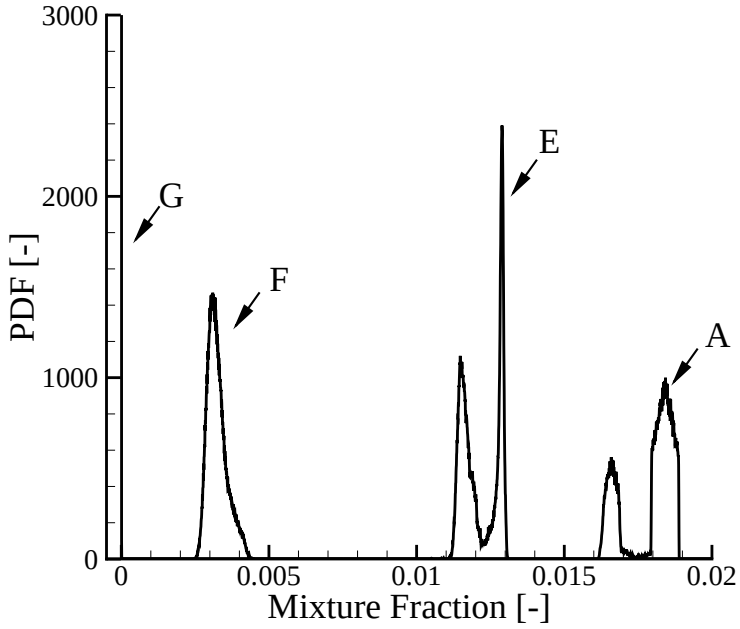

Fig. 4.8: PDFs of the mixture fraction, radial line.

the principal shape of the PDFs does not change. The mean value of the mixture fraction is reduced. According to Eq. (2.64), the difference of the mean mixture fraction is

$$\Delta\widetilde{\xi_C} = -\frac{2}{C_\phi}\frac{\tilde{k}}{\tilde{\epsilon}}\bar{S}_{l,1}, \tag{4.1}$$

compared to the case with the spray source.

4.1.2.2 Comparison of the PDFs

The results of the present transported PDF method are compared with the results from the presumed PDFs. The presumed PDFs used here are the standard β function (see Eq. (2.142)) and the modified β function (see Eq. (2.145)). The comparisons are illustrated in Figs. 4.9–4.11. Solid lines indicate the results of the transported PDF method. Dash-dotted lines indicate standard β function (β_1). Dashed lines indicate the modified β function (β_2). The symbol $\widetilde{\xi_C}$ in the figures indicates the position of the mean value of mixture fraction computed using the transported PDF method. The values of $\xi_{C,\max}$ and $\xi_{C,\min}$ are indicated on the axis of mixture fraction by arrows in Figs. 4.9–4.11. With the mean of the mixture fraction $\widetilde{\xi_C}$ and the variance of mixture fraction $\widetilde{\xi_C''^2}$ computed using the transported PDF method, the α and β in the standard β function (Eq. (2.142)) can be determined from the Eqs. (2.143-2.144).

However, as shown in the figures, the standard β function always shows a Gaussian-

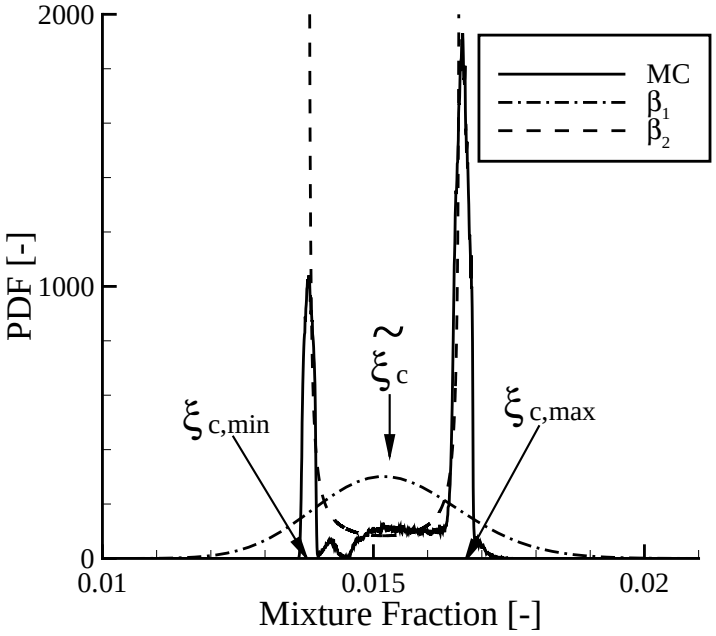

Fig. 4.9: Comparison of standard (β_1) and modified (β_2) β function with the results computed by Monte-Carlo method (MC), position H. The positions of $\xi_{c,\max}$ and $\xi_{c,\min}$ are used in the modified β function.

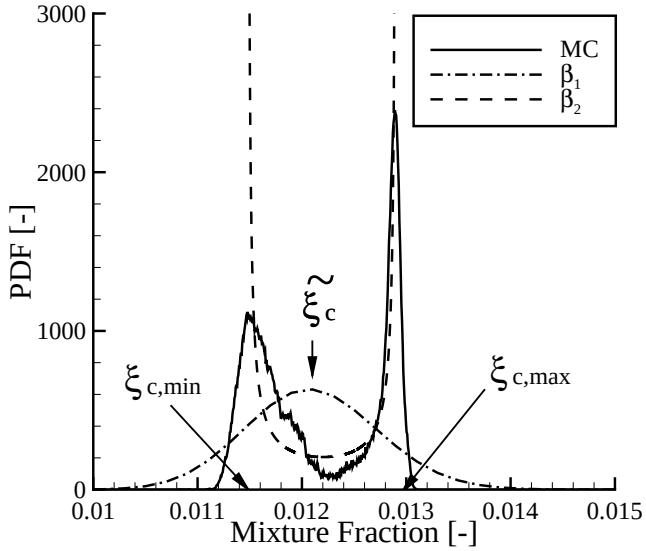

Fig. 4.10: Comparison of standard (β_1) and modified (β_2) β function with the results computed by Monte-Carlo method (MC), position E. The positions of $\xi_{c,\max}$ and $\xi_{c,\min}$ are used in the modified β function.

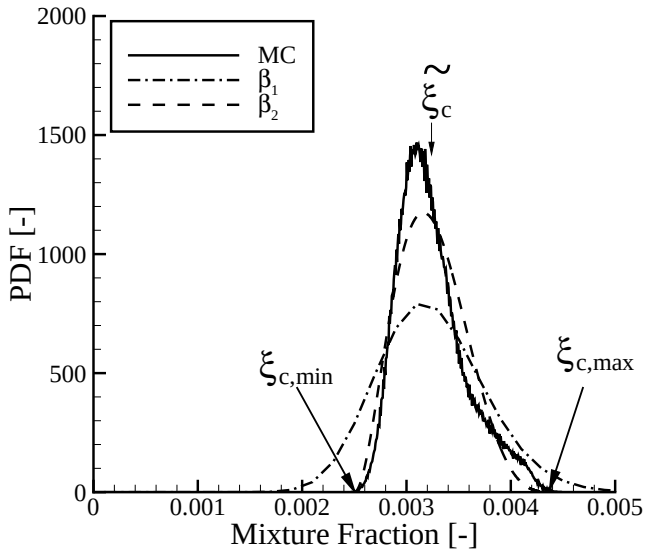

Fig. 4.11: Comparison of standard (β_1) and modified (β_2) β function with the results computed by the transported method (MC), position F. The positions of $\xi_{c,\max}$ and $\xi_{c,\min}$ are used in the modified β function.

like (unimodal) distribution for the conditions of the current flow field. This shape does not represent the results of the transported PDF method, in particular when the PDF of mixture fraction shows a bimodal shape (see Figs. 4.9–4.10). With the same mean and variance of mixture fraction from the transported PDF method, and the local maximum and minimum values of mixture fraction $\xi_{C,\max}$ and $\xi_{C,\min}$, the α and β in the modified β function (c.f. Eq. (2.145)) can be determined from the Eqs. (2.146–2.147).

With appropriate values of $\xi_{C,\max}$ and $\xi_{C,\min}$, the modified β function represents the results computed using the transported PDF method very well. Even when the results of the transported PDF method shows a Gaussian-like shape (see Fig. 4.11), the modified β function still fits it very well. It has been mentioned that the standard β function is a special form of the modified β function with $\xi_{C,\max} = 1$ and $\xi_{C,\min} = 0$ in Section 2.2.2.6. The predictive ability of the standard β function in turbulent spray flow mainly depends on the value of $(1 - \xi_{C,\max})$ and $(\xi_{C,\min} - 0)$. In the current situation, these deviations are quite large. Assuming that the spray stream has reached the saturation, the maximum mass fraction of methanol vapor at the droplet surface is roughly 0.1. The corresponding mixture fraction is 0.1 which is considerably smaller than 1. Therefore, the standard β function is far away from the results of the transported PDF method. When the value of the local $\xi_{C,\max}$ and $\xi_{C,\min}$ are close enough to unity and zero, respectively (which is the case in the turbulent gas-phase flows),

the standard β function is reasonable to give good estimations to the results of the transported PDF method. This is the reason why standard β function works well in the turbulent gas-phase flows.

If the local maximum and minimum values of the mixture fraction $\xi_{C,\max}$ and $\xi_{C,\min}$ is close enough to a constant in the whole computational domain, say,

$$\left| \frac{\xi_{C,\max} - \xi_{C,1}}{\xi_{C,\max} - \xi_{C,\min}} \right| \leq \varepsilon \tag{4.2}$$

or

$$\left| \frac{\xi_{C,\min} - \xi_{C,0}}{\xi_{C,\max} - \xi_{C,\min}} \right| \leq \varepsilon \tag{4.3}$$

the unknown parameters $\xi_{C,\max}$ (or $\xi_{C,\min}$) can be replaced by the constant $\xi_{C,1}$ (or $\xi_{C,0}$). When either Eq.(4.2) or Eq.(4.3) holds, the 4-parameter β function reduces to a 3-paramter β function. Here ε is the tolerant error. If Eqs.(4.2) and (4.3) are both true, it will reduce to a 2-parameter β function. In this case, the left two parameters α and β can be determined from the local value of the mean and variance of mixture fraction directly.

4.1.3 Joint Velocity-Scalar PDF for the Turbulent Non-Reactive Methanol/Air Spray Flows

A joint velocity-scalar PDF is proposed in [141]. Its definition and transport equation are presented in Section 2.2.1.3. The velocity model and mixing model are described in Section 2.2.1.5 and 2.2.1.6, respectively. The same numerical method is used to solve its transport equation.

A turbulent non-reactive methanol/air spray flow is simulated using this joint velocity-scalar PDF formulation. Figure 4.12 shows the radial profiles of the mean axial gas velocities at four different cross sections: $x = 25$ mm, 50 mm, 75 mm, and 100 mm. Symbols indicate the experimental data [240]; solid lines indicate the results of the present transported PDF method; dashed lines indicate the results of former moment closure modeling [178]. The results of the transported PDF method are in very good agreement with experimental data. The transported PDF method improves the results of the moment closure method particularly for the velocity near the center-line which is shown in Fig. 4.13. The present extended simplified Langevin model is suitable for use in turbulent spray flows. This simplified Langevin model neglects the effects of the mean velocity gradient, which is mean source of the discrepancies found in the current simulation. In the region close to the nozzle, the mean velocity gradient is large and should not be neglected. Therefore, the results at the section $x = 25$ mm do not fit the experimental data very well. Excellent agreement is found downstream

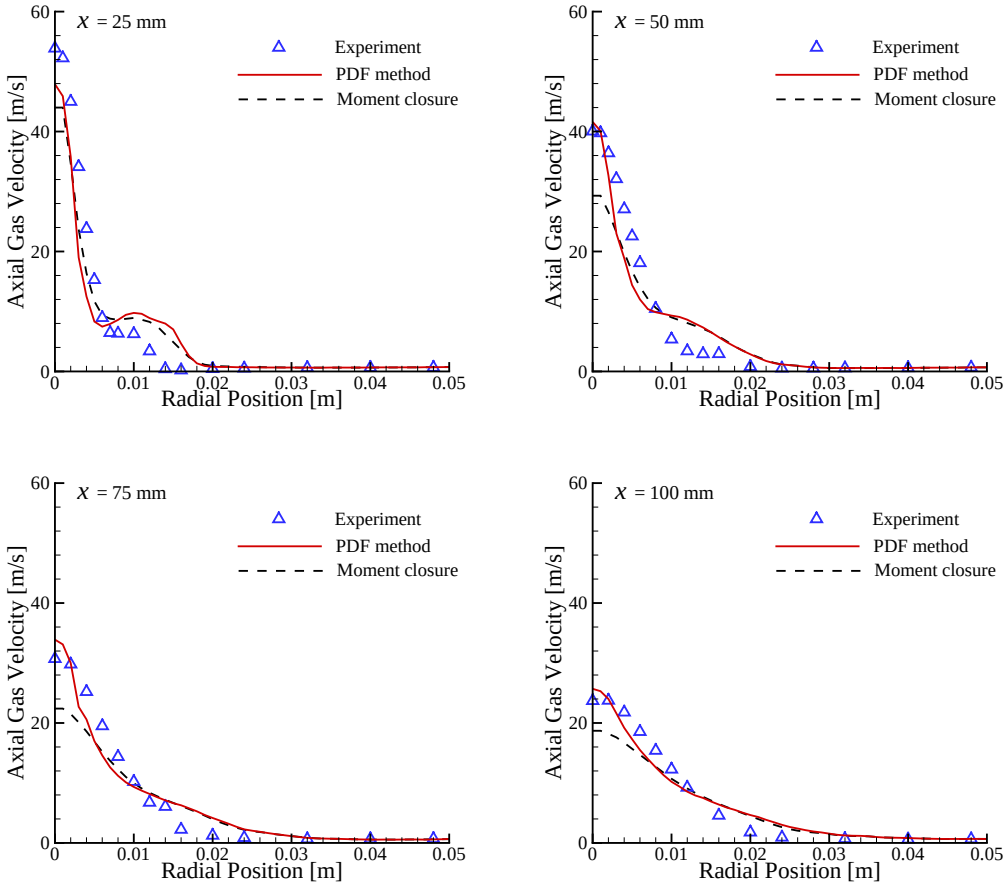

Fig. 4.12: Radial profiles of the mean axial gas velocity at $x = 25$ mm, 50 mm, 75 mm, and 100 mm.

where the mean velocity gradient is relatively smaller and its effects are negligible. The generalized Langevin model [199] takes into account the effects of the mean velocity gradient. In this sense, the generalized Langevin model could offer better results of the gas-phase velocity.

Figure 4.14 shows the radial profiles of the Sauter mean radius at sections $x =$ 25 mm and 100 mm. Both the transported PDF method and the moment closure method are in qualitative agreement with the measurements. The results from the two models are almost identical. For the non-reactive case, the gas temperature gradients and concentration gradients in the flow field are very small. The improvements in the results of the transported PDF method do not affect the liquid phase very strongly.

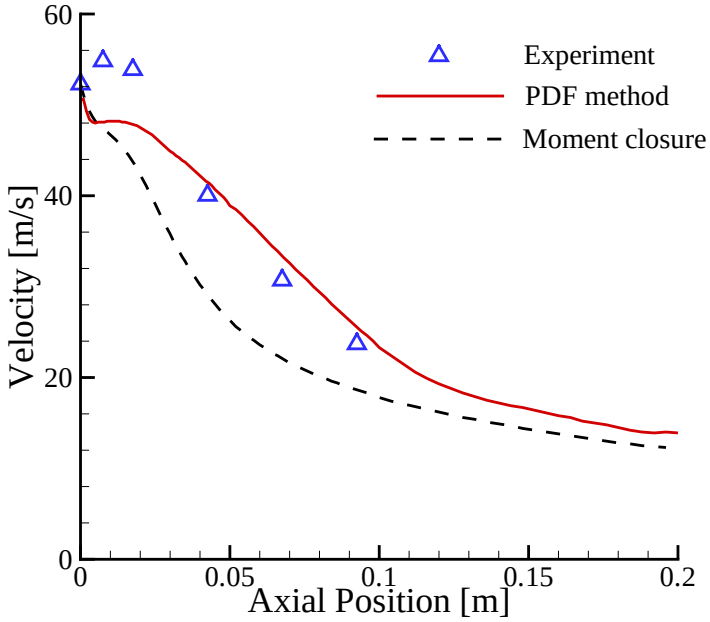

Fig. 4.13: Axial profile of the gas-phase mean axial velocity along the centerline.

4.1.4 Joint Enthalpy-Mixture Fraction PDF for the Turbulent Methanol/Air Spray Flames

A joint mixture fraction-enthalpy PDF is proposed for the turbulent spray combustion [142]. Its definition and transport equation are presented in Section 2.2.1.2. The same models are used as the single-scalar PDF. A turbulent methanol/air spray flame is modeled using this joint mixture fraction–enthalpy PDF. A detailed methanol/air combustion mechanism is implemented through a spray flamelet model [180]. The mechanism [245] consists of 23 species and 168 elementary reactions. The spray flamelet library

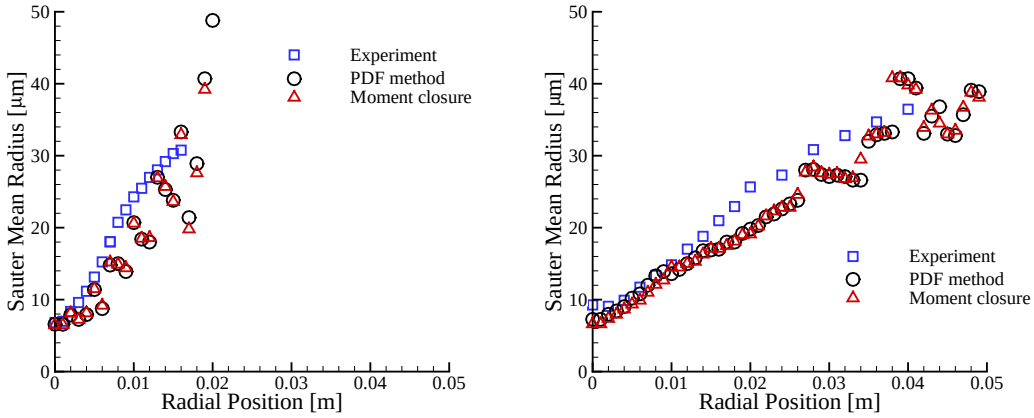

Fig. 4.14: Radial profiles of the Sauter mean radius at $x = 25$ mm (left) and 100 mm (right).

is pre-calculated from laminar counterflow spray flame. The library [180] consists of the data with two different initial droplet radius of $r_{l0} = 25$ μm and 10 μm, and one equivalence ratio $E_r = 3$, one initial spray velocity $v_0 = 0.44$ m/s. The species concentrations of a gas particle are determined from the spray flamelet library. The droplet size r^* is determined by interpolating the local Sauter mean radius at the nodes into the gas particle's position. The instantaneous dissipation rate of the gas particle, χ^*, is sampled from a log-normal distribution using a Monte-Carlo method [99]. The parameter $\mu_{\log}$ in the log-normal distribution (c.f. Eq. (2.148)) is calculated from the mean of the dissipation rate, which is computed from the local variance of the mixture fraction. The composition vector of the gas particle, $\mathbf{Y}^*(\xi_C^*, \chi^*, r^*, E_{l0}, v_{l0})$, are computed by interpolating the data from the spray flamelet library. The temperature of the gas particle is computed from the composition vector and the enthalpy h_s^*. The mean values at the node are obtained using the Eq. (3.45).

Figure 4.15 shows the contour plot of the mean gas temperature computed using the present transported PDF method. The points A–H indicate the monitor positions, where the PDFs of the mixture fraction, gas temperature, and enthalpy are analyzed. The coordinates of these points (x, r) in mm are: A(50, 0), B(50,5), C(50, 10), D(50, 15), E(150, 0), F(150, 20), G(150, 40), H(150, 60).

Figure 4.16 shows the radial profiles of the mean axial gas velocity at the section $x = 25$ mm, 50 mm, 100 mm, and 150 mm. Symbols are the experimental data [240]. Solid lines indicate the results from the present transported PDF method. Dashed lines indicate the results from the moment closure method using $k - \epsilon$ model [180]. The results of the transported PDF method are in good agreement with experimental data. Compared to the results of the moment closure method, the velocity profiles are

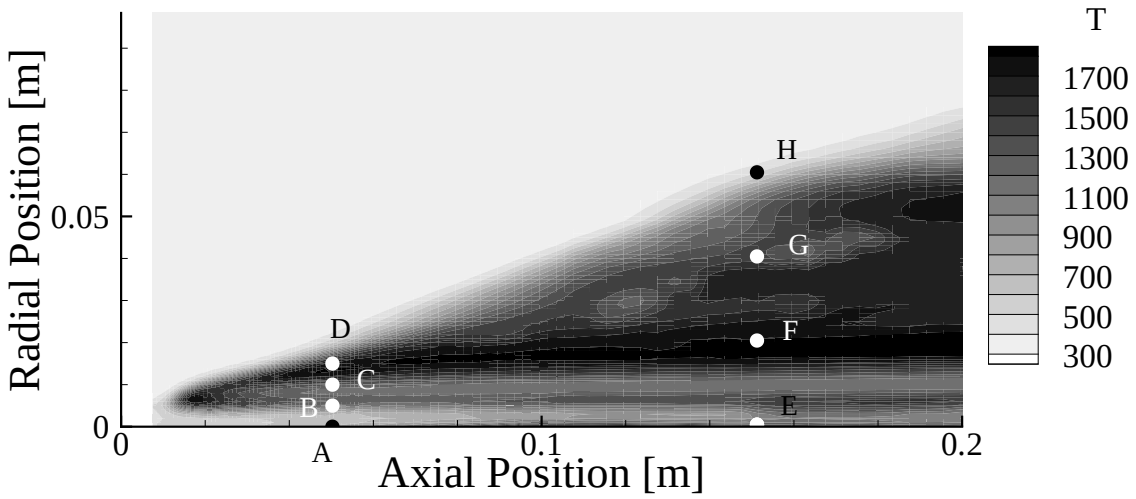

Fig. 4.15: Contour plot of the mean gas temperature computed by the transported PDF method. PDFs of the mixture fraction are analyzed at marked positions.

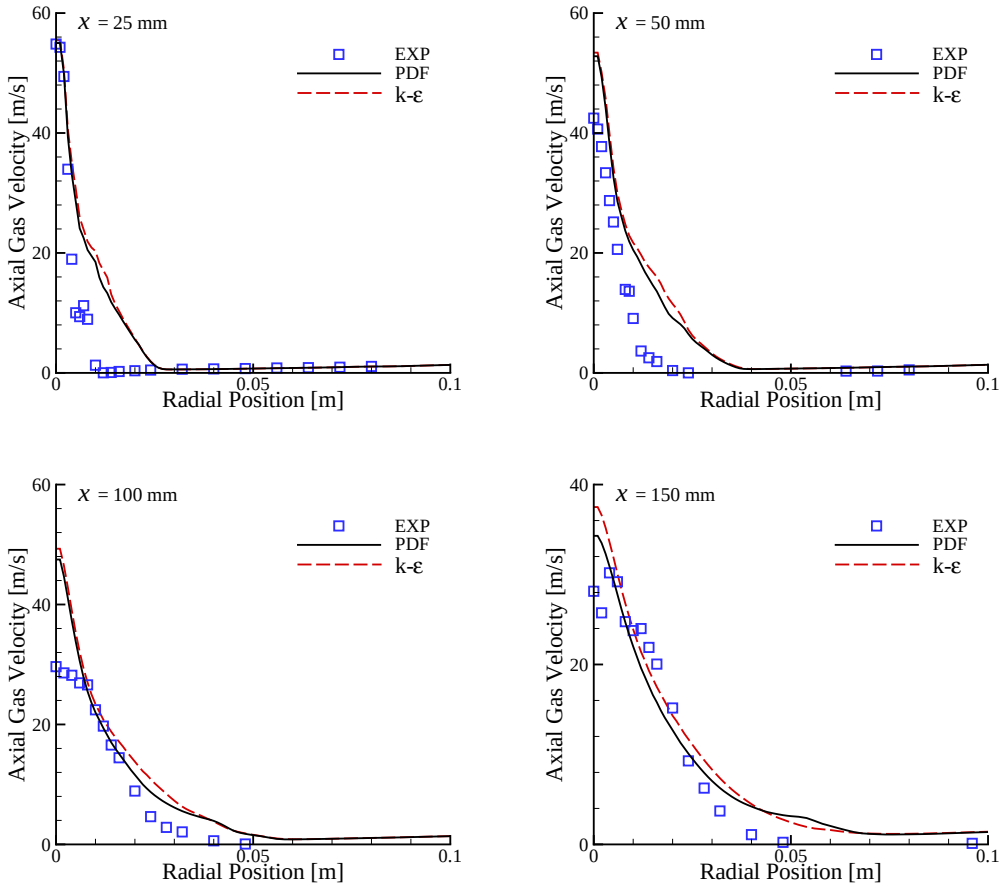

Fig. 4.16: Radial profiles of the mean axial gas velocity at sections $x = 25$ mm, 50 mm, 100 mm, and 150 mm.

slightly improved by the transported PDF method. The velocity field is also computed using the $k-\epsilon$ model in the present PDF simulation. More accurate composition fields enable the current transported PDF method to give a little better results in the velocity field. This improvement would be even better if the joint velocity-mixture fraction PDF is used [141].

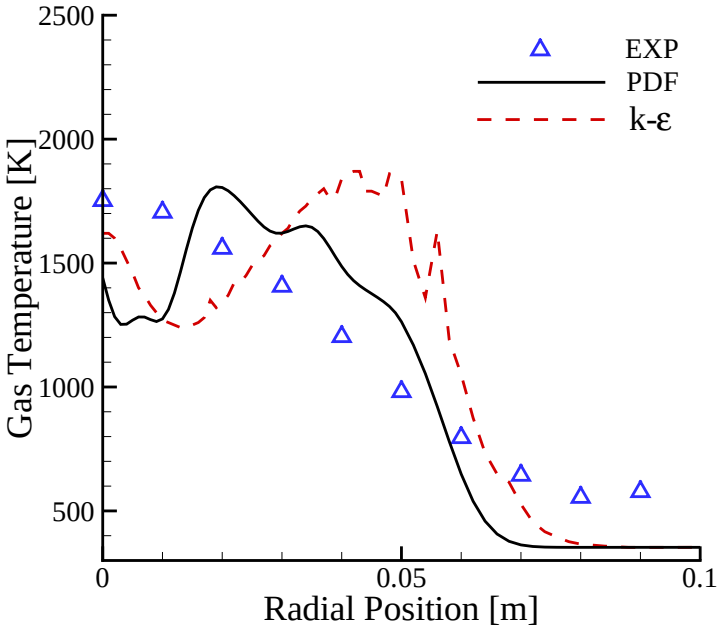

Fig. 4.17: Radial profiles of the mean gas temperature at section $x = 150$ mm.

Figure 4.17 shows the radial profile of the mean gas temperature at the section $x = 150$ mm. The same captions are used as the Fig. 4.16. The profile obtained using the transported PDF method improves the moment closure method between about 0.02 and 0.05 m from the centerline. At the centerline itself, both methods underpredict the experimental value which may be due to the inappropriate initial distribution of the liquid flux. The $k-\epsilon$ model yields some better agreement compared to the PDF model, however, experimental error may also contribute to the discrepancies here.

Figure 4.18 shows the radial profiles of the mean mass fraction of methanol vapor at the sections $x = 25$ mm, 50 mm, 100 mm, and 150 mm. The same captions in figures are the same as the Fig. 4.16. The results of the transported PDF method are in good agreement with the experimental data, whereas the moment closure method over-predicts the methanol vapor mass fraction. In the moment closure method, the mixture fraction is assumed to follow a standard β distribution. In the present method, the presumed PDF of mixture fraction is replaced by the marginal PDF of mixture fraction from Eq. (2.54), $\tilde{f}_{\xi_C}(\xi_C; \mathbf{x}, t)$. This PDF of the mixture fraction, which is computed by

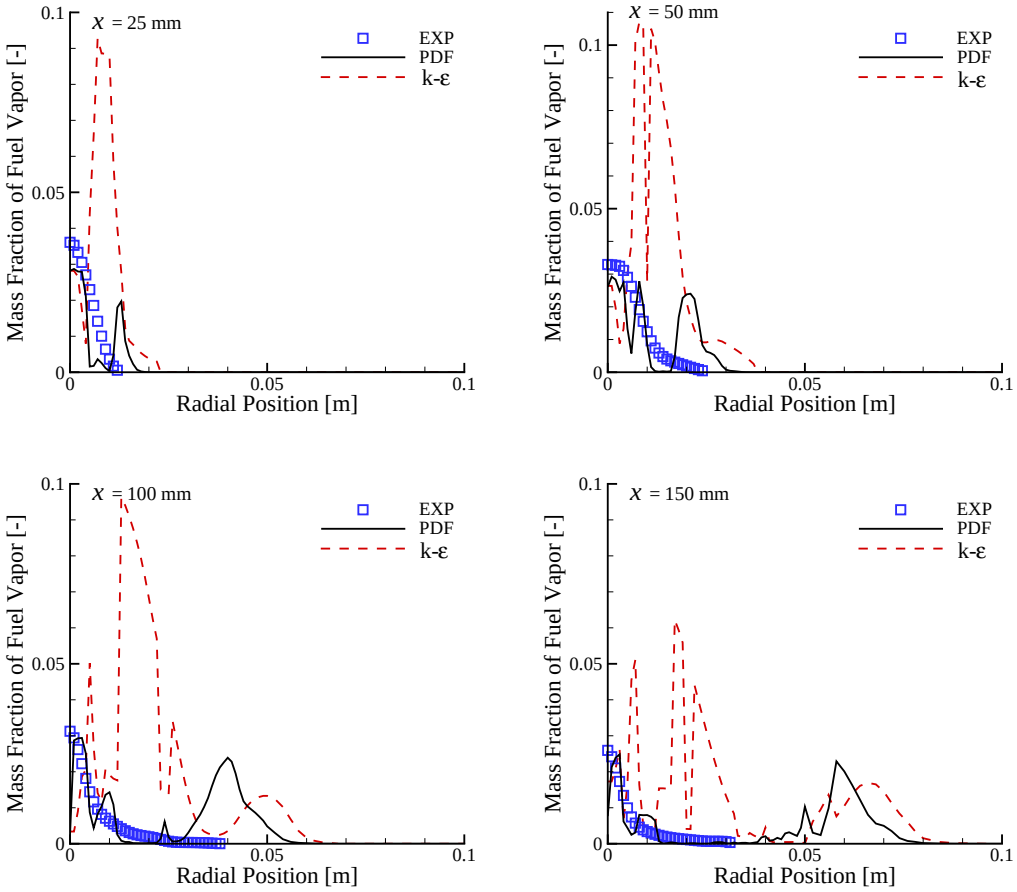

Fig. 4.18: Radial profiles of the methanol vapor mass fraction at sections $x = 25$ mm, 50 mm, 100 mm, and 150 mm.

solving the PDF transport equation, is more physical in the area where both chemical reactions and evaporation occur. Unfortunately, there are no experimental values of the fuel vapor mass fraction at higher distances of the centerline where the simulations predict a second peak.

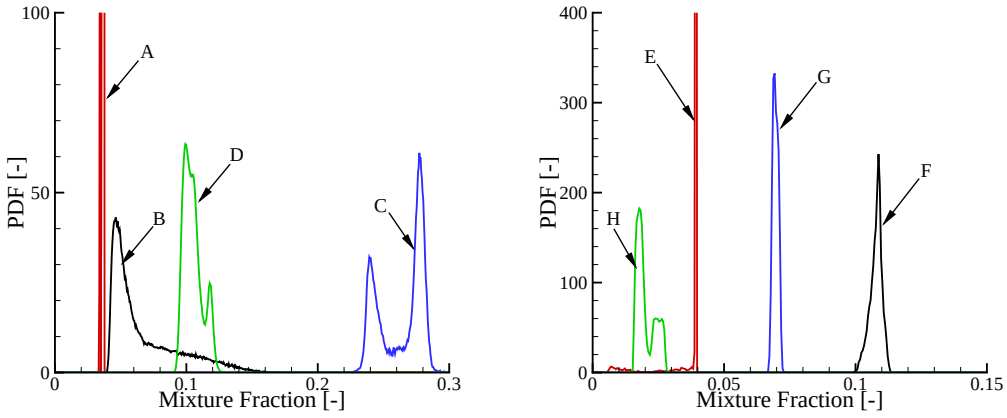

Fig. 4.19: PDFs of the mixture fraction at sections $x = 50$ mm (left) and 150 mm (right).

Figure 4.19 shows the PDFs of the mixture fraction at the monitor positions in the present transported PDF method. The PDFs at the points A and E are cut off in the figures. Their maximum value are about 1160 and 1820, respectively. Figure 4.19 (left) shows that the shape varies from a bivariate to a unimodal PDF as the positions C–D–B–A are passed which extend from the mixing layer of the jet to the centerline at $x = 50$ mm from the exit nozzle. The mean value of the mixture fraction in these positions varies from about 0.26 at C to 0.04 at A. The figure reveals that the mixture fraction profile in radial direction is non-monotonic, and it attains a maximal value of approximately 0.32 at about 2 mm from the centerline. The shape of the PDF varies also at higher distances from the exit nozzle as may be seen from Fig. 4.19 (right).

Figure 4.20 shows the comparison of the PDFs of the mixture fraction at selected monitor positions in the present transported PDF method and the moment closure method. Solid lines indicate the results of the present transported PDF method. Dashed lines indicate the presumed standard β PDFs used in the moment closure method [180]. All the PDFs used in the moment closure method show unimodal shapes, while the PDFs computed by the present method show bimodal, unimodal, or Dirac delta distributions. The standard β PDFs assume that the maximum mixture fraction in spray flow is unity, which is not true [233, 140]. Thus, the PDFs of the mixture fraction computed by the present method are more accurate. That is the reason why the present method gives better predictions with respect to the mass fraction

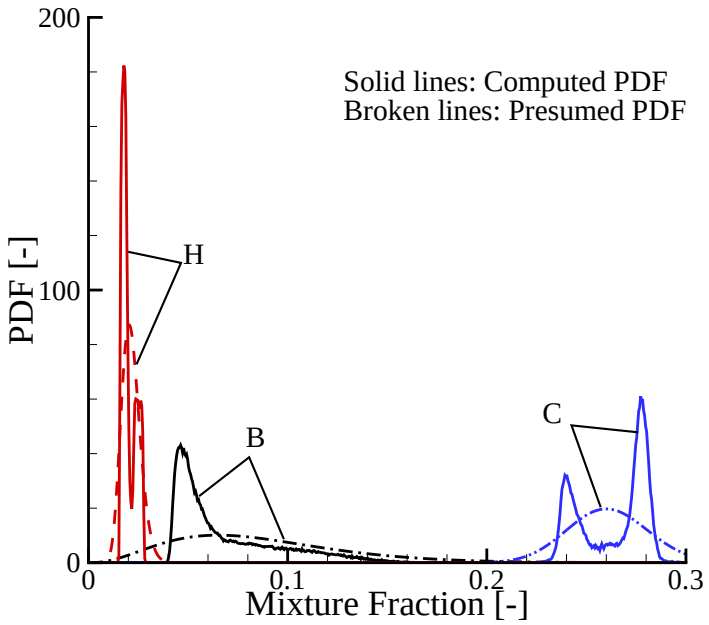

Fig. 4.20: Comparison of the PDFs of mixture fraction with the presumed β function.

of methanol vapor. The moment closure method can give a better prediction with an improved presumed PDF for the mixture fraction.

Figure 4.21 shows the PDFs of the enthalpy at the monitor positions computed by the present transported PDF method. The PDF at the point E is cut off in the figure, whose maximum value is about 0.17. The basic shapes of these PDFs are bimodal (point H) and unimodal (points E, F, G) shapes. The fluctuation in the enthalpy is weaker near the centerline than at other positions. The PDF of the enthalpy is close to a Dirac delta distribution at the point E.

Figure 4.22 shows the PDFs of the gas temperature at the monitor positions computed by the present transported PDF method. The PDFs at the points E and F are cut off in the figure. Their maximum values are about 0.16 and 0.067, respectively. The gas temperature is a nonlinear function of the enthalpy and the mixture fraction. Therefore, the PDFs of the gas temperature are more complicate than the PDFs of the mixture fraction and the PDFs of the gas temperature. Bi- and tri-modal shapes are observed in the PDFs of the gas temperature.

Figure 4.23 shows the radial profiles of the Sauter mean radius at the sections $x = 50$ mm and 100 mm, respectively. Squares are the experimental data. Circles indicate the results of the transported PDF method. Triangles indicate the results of the moment closure method. The numerical results are in good agreement with the experimental data. The results of the transported PDF method are close to the

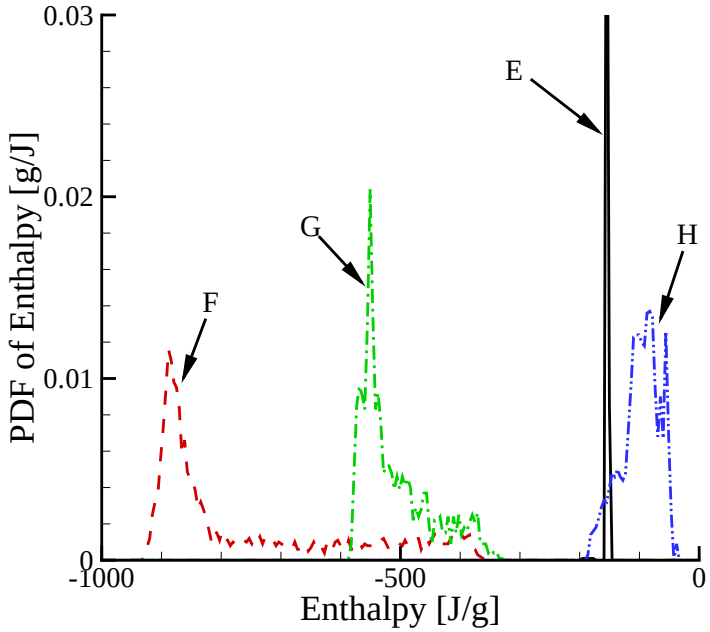

Fig. 4.21: PDFs of the enthalpy at section $x = 150$ mm.

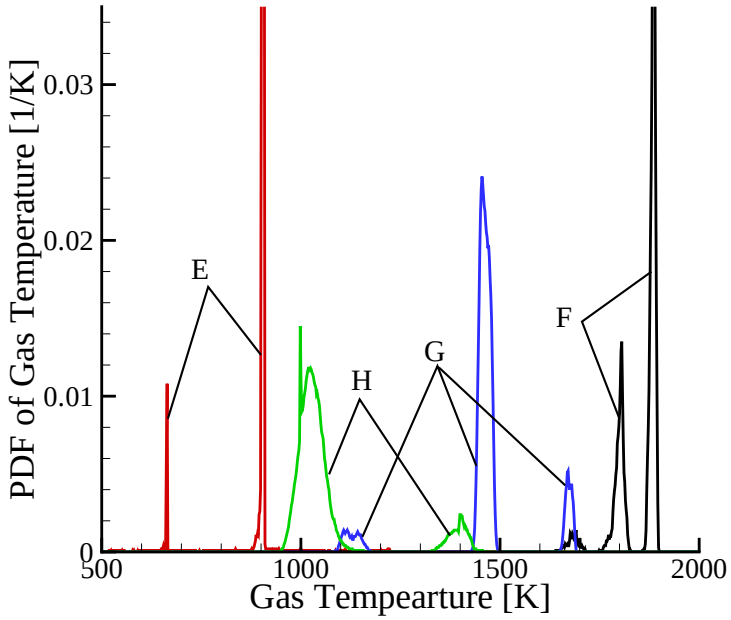

Fig. 4.22: PDFs of the gas temperature at section $x = 150$ mm.

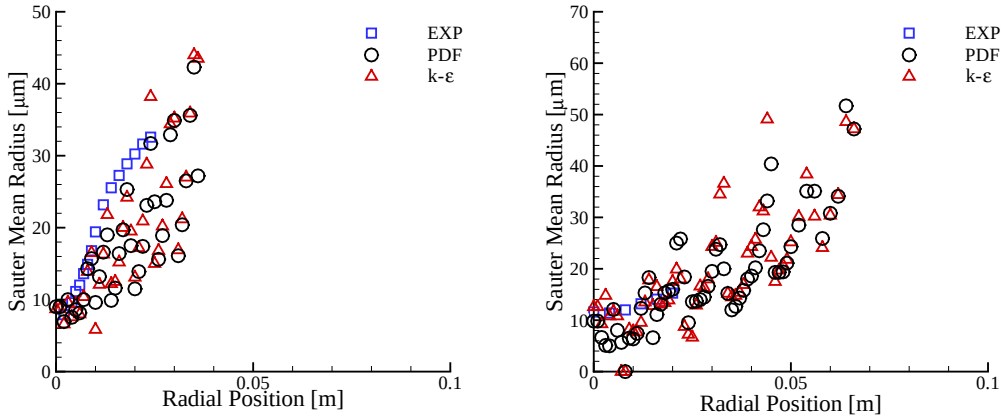

Fig. 4.23: Radial profiles of Sauter mean radius at sections $x = 50$ mm (left) and 100 mm (right).

results from the moment closure method. It implies that the dynamics of droplets are controlled by their inertia, and the effects of the gas-phase flow on the droplets is small. Two different initial droplet radius, $r_{l0} = 25$ μm and 10 μm, are considered in the present spray flamelet library. When the local Sauter mean radius is larger than 10 μm, the library with $r_{l0} = 25$ μm is used. When the local Sauter mean radius is smaller than 10 μm and larger than 1 μm, the library with $r_{l0} = 10$ μm is used. Referring to the Fig. 4.18, the fluctuation in the profiles of the methanol vapor mass fraction is observed. According to Fig. 4.23, the fluctuations in the results of both transported PDF method and moment closure method are observed just at the positions when the Sauter mean radius equals to 10 μm. Thus, such fluctuation must result from the insufficient resolution of initial droplet radius in current flamelet library. More data of laminar spray flame with different initial droplet radius should be included into the flamelet library in the future. Furthermore, it implies that the effects of droplets are very important for spray flame.

4.2 Turbulent Ethanol/Air Spray Flows

4.2.1 Experimental Setup

Recently, a novel spray jet flame burner has been set up at the Institute of Physical Chemistry, University of Heidelberg [246]. The burner is developed in cooperation with the University of California at Berkeley. The burner consists of a central fuel nozzle (Delavan 67700-5), a perforated brass plate that provides a homogeneous air co-flow on the top of the central burner bowl (see Fig. 4.24). The nozzle has a diameter of

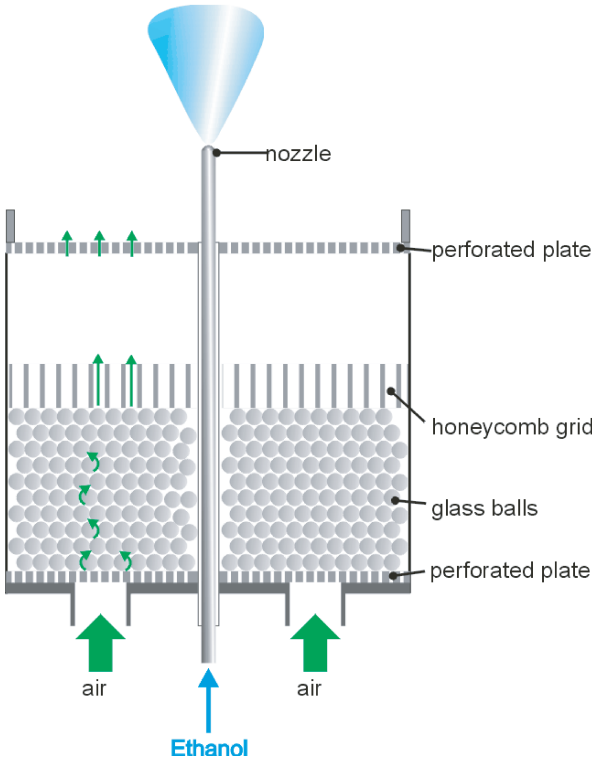

Fig. 4.24: Schematic set-up of the spray burner.

10 mm and produces a hollow-cone spray. It is fixed about 80 mm above the center of the plate. The geometric Reynolds number Re = 19,565 of the non-reactive flow is calculated from the mean droplet velocity which is measured by particle imaging velocimetry (PIV) measurements [247]. As an improvement to the conventional simple jet flame burner, there is no bluff body in this burner, and obscurations caused by the fluid mechanics are avoided. The burner in Berkeley uses vitiated co-flows. The oxygen rich combustion products from the co-flows ignite and stabilize the central jet flame. The droplet size distribution and liquid volume fraction of a methanol/air spray in a vitiated co-flow are measured using ensemble light diffraction (ELD) technique [248].

The burner in the present work uses air co-flows. An igniter is needed to initiate the flame. Ethanol is heated to 45°C before injection into quiescent air at room temperature. The resulting flame has two flame zones. The inner flame is located 1 mm above the nozzle exit while the outer flame position depends on the fuel pressure and is located 5 – 15 mm above the nozzle. The fuel pressure was varied between 1.4 and 2.6 bar. The resulting liquid flow rate varies between 0.39 g/s and 0.54 g/s. The air co-flow velocity was varied between 0 and 0.64 m/s. The Sauter mean radius in an ethanol/air spray flame is measured using a combined LIF/Mie technique [249]. Fuel tracers with different volatilities have been tested in planar LIF/Mie dropsizing measurements [249]. Droplet size and velocity distributions of a non-reactive ethanol/air

spray flow were measured using phase Doppler anemometry (PDA) [246]. Imaging of the gas-phase temperature in and around the spray flame was performed based on multi-line laser-induced fluorescence measurements with seeded NO [250, 251]. The temperature of the liquid phase is measured using two-color LIF thermometry [252].

4.2.2 Turbulent Non-Reactive Ethanol/Air Spray Flows

PDA measurements provide a set of amenable data for the numerical simulation. The well-known Eulerian/Lagrangian formulation is adopted to model the turbulent non-reactive ethanol/air spray flow. The conventional droplet parcel method [194] is used to solve the droplet evolution equation. The computed ensemble-averaged droplet velocities, the Sauter mean radius (SMR), as well as the droplet size distribution are compared with the experimental data.

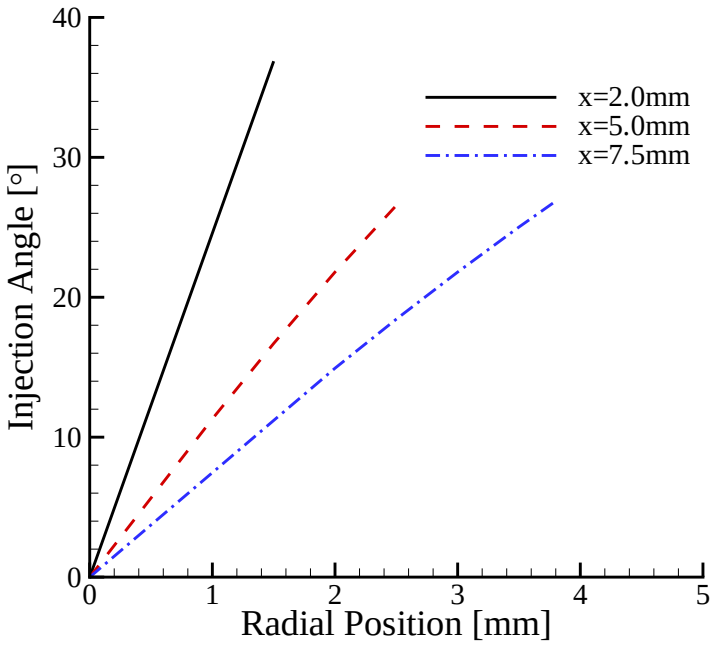

Fig. 4.25: Radial profiles of the spray injection angle at different sections.

Droplet size and droplet velocity distributions in a non-reactive spray without co-flow were measured close to the nozzle exit. Cabra's [248] experiment shows that the droplet sizes do not change considerably before the droplets reach the flame front. Therefore, the differences of the droplet sizes between reactive and non-reactive cases are expected to be small for the position close to the nozzle. Both droplet sizes and velocities were measured using phase Doppler anemometry (PDA). The droplet velocity perpendicular to the plane defined by the laser beams is measured. The droplet velocity

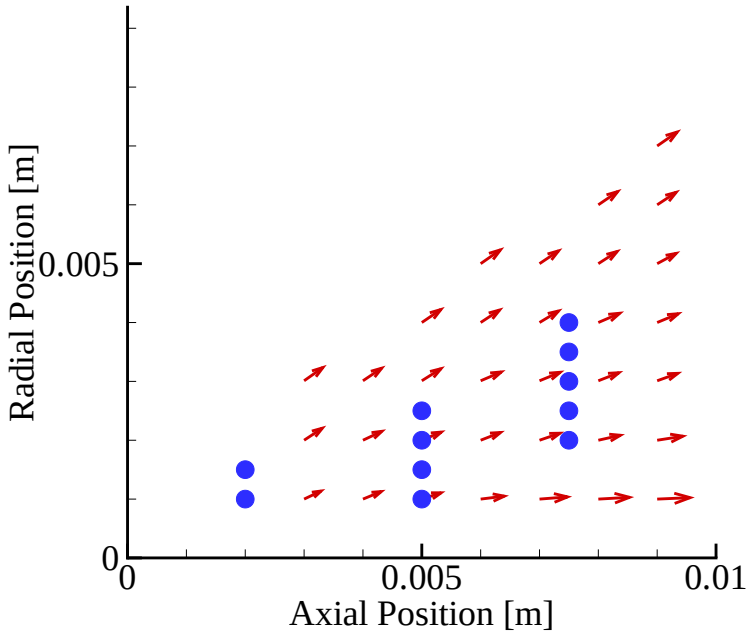

Fig. 4.26: Vector plot of the ensemble-averaged droplet velocities. Marked points indicate the experimental positions.

parallel to the plane is calculated from the perpendicular component and the injection angle. In the present work, the axial component of droplet velocity, U_x is measured. The radial component is calculated using

$$U_r = U_x \tan\theta, \tag{4.4}$$

where θ is the spray injection angle estimated from the data provided by the nozzle producer. The radial profiles of the spray injection angle at different sections are illustrated in Fig. 4.25.

The droplet radius and its axial velocity are measured at three different axial sections: $x = 2.0$ mm, 5.0 mm, and 7.5 mm. Three cases with different injection pressures $p = 1.4$ bar, 2.0 bar, and 2.4 bar are investigated. In the case of $p = 2.0$ bar, spray breakup occurs closer to the nozzle. Thus, the overall number of non-spherical droplets is smaller and the PDA data is more reliable [246]. Therefore, this case is used for the comparison between experiment and simulation.

Figure 4.26 shows the simulated vector plot of the ensemble-averaged droplet velocity. The marked points indicate the experimental positions. The first section where experimental data are available is $x = 2$ mm, which is taken as the inlet profile for the computation.

Figure 4.27 shows the radial profiles of the Sauter mean radius and ensemble-

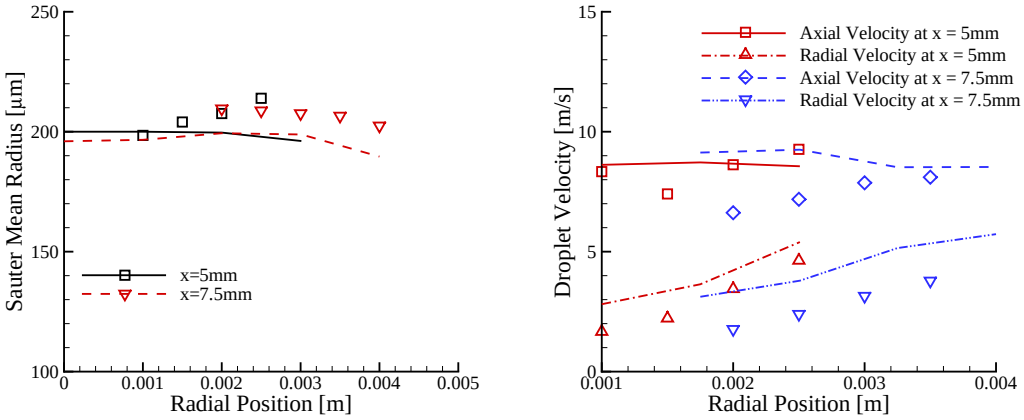

Fig. 4.27: Radial profiles of the Sauter mean radius (left) and ensemble-averaged droplet velocity (right) at sections $x = 5$ mm and 7.5 mm. Symbols: experimental data. Lines: simulation.

averaged droplet velocity at the two different axial positions $x = 5$ mm and 7.5 mm. Considering the fact that there is no measurement about the gas-phase, the agreement of the computed results and the experimental data is good. The simulated droplet velocities are systematically higher than the measured values by up to 30%. This causes a higher droplet evaporation rate leading to smaller droplet radius compared to the experimental values by up to 10%. The discrepancies between experiment and simulation in the droplet velocities can be attributed from the imprecise approximation of the radial droplet velocity, unknown initial gas flow properties for the simulation and the coarse initial droplet size in the experiment. All spray calculations are very sensitive to the initial conditions of both, the gas and the liquid phase. The experimental data of the droplet distribution at $x = 2$ mm have a coarse spatial resolution in radial direction. Therefore, there is some ambiguity in determining appropriate initial conditions for the computations. Moreover, the PDA measurements discard droplets that deviate from spherical symmetry as well as measurements with, too low droplet density. Therefore, the experimental data also have a certain error range. Moreover, the radial velocity component has been extrapolated from the spray angle given by the nozzle producer again causing some uncertainties.

Figures 4.28–4.29 show the comparison of the droplet size distributions from the numerical simulation and experiment. The droplet size distributions at the positions (5.0, 1.0), (5.0, 2.0), (7.5, 3.0), and (7.5, 3.5) are illustrated. The size of the droplet radius ranges from 0 to 300 μm. In the present computation, the droplet size range is split into 50 equal-sized class intervals. The number fraction of each class interval is calculated, and then the PDFs of the droplet radius are evaluated. In general,

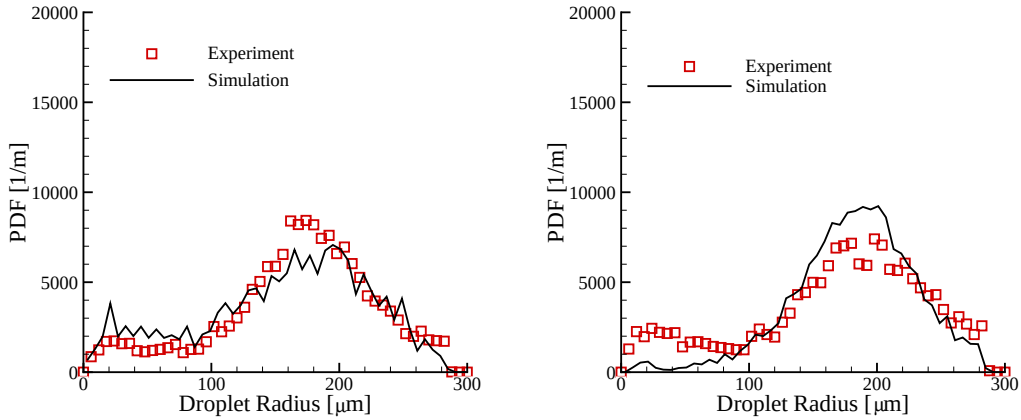

Fig. 4.28: Droplet size distribution at the positions (5.0 mm, 1.0 mm) (left) and (5.0 mm, 2.0 mm) (right). Symbols: experimental data. Lines: simulation.

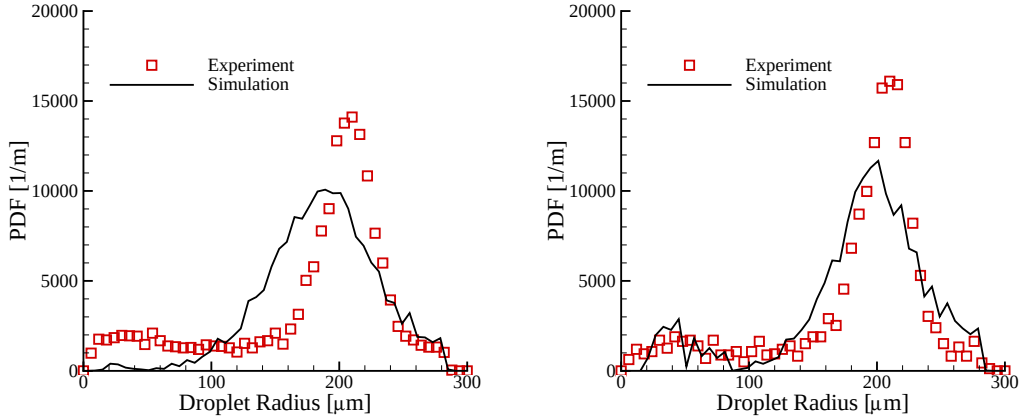

Fig. 4.29: Droplet size distribution at the positions (7.5 mm, 3.0 mm) (left) and (7.5 mm, 3.5 mm) (right). Symbols: experimental data. Lines: simulation.

the numerical results agree reasonably well with experimental data. Comparing the sections at $x = 5$ mm and 7.5 mm, the peak values of the droplet size distribution shift towards larger drop radius, which indicates the progress of evaporation. The probability of small droplets at the positions (5.0, 2.0) and (7.5, 3.0) are under-predicted. This may result from an inappropriate guess of the gas velocity and liquid flux at the inlet profile. More experimental studies in this direction are encouraged.

4.2.3 Turbulent Ethanol/Air Spray Flames

Gas temperature of the turbulent ethanol/air spray flame is measured using multi-line NO-LIF thermometry. 1000 ppm of NO is seeded to the co-flow gas and therefore allow measurements in both co-flow and flame.

The gas temperatures in the co-flow are 300 ± 4 K ($\pm1\%$). For the case with injection pressure 2.0 bar and co-flow velocity 0.32 m/s, we find 1775 ± 75 K ($\pm4\%$) in the center of the flame 20 mm above the nozzle exit. The accuracy of the present technique has been proven by comparisons to thermocouple measurements at ambient temperature [251] and by CARS at flame temperatures in [250]. The turbulent ethanol/air spray flame is simulated using Eulerian/Lagrangian formulation. The same physical models and numerical methods are used as Section 4.2.2. A spray flamelet model [180] is used to include the detailed ethanol/air combustion mechanism. The mechanism [245] consists of 38 species and 337 elementary reactions. The spray flamelet library has been built up from the results of laminar counterflow spray flame [183].

The case with injection pressure 2.0 bar and assistant gas velocity 0.32 m/s is simulated. The gas velocity is estimated from the volume flux of the assistant gas. The section at $x = 2$ mm is taken as the inlet profile. The gas temperature profile at the inlet is taken from the measurements of 2D NO-LIF [253]. The gas velocity at the inlet is set to 0.32 m/s. Assuming that the difference in dropsize and velocity between reactive and non-reactive spray is small, the droplet size distribution and droplet velocity distribution at the inlet are taken from the measurements of PDA, in which the injection pressure is 2.0 bar, too [254].

Figure 4.30 shows the radial profiles of gas temperature at the section $x = 6$ mm, 10 mm, 20 mm, and 30 mm. Symbols are the experimental data [253]. The lines indicate the numerical results. The numerical results are in good agreement with the experimental data, especially near the center line. However, the present simulation fails to predict the hot wings of the spray flame that were found in the experiment for $x = 20$ and 30 mm. The discrepancies are mainly from the unknown local liquid flux, coarse droplet size distribution and droplet velocity distribution, and many unknown gas-phase properties at the inlet. The numerical results are very sensitive to these variables. In the present simulation, we assume a homogeneous distribution of the

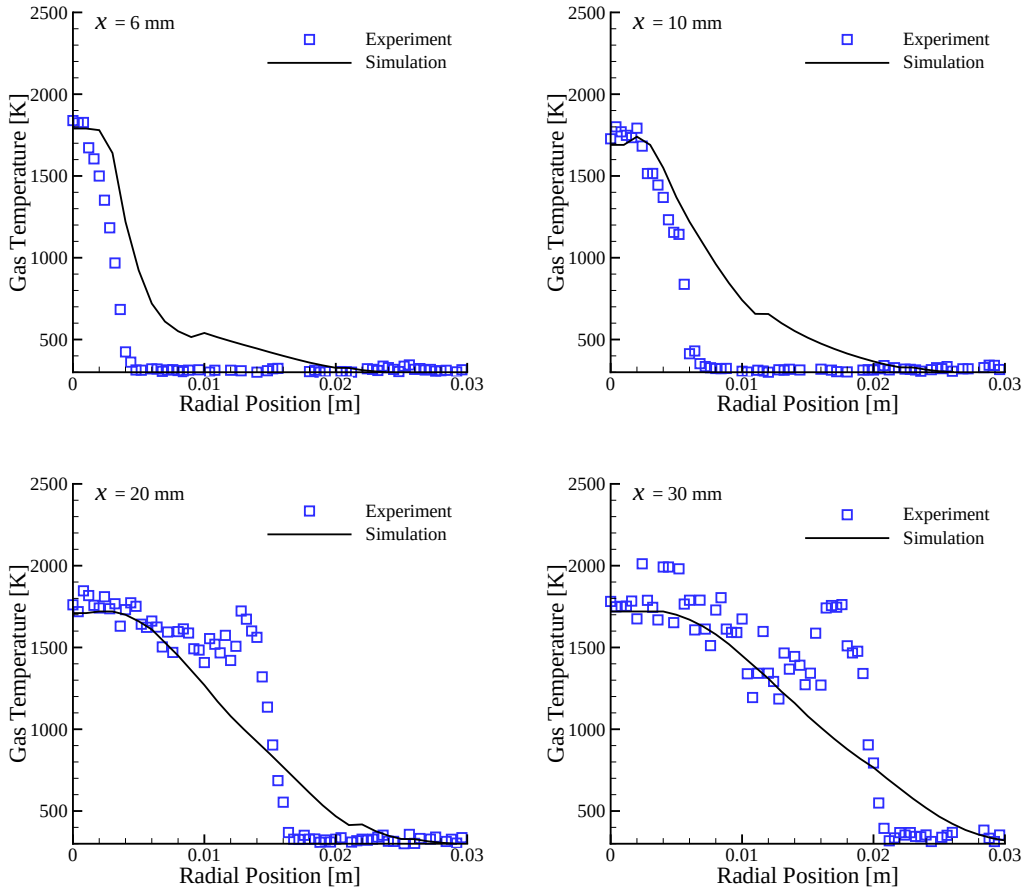

Fig. 4.30: Radial profiles of the mean gas temperature at section $x = 6$ mm, 10 mm, 20 mm, and 30 mm.

liquid flux at the inlet, which may not be true. On the section close to the nozzle ($x = 2$ mm), the simulated gas temperature profile is broader than the experimental one. It may be partly due to the $k - \epsilon$ model used in the present work, because the $k - \epsilon$ model always over-predicts the spread rate of the round jet flow. Another reason may be the inappropriate guess of the gas-phase properties, particularly the turbulent kinetic energy and its dissipation rate.

Next step, the turbulent ethanol/air spray flame will be simulated using the transported PDF method. More quantities of the spray flame need to be measured, especially the local liquid flux.

5. Conclusions and Perspective

In this dissertation, turbulent spray flows are investigated using probability density function (PDF) methods. Two methodologies are used: the presumed PDF method and the transported PDF method. The turbulent non-reactive spray flows are simulated using the transported PDF method. The numerical results are analyzed by comparing with the experimental data, the numerical results available in the literature, and the presumed PDFs.

A PDF of mixture fraction for turbulent spray flows is proposed. The PDF transport equation is deduced. The unclosed term of molecular mixing is described using an extended Interaction-by-Exchange-with-the-Mean (IEM) model. The PDF transport equation is closed through coupling with an extended $k-\epsilon$ model for turbulent multi-phase flows. The PDF transport equation is solved using a hybrid finite volume/Lagrangian Monte-Carlo particle method. A turbulent non-reactive spray flow is simulated using this method. The numerical results of the PDF method are in good agreement with experimental data [241] and improve the results from the moment closure method [180]. Furthermore, the shapes of the PDFs of mixture fraction at different positions, which are computed by the transported PDF method, are presented and analyzed. It appears that the spray source changes the value of the mean mixture fraction, but it does not change the shape of its PDF. A comparison of the transported PDF results with the standard β function shows that the standard β function fails to describe the shape of the PDF. With the definition of appropriate local maximum and minimum values of the mixture fraction, a modified four-parameter β function is suitable to reflect the shape of the Monte-Carlo PDF very well [140].

A joint velocity-scalar PDF for turbulent spray flows is proposed. Its transport equation is deduced and modeled. The simplified Langevin model is extended to model the gas velocity. The molecular mixing is modeled using the extended IEM model. Simulations of a turbulent non-reactive spray flow show that the profiles of gas velocity are well predicted by this joint PDF model [141].

A joint enthalpy-mixture fraction PDF for turbulent spray flames is proposed. Its transport equation is deduced. The molecular mixing is modeled using the extended IEM model. A turbulent methanol/air spray flame is simulated. Detailed chemistry consisting of 23 species and 168 elementary reactions is implemented through a spray flamelet model [180]. The numerical results of gas velocity, gas temperature, mass

fraction of fuel vapor, and Sauter mean radius are compared with experimental data [241] and the results from the moment closure method [180]. Good agreements with experiment are observed. The present method improves the results of the moment closure method with respect to the mass fraction of methanol vapor. The presumed PDFs of mixture fraction used in moment closure method are compared with the computed PDFs of mixture fraction from the transported PDF method. The results show that the latter ones are more accurate. Thus, the composition spaces computed by present transported PDF method are more accurate [142].

Applications of the presumed PDF method in turbulent spray flows are discussed. The normal distribution, log-normal distribution, Nukiyama-Tanasawa distribution, Rosin-Rammler distribution, standard β distribution, and modified four-parameter β distribution are discussed and analyzed. The relationships between them are pointed out. Comparisons of modified β distribution with normal distribution, log-normal distribution, and Rosin-Rammler distribution show that modified β distribution can reproduce these distributions.

A turbulent ethanol/air spray flow is simulated using second moment closure modeling. A conventional Eulerian/Lagrangian formulation is employed. The numerical results of the non-reactive case are compared with the measurements obtained by phase Doppler anemometry [184]. The Sauter mean radius, mean droplet velocity, as well as droplet size distribution are well predicted [246]. For the reactive case, the detailed chemistry is implemented through a spray flamelet model [183]. The ethanol/air combustion mechanism consists of 38 species and 337 elementary reactions. The profiles of gas temperature are compared with the experimental data which is measured using 2D NO-LIF [251]. Good agreement to the experimental data is found [184].

An implicit scheme is designed to compute the particle velocity in the convective environment. A numerical test shows that the implicit scheme is more robust, accurate and efficient than conventional explicit scheme.

This work shows that transported PDF methods are feasible for the simulation of turbulent non-reactive and reactive spray flows. The results of the transported PDF method are in good agreement with the experimental data. Improvements to the conventional moment closure methods are found. The statistical distribution of the mixture fraction in the turbulent spray flows are exerted from the results of transported PDF methods and are compared with the presumed PDFs.

There are still many unsolved problems associating with the transported PDF methods for the turbulent spray flows. Great efforts should be paid on them. Physical models, including the mixing model and Langevin model, need to be validated in benchmark cases. Advanced models should be implemented into the code, such as EMST mixing model, generalized Langevin model. The effects of liquid phase, for instance, volume

fraction, fluctuating in the spray source terms, should be taken into account in the PDF models. The joint velocity-scalar PDF coupling with the spray flamelet model will be employed to simulate the turbulent spray flames. Joint velocity-turbulent frequency-composition PDF might be an interesting topic. The turbulent frequency provides a turbulent time scale for the PDF transport equation. The resulting PDF transport equation appears a closed form. Therefore, the turbulent spray flows can be simulated without turbulent viscosity model or Reynolds-stress model. However, a physical model for the turbulent frequency needs to be developed at first. Numerical accuracy issues deserve our attention. The effects of grid size and gas particle number on the results should be investigated.

Appendix

A. Nomenclature

Symbol	Unit	Description
A	m^2	Surface area of control volume
B_M		Spalding mass transfer number
B_T		Spalding heat transfer number
C_0		Constant in Langevin model
C_{CFL}		Constant in Courant–Friedrichs–Lewy condition
C_d		Coefficient in spray model
$C_{p\alpha}$		Constant-pressure specific heat of species α
C_s		Constant in extended $k-\epsilon$ model for spray flows
C_ϕ		Constant in IEM model
c_{tr}		Constant in spray model
$c_{\epsilon,1}$		Constant in $k-\epsilon$ model
$c_{\epsilon,2}$		Constant in $k-\epsilon$ model
c_μ		Constant in $k-\epsilon$ model
D	m^2/s	Diffusion coefficient
$D(x)$		Cumulative distribution function
D_M	m^2/s	Mean diffusion coefficient of mixture
E_r		Equivalence ratio in counterflow spray flame
$\mathrm{erfc}(x)$		Error function
$\mathbf{F}$	m/s^2	Acceleration of droplet
$\mathbf{F}$		Vector of convective terms
f		Probability density function
f_d		droplet density function
Δh_f^0	J/g	Specific enthalpy of formation
$h_{s,\alpha}$	J/g	Specific sensible enthalpy of species α
h_t	J/g	Specific total non-chemical enthalpy
$h_{t,c}$	J/g	Specific total enthalpy
$\mathbf{J}_q^c$	$\mathrm{J}/(\mathrm{m}^2\mathrm{s})$	Heat flux due to thermal conductivity
$\mathbf{J}_q^d$	$\mathrm{J}/(\mathrm{m}^2\mathrm{s})$	Heat flux due to molecular diffusion
k	$\mathrm{m}^2/\mathrm{s}^2$	Turbulent kinetic energy
L	m	Turbulent length scalar

L_v	J/g	Latent heat of fuel
$\dot{M}_{d,k}$	g/s	Liquid mass flux represented by k-th droplet parcel
N		Particle number, sample number
$\mathbf{N}$		Vector of viscious terms
$N_{\max}$		Maximum particle number in one cell
$N_{\min}$		Minimum particle number in one cell
N_s		Species number
Nu^*		Modified Nusselt number
Nu_0		Nusselt number
p	Pa	Pressure
P		Presumed probability density function
p_{crit}	Pa	Critical pressure of liquid phase
p_F	Pa	Vapor pressure
Pr		Prandtl number
$\dot{Q}$	J/s	Chemical production rate of heat
r_d	m	Droplet radius
R_α	J/(mol·K)	Gas constant of species α
Re		Reynolds number
Re_d		Droplet Reynolds number
r_{l0}	m	Initial droplet radii in counterflow spray flame
$\mathbf{S}$		Vector of source terms
S_g		Source term due to gas phase
S_l		Source term due to liquid phase
S_α	g/s	Chemical production rate of species α in mass
Sc		Schmit number
Sh^*		Modified Sherwood number
Sh_0		Sherwood number
T	K	Temperature
T_b	K	Boiling temperature of liquid phase
T_{crit}	K	Critical temperature of liquid phase
t	s	Time
t_{corr}	s	Droplet-eddy interaction time scalar
t_{drag}	s	Time scalar for drag force
t_{tr}	s	Time scalar for droplet to traverse the eddy
t_τ	s	Turbulent time scalar
$\mathbf{U}$	m/s	Velocity
$\mathbf{U}_d$	m/s	Droplet velocity
$\mathbf{U}_r$	m/s	Relative velocity between liquid phase and gas phase

$\mathbf{V}$	m/s	Velocity in sample space
$\mathbf{V}_d$	m/s	Droplet velocity in sample space
v_{l0}	m/s	Initial droplet velocity in counterflow spray flame
$\mathbf{W}$		Vector of conservation variables
dW_i	$s^{1/2}$	i–component of an increment of a Wiener process
W_α	g/mol	molecular weight of species α
X_α		Mole fraction of species α
$\mathbf{x}$	m	Coordination
Y_{Fs}		Mass fraction of fuel vapor at droplet surface
$Y_{F\infty}$		Mass fraction of fuel vapor at outer boundary of film
Y_α		Mass fraction of species α
Z_C		Mass fraction of element carbon
ϵ	m^2/s^3	Dissipation rate of turbulent kinetic energy
ζ_C		Mixture fraction in sample space
η_s		Sensible enthalpy in sample space
θ_d	K	Droplet temperature in sample space
ι_d	m	Droplet radius in sample space
λ	J/(msK)	Thermal conductivity
μ	g/(ms)	Viscosity coefficient
μ		Mean of a distribution
μ_t	g/(ms)	Turbulent viscosity coefficient
μ_l	g/(ms)	Laminar viscosity coefficient
μ_{eff}	g/(ms)	Effective viscosity coefficient
ξ_C		Mixture fraction
$\xi_{C,\text{st}}$		Mixture fraction at stoichiometric condition
ρ	kg/m^3	mass density
σ		Variance of a distribution
σ_k		Effective Schmit number for k
σ_ϵ		Effective Schmit number for ϵ
χ	s^{-1}	Dissipation rate of mixture fraction
χ_{st}	s^{-1}	Dissipation rate of mixture fraction at stoichiometric condition
$\dot{\omega}_\alpha$	s^{-1}	Chemical production rate of species α
$\Gamma(x)$		Gamma function
Γ_h	g/(ms)	Thermal diffusion coefficient
$\Gamma_{h,\text{eff}}$	g/(ms)	Effective thermal diffusion coefficient
$\Gamma_{h,t}$	g/(ms)	Turbulent thermal diffusion coefficient

$\Gamma_{k,\text{eff}}$	g/(ms)	Effective exchange coefficient for k
$\Gamma_{\epsilon,\text{eff}}$	g/(ms)	Effective exchange coefficient for ϵ
Γ_M	g/(ms)	Mean mass diffusion coefficient of the mixture
$\Gamma_{M,\text{eff}}$	g/(ms)	Effective mean mass diffusion coefficient of the mixture
$\Gamma_{M,t}$	g/(ms)	Turbulent mean mass diffusion coefficient of the mixture
Δt	s	Time step
Ω		Control volume

Subscripts and Superscripts

Symbol	Quantity
d	Droplet
F	Fuel
l	Liquid phase
O	Oxygen
s	Species, sensible
$\tilde{}$	Favre average
$\bar{}$	Time average
$''$	Fluctuating component in Favre average
$'$	Fluctuating component in time average
$*$	Sample properties
$\langle\ \rangle$	Ensemble average
$\hat{}$	Estimated property

Physical Constants

Symbol	Quantity
$\mathcal{R} = 8.31451$ J/(mol·K)	Universal gas constant
$g = 9.8$ m/s^2	Gravitational acceleration

B. Acknowledgements

First of all, I would like to thank Prof. Eva Gutheil who patiently taught, helped, and guided me on my research during these years. Prof. Gutheil led me to the topic of this work, and supported me to apply the scholarship provided by Graduate College at IWR. She advised me whenever necessary. She corrected in great patience the reports, papers, presentations, and this thesis I wrote. My future career will benefit a lot from it. And she provided me the timely help in my normal life, too. Without her invaluable help and advice, this thesis could not have been finished.

I am grateful to my co-advisor, Prof. Jürgen Wolfrum, for his confidence in my potential and my work, for his guidance in research, and for his efforts on this joint project.

I want to thank my colleagues, Markus Vogelgesang, Marco de Rosa, Yarlanki Srinivas, Daniela Urzica, Peter Groppenbächer. Thanks to Prof. Gutheil, Prof. Wolfrum, Marco de Rosa, Daniela Urzica, Peter Groppenbächer, Thomas Dunne, Sreejith Pulloor Kuttanikkad, and Yi-Lin Liu who helped to correct my English in the thesis. Special thanks to Mr. Peter Groppenbächer, who corrected the german abstract of this thesis with great patience. Many thanks to Prof. Christof Schulz, Isabell Düwel, Helmut Kronemayer for the comments and suggestions on this work, especially for providing the experimental data of ethanol spray flows. Thanks to Prof. Yi-Liang Chen and Dr. Min-Ming Zhu for fruitful discussions on the theory and numerical methods of the PDF methods.

Thanks to Steffen Wunderlich and Pavel Popov for their help on computer facilities.

I wish to give special thanks to my wife, Mrs. Yi-Lin Liu, and my father, Mr. Gui-Jun Ge, for their loves, their continuous encouragements and supports.

Finally, I acknowledge German Science Foundation (Deutsche Forschungsgemeinschaft - DFG) for the finacial support of through the International Graduiertenkolleg (IGK) 710 “Complex processes: Modeling, Simulation and Optimization”.

C. Curriculum Vitae

Name Hai-Wen GE

Nationality Chinese

Birth Zhejiang, P. R. China
April 7, 1977

Address Interdisziplinäres Zentrum für Wissenschaftliches Rechnen,
Universität Heidelberg,
Im Neuenheimer Feld 368,
D69120, Heidelberg, Germany

Phone +49-6221-54-4988

Fax +49-6221-54-6111

Email heaveng@iwr.uni-heidelberg.de

Webpage http://www.iwr.uni-heidelberg.de/groups/mfc/

Education 1983.9 - 1988.7: "Jiatang" Primary School, Shangyu, Zhejiang, P. R. China

1988.9 - 1991.7: "Jiatang" Middle School, Shangyu, Zhejiang, P. R. China

1991.9 - 1994.7: "Chunhui" Middle School, Shangyu, Zhejiang, P. R. China

1994.9 - 1999.7: Undergraduate student, Department of Thermal Science and Energy Engineering, University of Science and Technology of China, P. R. China

1999.7: Bachelor of Science, Department of Thermal Science and Energy Engineering, University of Science and Technology of China, P. R. China

1999.9 - 2002.7: Graduate student, Department of Thermal Science and Energy Engineering, University of Science and Technology of China, P. R. China

2002.7: Master of Engineering, Department of Thermal Science and Energy Engineering, University of Science and Technology of China, P. R. China

2002.9 - present: PhD student, Interdisciplinary Center of Scientific Computing, University of Heidelberg, Germany.

Experience 1999.9 - 2002.7: Research assistant, Department of Thermal Science and Energy Engineering, University of Science and Technology of China, P. R. China.

2001.2 - 2001.7: Teaching assistant for "Advanced Mathematics", Department of Thermal Science and Energy Engineering, University of Science and Technology of China, P. R. China.

2002.8 - present: Research assistant, Interdisciplinary Center of Scientific Computing, University of Heidelberg, Germany.

2004.10 - present: Teaching assistant for "Mathematics for Natural Scientists", Faculty of Chemistry and Earth Sciences, University of Heidelberg, Germany.

Awards Shunjie scholarship, 1994
Guanghua scholarship, 2002
Dr.-Sophie-Bernthsen-Fonds, 2004

Publications **Master Thesis**: Hybrid finite-volume/Monte-Carlo method for joint PDF equations of turbulent (non-)reactive flows on unstructured mesh. University of Science and Technology of China, Hefei, China, 2002, in Chinese. Advisor: Prof. Yi-Liang Chen.

PhD Thesis: Probability density function modeling of turbulent non-reactive and reactive spray flows. University Heidelberg, Heidelberg, Germany, 2005. Advisor: Prof. Eva Gutheil; Co-advisor: Prof. Jürgen Wolfrum.

Articles in Books, Journals and Conference Proceedings

1. **Ge HW**, Zhu MM, Hu GH, Chen YL. Hybrid finite-volume/particle method to solve joint PDF equations. *J. Univ. Sci. Tech. China*, 32(5): 607–617 (2002), in Chinese.
2. Zhu MM, **Ge HW**, Chen YL. PDF simulation of bluff-body stabilized turbulent premixed combustion. *Proc. Combust. Meeting Chinese Soc. Engng. Thermophys.*, 109–115 (2002), in Chinese.

3. **Ge HW**, Zhu MM, Chen YL. PDF simulation of bluff-body stabilized turbulent premixed combustion. *J. Engr. ThermoPhys.*, 24(3): 519–523 (2003), in Chinese.

4. Zhu MM, **Ge HW**, Chen YL, Hu GH. FV/MC hybrid algorithm for axisymmetric bluff body stabilized turbulent flows. *Acta Mechanics*, 35(3): 332–337 (2003), in Chinese.

5. **Ge HW**, Dong G, Chen YL. Numerical study of stretch effects on premixed methane-air flame. *J. Univ. Sci. Tech. China*, 33(3): 369–374(2003), in Chinese.

6. **Ge HW**, Gutheil E. PDF simulation of turbulent spray flow. *Proc. 2nd Int. SFB568 workshop*, 227–233, Heidelberg, Germany, 2004.

7. **Ge HW**, Gutheil E. PDF simulation of turbulent spray flow. *Proc. 19th ILASS-Europe*, 136–142, Nottingham, UK, 2004.

8. **Ge HW**, Gutheil E. PDF simulation of turbulent spray flow. *Atomiz. Sprays*, 2005, accepted.

9. **Ge HW**, Vogelgesang M, Gutheil E, Düwel I, Kronemayer H, Schulz C. Experimental and numerical investigation of turbulent spray flows. *SPRAY–05*, Antalya, Turkey, 2005.

10. **Ge HW**, Zhu MM, Chen YL, Gutheil E. Hybrid unsteady RANS and PDF method for turbulent flows. *Proc. 1st Workshop on Quality Assessment of Unsteady Methods for Turbulent Combustion Prediction and Validation*, Darmstadt (Seeheim-Jugenheim), Germany, June 16–17, 2005.

11. Zhu MM, **Ge HW**, Chen YL. PDF simulation of vortex shedding behind bluff body. *Proc. 1st Workshop on Quality Assessment of Unsteady Methods for Turbulent Combustion Prediction and Validation*, Darmstadt (Seeheim-Jugenheim), Germany, June 16–17, 2005.

12. **Ge HW**, Gutheil E. PDF modeling of the mixing process in turbulent spray flows. *ICDERS 2005*, Montreal, Canada, 2005.

13. Düwel I, Kronemayer H, Schulz C, **Ge HW**, Gutheil E. Numerical simulation and experimental investigation of droplet size distribution in non-reactive turbulent spray flows. *Proc. 20th ILASS-Europe*, 349–354, Orléans, France, 2005.

14. **Ge HW**, Gutheil E. Joint velocity-scalar PDF modeling of turbulent spray flows. *Proc. 20th ILASS-Europe*, 115–120, Orléans, France, 2005.

15. **Ge HW**, Zhu MM, Chen YL, Gutheil E. Hybrid unsteady RANS and PDF method for turbulent non-reactive/reactive flows. *Flow Turbul. Combust.*, 2005, submitted.
16. Zhu MM, Chen YL, **Ge HW**, Gutheil E. PDF simulation of vortex shedding behind bluff body. *J. Turbul.*, 2005, submitted.
17. **Ge HW**, Gutheil E. PDF modeling coupling with the spray flamelet model for the simulation of a turbulent spray flame. *Proc. Combust. Inst.*, 2005, submitted.
18. Düwel I, **Ge HW**, Kronemayer H, Dibble R, Gutheil E, Schulz C, Wolfrum J. Experimental and numerical characterization of a turbulent spray flame. *Proc. Combust. Inst.*, 2005, submitted.
19. **Ge HW**, Urzica D, Vogelgesang M, Gutheil E. Modeling and simulation of turbulent non-reacting and reacting spray flows. *In: Reactive flow, diffusion and transport* (R. Rannacher, Ed.), Springer, 2006, to appear.

Talks in Conferences and Symposiums

1. PDF simulation of turbulent spray flow. *19th Ann. Conf. ILASS-Europe*, Nottingham, UK, 2004.
2. Experimental and Numerical Investigation of Turbulent Spray Flows. *SPRAY–05*, Antalya, Turkey, 2005.
3. Joint velocity-scalar PDF modeling of turbulent spray flows. *20th Ann. Conf. ILASS-Europe*, Orléans, France, 2005.

Talks in Workshops

1. Numerical simulation of non-reactive and reactive turbulent spray flows. *3rd Fall Workshop on "Complex processes: modelling, simulation and optimization"*, Warsaw, Poland, Dec. 5–8, 2003.
2. Stochastic Stochastic Modeling of Turbulent Spray Flows. *Joint Workshop on "Modeling, Simulation and Control in Chemical Engineering"*, Warsaw, Poland, Apr. 14–17, 2005.
3. PDF modeling of turbulent non-reactive and reactive flows. *Workshop on "Understanding and Control of Complex Chemical Processes"*, Heidelberg, Oct. 10–11, 2005.

Bibliography

[1] International Energy Agency Paris: *Key Word Energy Statistic* (2003)

[2] G. M. Faeth: Evaporation and combustion of sprays. *Prog. Energy Combust. Sci.*, **9**, 1–76 (1983)

[3] C.-K. Law: Heat and mass transfer in combustion: Fundamental concepts and analytical techniques. *Prog. Energy Combust. Sci.*, **10**, 295–318 (1984)

[4] K.-K. Kuo: *Principles of combustion*, New York: John Wiley & Sons (1986)

[5] G. M. Faeth: Mixing, transport and combustion in sprays. *Prog. Energy Combust. Sci.*, **13**, 293–345 (1987)

[6] C. T. Crowe, J. N. Chung, T. R. Trout: Particle mixing in free shear flows. *Prog. Engery Combust. Sci.*, **14**, 171–194 (1988)

[7] G. M. Faeth: Spray combustion phenomena. *Proc. Combust. Inst.*, **26**, 1593–1612 (1996)

[8] W. A. Sirignano: *Fluid dynamics and transport of droplets and sprays*, Cambridge: Cambridge University Press (1999)

[9] G. Gouesbet, A. Berlemont: Eulerian and Lagrangian approaches for predicting the behaviour of discrete particles in turbulent flows. *Prog. Energy Combust. Sci.*, **25**, 133–159 (1999)

[10] F. Mashayek, R. V. R. Pandya: Analytical description of particle/droplet-laden turbulent flows. *Prog. Energy Combust. Sci.*, **29**, 329–378 (2003)

[11] E. Loth: Numerical approaches for motion of dispersed particles, droplets and bubbles. *Prog. Energy Combust. Sci.*, **26**, 161–223 (2000)

[12] T. Baritaud, T. Poinsot, M. Baum: *Direct numerical simulation for turbulent reacting flows*, Paris: Editions Technip (1996)

[13] P. K. Yeung, S. B. Pope: Lagrangian statistics for direct numerical simulations of isotropic turbulence. *J. Fluid Mech.*, **207**, 531–586 (1989)

[14] P. Moin, K. Mahesh: DNS: a tool for turbulence research. *Annu. Rev. Fluid Mech.*, **30**, 539–578 (1998)

[15] J. J. Riley, G. Patterson: Diffusion experiments with numerically integrated isotropic turbulence. *Phys. Fluids*, **17**, 292–297 (1974)

[16] K. D. Squires, J. K. Eaton: Measurements of particle dispersion obtained from direct numerical simulations of isotropic turbulence. *J. Fluid Mech.*, **226**, 1–35 (1991)

[17] C.-Y. Yang, U. Lei: Role of the turbulent scales in the settling velocity of heavy particles in homogeneous isotropic turbulence. *J. Fluid Mech.*, **371**, 179–205 (1998)

[18] F. Mashayek, F. A. Jaberi, R. S. Miller, P. Givi: Dispersion and polydispersity of droplets in stationary isotropic turbulence. *Int. J. Multiphas. Flow*, **23**, 337–355 (1997)

[19] W. Ling, J.-N. Chung, T. R. Troutt, C. T. Crowe: Direct numerical simulation of a three-dimensional temporal mixing layer with particle dispersion. *J. Fluid Mech.*, **358**, 61–85 (1998)

[20] I. Iliopoulos, Y. Mito, T. J. Hanratty: A stochastic model for solid particle dispersion in a nonhomogeneous turbulent field. *Int. J. Multiphas. Flow*, **29**, 375–394 (2003)

[21] K. D. Squires, J. K. Eaton: Particle response and turbulence modification in isotropic turbulence. *Phys. Fluids A*, **2**, 1191–1203 (1990)

[22] S. Elghobashi, G. C. Truesdell: On the two-way interaction between homogeneous turbulence and dispersed solid particles, I: turbulence modification. *Phys. Fluids*, **5**, 1790–1801 (1993)

[23] M. Boivin, O. Simonin, K. D. Squires: Direct numerical simulation of turbulence modulation by particles in isotropic turbulence. *J. Fluid Mech.*, **375**, 235–263 (1998)

[24] A. M. Ahmed, S. Elghobashi: On the mechanisms of modifying the structure of turbulent homogeneous shear flows by dispersed particles. *Phys. Fluids*, **12**, 2906–2930 (2000)

[25] S. Sundaram, L. R. Collins: Collision statistics in an isotropic particle-laden turbulent suspension. Part 1: direct numerical simulations. *J. Fluid Mech.*, **335**, 75–109 (1997)

[26] T. Tsuji, R. Narutomi, T. Yokomine, S. Ebara, A. Shimizu: Unsteady three-dimensional simulation of interactions between flow and two particles. *Int. J. Multiphas. Flow*, **29**, 1431–1450 (2003)

[27] Y. Sato, E. Deutsch, O. Simonin: Direct numerical simulation of heat transfer by solid particles suspended in homogeneous isotropic turbulence. *Int. J. Heat Fluid Flow*, **19**, 187–192 (1998)

[28] F. A. Jaberi: Temperature fluctuations in particle-laden homogeneous turbulent flows. *Int. J. Heat Mass Tran.*, **41**, 4081–4093 (1998)

[29] F. A. Jaberi, F. Mashayek: Temperature decay in two-phase turbulent flows. *Int. J. Heat Mass Tran.*, **43**, 993–1005 (2000)

[30] R. V. R. Pandya, F. Mashayek: Non-isothermal dispersed phase of particles in turbulent flow. *J. Fluid Mech.*, **475**, 205–245 (2003)

[31] F. Mashayek: Droplet-turbulence interactions in low mach number homogeneous shear two-phase flows. *J. Fluid Mech.*, **367**, 163–203 (1998)

[32] F. Mashayek: Direct numerical simulation of evaporating droplet dispersion in forced low mach number turbulence. *Int. J. Heat Mass Tran.*, **41**, 2601–2617 (1998)

[33] F. Mashayek: Dynamics of evaporating drops. Part I: formulation and evaporation model. *Int. J. Heat Mass Tran.*, **44**, 1517–1526 (2001)

[34] F. Mashayek: Dynamics of evaporating drops. Part II: free oscillations. *Int. J. Heat Mass Tran.*, **44**, 1527–1541 (2001)

[35] R. S. Miller, J. Bellan: Direct numerical simulation of a confined three-dimensional gas mixing layer with one evaporating hydrocarbon-droplet-laden stream. *J. Fluid. Mech.*, **384**, 293–338 (1999)

[36] R. S. Miller, J. Bellan: Direct numerical simulation and subgrid analysis of a transitional droplet laden mixing layer. *Phys. Fluids*, **12**, 650–671 (2000)

[37] H. Abdel-Hameed, J. Bellan: Direct numerical simulations of two-phase laminar jet flows with different cross-section injection geometrie. *Phys. Fluids*, **14**, 3655–3674 (2002)

[38] N. A. Okong'o, J. Bellan: Consistent large-eddy simulation of a temporal mixing layer laden with evaporating drops. Part 1. Direct numerical simulation, formulation and *a priori* analysis. *J. Fluid Mech.*, **499**, 1–47 (2004)

[39] A. Leboissetier, N. A. Okong'o, J. Bellan: Consistent large-eddy simulation of a temporal mixing layer laden with evaporating drops. Part 2. *A posteriori* modelling. *J. Fluid Mech.*, **523**, 37–78 (2005)

[40] P. C. L. Clercq, J. Bellan: Direct numerical simulation of gaseous mixing layers laden with multicomponent-liquid drops: liquid-specific effects. *J. Fluid Mech.*, **533**, 57–94 (2005)

[41] K. K. Varanasi, H. L. Clack, R. S. Miller: On preferential diffusion of binary component liquid droplets evaporating in a two-phase mixing layer. *Int. J. Multiphas. Flow*, **30**, 1235–1257 (2004)

[42] N. A. Okong'o, J. Bellan: Direct numerical simulation of a transitional supercritical binary mixing layer: heptane and nitrogen. *J. Fluid Mech.*, **464**, 1–34 (2002)

[43] R. S. Miller, K. G. Harstad, J. Bellan: Direct numerical simulations of supercritical fluid mixing layers applied to heptane - nitrogen. *J. Fluid. Mech.*, **436**, 1–39 (2001)

[44] H. Lou, R. S. Miller: On the scalar probability density function transport equation for binary mixing in isotropic turbulence at supercritical pressure. *Phys. Fluids*, **13**, 3386–3399 (2001)

[45] R. S. Miller, J. Bellan: On the validity of the assumed probability density function method for modeling binary mixing/reaction of evaporated vapor in gas/liquid-droplet turbulent shear flow. *Proc. Combust. Inst.*, **27**, 1065–1072 (1998)

[46] R. S. Miller: Turbulence-flame modification in particle laden reacting shear flow. *AIAA paper*, 2001–0193 (2001)

[47] F. Mashayek: Simulations of reacting droplets dispersed in isotropic turbulence. *AIAA J.*, **37**, 1420–1425 (1999)

[48] F. Mashayek: Numerical investigation of reacting droplets in homogeneous shear turbulence. *J. Fluid Mech.*, **405**, 1–36 (2000)

[49] F. Mashayek: Velocity and temperature statistics in reacting droplet-laden homogeneous shear turbulence. *J. Propul. Power*, **17**, 197–202 (2001)

[50] P. Domingo, L. Vervisch, J. Réveillon: DNS analysis of partially premixed combustion in spray and gaseous turbulent flame-bases stabilized in hot air. *Combust. Flame*, **140**, 172–195 (2005)

[51] S. B. Pope: *Turbulent flow*, Cambridge: Combridge University Press (2000)

[52] K. Akselvoll, P. Moin: Large-eddy simulation of turbulent confined coannular jets. *J. Fluid Mech.*, **315**, 387–411 (1996)

[53] D. C. Haworth, K. Jansen: Large-eddy simulation on unstructured deforming meshes: toward reciprocating IC engines. *Comput. Fluids*, **29**, 493–524 (2000)

[54] S. B. Pope: Ten questions concerning the large-eddy simulation of turbulent flows. *New J. Phys.*, **6**, art. no. 35 (2004)

[55] J. Janicka, A. Sadiki: Large eddy simulation of turbulent combustion systems. *Proc. Combust. Inst.*, **30**, 537–547 (2005)

[56] P. Givi: Quality assessment of the filtered density function for large eddy simulation. *1st workshop on "Quality Assessment of Unsteady Methods for Turbulent Combustion Prediction and Validation"*, Darmstadt (Seeheim -Jugenheim), Germany (June 2005)

[57] F. Yeh, U. Liu: On the motion of small particles in a homogeneous turbulent shear flow. *Phys. Fluids*, **3**, 2758–2776 (1991)

[58] Q.-Z. Wang, K. D. Squires: Large eddy simulation of particle-laden turbulent channel flows. *Phys. Fluids*, **8**, 1207–1223 (1996)

[59] S. K. Aggarwal, Y. Xiao: Effects of external forcing on droplet dispersion in a developing shear layer. *J. Propul. Power*, **10**, 395–401 (1994)

[60] V. Armenio, U. Piomelli, V. Fiorotto: Effect of the subgrid scales on particle motion. *Phys. Fluids*, **11**, 3030–3042 (1999)

[61] M. Boivin, O. Simonin, K. D. Squires: On the prediction of gas-solid flows with two-way coupling using large eddy simulation. *Phys. Fluids*, **12**, 2080–2090 (2000)

[62] V. Sankaran, S. Menon: LES of spray combustion in swirling flows. *J. Turbul.*, **3**, no.11 (2002)

[63] R. V. R. Pandya, F. Mashayek: Two-fluid large-eddy simulation approach for particle-laden turbulent flows. *Int. J. Heat Mass Tran.*, **45**, 4753–4759 (2002)

[64] S. V. Apte, M. Gorokhovsk, P. Moin: LES of atomizing spray with stochastic modeling of secondary breakup. *Int. J. Multiphas. Flow*, **29**, 1503–1522 (2003)

[65] R. Borghi: Turbulent combustion modelling. *Prog. Engery Combust. Sci.*, **14**, 245–292 (1988)

[66] A. K. Tolpadi, S. M. Correa, D. L. Burrus, H. C. Mongia: Monte Carlo Probability density function method for gas turbine combustor flowfield predictions. *J. Propul. Power*, **13**, 218–225 (1997)

[67] N. Peters: Laminar diffusion flamelet models in non-premixed turbulent combustion. *Prog. Enery Combust. Sci.*, **10**, 319–339 (1984)

[68] D. Veynante, L. Vervisch: Turbulent combustion modeling. *Prog. Engery Combust. Sci.*, **28**, 193–266 (2002)

[69] H.-W. Ge, M.-M. Zhu, Y.-L. Chen, E. Gutheil: Hybrid unsteady RANS and PDF method for turbulent non-reactive/reactive flows. *Flow Turbul. Combust.*, (2005), submitted

[70] M.-M. Zhu, Y.-L. Chen, H.-W. Ge, E. Gutheil: PDF simulation of vortex shedding behind bluff body. *J. Turbul.*, (2005), submitted

[71] S. B. Pope: PDF methods for turbulent reactive flows. *Prog. Energy Combust. Sci.*, **11**, 119–192 (1985)

[72] S. B. Pope: Lagrangian PDF methods for turbulent flows. *Annu. Rev. Fluid Mech.*, **26**, 23–63 (1994)

[73] E. Hopf: Statistical hydromechanics and functional calculus. *J. Rational Mech. Anal.*, **1**, 87–123 (1952)

[74] R. M. Lewis, R. H. Kraichnan: A space-time functional formalism for turbulence. *Comm. Pure Appl. Math.*, **15**, 397–411 (1962)

[75] C. A. Petty, X. B. J. Reed: Asympototic solutions of Hopf's equation for turbulent chemical reactions. *AIChE J.*, **18**, 751–753 (1972)

[76] T. S. Lundgren: Distribution functions in statistical theory of turbulence. *Phys. Fluids*, **10**, 969–975 (1967)

[77] T. S. Lundgren: Model equation for non-homogeneous turbulence. *Phys. Fluids*, **12**, 485–497 (1969)

[78] C. Dopazo, E. E. O'Brien: An approach to the autoignition of a turbulent mixture. *Acta. Astronaut.*, **1**, 1239–1266 (1974)

[79] C. Dopazo, E. E. O'Brien: Functional formulation of nonisothermal turbulent reactive flows. *Phys. Fluids*, **17**, 1968–1975 (1975)

[80] C. Dopazo, E. E. O'Brien: Statistical treatment of non-isothermal chemical reactions in turbulence. *Combust. Sci. Technol.*, **13**, 99–112 (1976)

[81] S. B. Pope: The probability approach to the modelling of turbulent reacting flows. *Combust. Flame*, **27**, 299–312 (1976)

[82] S. B. Pope: Computations of turbulent combustion: progress and challenges. *Proc. Combust. Inst.*, **23**, 591–612 (1990)

[83] S. B. Pope: Advances in PDF methods for turbulent reactive flows. *H. I. Andersson, P. A. Krogstad (Eds.), Advances in Turbulence X*, (2004)

[84] R. W. Bilger, S. B. Pope, K. N. C. Bray, J. F. Driscoll: Paradigms in turbulent combustion research. *Proc. Combust. Inst.*, **30**, 21–42 (2005)

[85] S. B. Pope, Y.-L. Chen: The velocity-dissipation probability density function model for turbulent flows. *Phys. Fluids A*, **2**, 1437–1449 (1990)

[86] P. R. V. Slooten, Jayesh, S. B. Pope: Advances in PDF modelling for inhomogeneous turbulent flows. *Phys. Fluids*, **10**, 246–265 (1998)

[87] S. Subramaniam, S. B. Pope: A mixing model for turbulent reactive flows based on euclidean minimum spanning trees. *Combust. Flame*, **115**, 487–514 (1998)

[88] J. P. Minier, J. Pozorski: Wall boundary conditions in PDF methods and application to a turbulent channel flow. *Phys. Fluids*, **11**, 2632–2644 (1999)

[89] M. Wacławczyk, J. Pozorski, J. P. Minier: PDF computation of turbulent flows with a new near-wall model. *Phys. Fluids*, **16**, 1410–1422 (2004)

[90] M. Muradoglu, S. B. Pope, P. Jenny, D. A. Caughey: A consistent hybrid finite-volume/particle method for the pdf equations of turbulent reactive flows. *J. Comp. Phys.*, **154**, 342–371 (1999)

[91] P. Jenny, S. B. Pope, M. Muradoglu, D. A. Caughey: A hybrid algorithm for the joint pdf equation of turbulent reactive flows. *J. Comp. Phys.*, **166**, 218–252 (2001)

[92] M. Muradoglu, S. B. Pope, D. A. Caughey: The hybrid method for the PDF equations of turbulent reactive flows: consistency conditions and correction algorithms. *J. Comp. Phys.*, **172**, 841–878 (2001)

[93] H.-W. Ge: *Hybrid Finite-Volume/Monte-Carlo method for joint PDF equations of turbulent (non-)reactive flows on unstructured mesh.* Master thesis, University of Science and Technology of China, Hefei, P. R. China (2002), in chinese

[94] M.-M. Zhu: *Hybrid finite volome/Monte-Carlo algorithm to solve the PDF equations of turbulent combustion.* PhD Thesis, University of Science and Technology of China, Hefei, P. R. China (2004), in chinese

[95] A. Y. Klimenko, S. B. Pope: A model for turbulent reactive flows based on multiple mapping conditioning. *Phys. Fluids*, **15**, 1907–1925 (2003)

[96] U. Maas, S. B. Pope: Simplifying chemical kinetics intrinsic low-dimensional manifolds in composition space. *Combust. Flame*, **88**, 239–264 (1992)

[97] S. B. Pope: Computationally efficient implementation of combustion chemistry using *in situ* adaptive tabulation. *CTM*, **1**, 41–63 (1997)

[98] J.-Y. Chen, J. A. Blasco, N. Fueyo, C. Dopazo: An economical strategy for storage of chemical kinetics: fitting *in situ* adaptive tabulation with artificial neural networks. *Proc. Combust. Inst.*, **28**, 115–121 (2001)

[99] D. C. Haworth, M. C. Drake, R. J. Blint: Stretched laminar flamelet modeling of a turbulent jet diffusion flame. *Combust. Sci. Technol.*, **60**, 287–318 (1988)

[100] H.-F. Wang, Y.-L. Chen: Flamelet modeling of turbulent jet non-premixed flame. *J. Propul. Tech.*, **24**, 58–62 (2003), in chinese

[101] H.-F. Wang, Y.-L. Chen: Unsteady flamelet modelling of turbulent non-premixed flame. *J. Engr. ThermoPhys.*, **25**, 329–332 (2004), in chinese

[102] S. Mazumder, M. F. Modest: A PDF approach to modeling turbulence-radiation interaction in nonluminous flames. *Int. J. Heat Mass Tran.*, **42**, 971–991 (1999)

[103] G.-N. Li, M. F. Modest: Application of composition PDF methods in the investigation of turbulence-radiation interactions. *J. Quant. Spectrosc. Ra.*, **73**, 461–472 (2002)

[104] P. J. Colucci, F. A. Jaberi, P. Givi, S. B. Pope: Filtered density function for large eddy simulation of turbulent reacting flows. *Phys. Fluids*, **10**, 499–515 (1998)

[105] F. A. Jaberi, P. J. Colucci, S. James, P. Givi, S. B. Pope: Filtered mass density function for large-eddy simulation of turbulent reacting flows. *J. Fluid Mech.*, **401**, 85–121 (1999)

[106] L. Y. M. Gicquel, P. Givi, F. A. Jaberi, S. B. Pope: Velocity filtered density function for large eddy simulation of turbulent flows. *Phys. Fluids*, **14**, 1196–1213 (2003)

[107] S. James, F. A. Jaberi: Large scale simulations of two-dimensional nonpremixed methane jet flames. *Combust. Flame*, **123**, 465–487 (2000)

[108] M. R. H. Sheikhi, T. G. Drozda, P. Givi, S. B. Pope: Velocity-scalar filtered density function for large eddy simulation of turbulent flows. *Phys. Fluids*, **15**, 2321–2337 (2003)

[109] V. Raman, D. Cook, H. Pitsch: Hybrid LES/FDF simulation of a non-premixed bluff-body stabilized flame. *B. Am. Phys. Soc.*, **49**, 57–58 (2004)

[110] A. Mura, R. Borghi: Introducing a new partial PDF approach for turbulent combustion modeling. *Combust. Flame*, **136**, 377–382 (2004)

[111] I. V. Derevich, L. I. Zaichik: The Equation for the probability density of the particle velocity and temperature in a turbulent flow simulated by the Gauss stochastic field. *Prikl. Mat. Mekh.*, **54**, 631–637 (1990)

[112] M. W. Reeks: On a kinetic equation for the transport of particles in turbulent flow. *Phys. Fluids A*, **3**, 446–456 (1991)

[113] D. C. Swailes, M. W. Reeks: Particle deposition from a turbulent flow. I. A steady-state model for high inertia particles. *Phys. Fluids*, **6**, 3392–3403 (1994)

[114] K. E. Hyland, S. McKee, M. W. Reeks: Derivation of a pdf kinetic equation for the transport of particles in turbulent flows. *J Phys. A-Math. Gen.*, **32**, 6169–6190 (1999)

[115] M. W. Reeks: On the continuum equations for a dispersed particles in non-uniform flows. *Phys. Fluids A*, **4**, 1290–1303 (1992)

[116] R. V. R. Pandya, F. Mashayek: Probability density function modeling of evaporating droplets dispersed in isotropic turbulence. *AIAA J.*, **39**, 1909–1915 (2001)

[117] M. W. Reeks: On the constitutive relations for dispersed particles in non-uniform flows I: Dispersion in a simple shear flow. *Phys. Fluids A*, **5**, 750–761 (1993)

[118] L. I. Zaichik: A statistical model of particle transport and heat transfer in turbulent shear flows. *Phys. Fluids*, **11**, 1521–1534 (1999)

[119] B. J. Devenish, D. C. Swailes, Y. A. Sergeev, V. N. Kurdyumov: A PDF model for dispersed particles with inelastic particle-wall collisions. *Phys. Fluids*, **11**, 1858–1868 (1999)

[120] I. V. Derevich: Statistical modelling of mass transfer in turbulent two-phase dispersed flows. I. Model development. *Int. J. Heat Mass Tran.*, **43**, 3709–3723 (2000)

[121] L. I. Zaichik, V. M. Alipchenkov: A statistical model for transport and deposition of high inertia colliding particles in turbulent flow. *Int. J. Heat Fluid Flow*, **22**, 365–371 (2001)

[122] L. I. Zaichik, V. M. Alipchenkov: Pair dispersion and preferential concentration of particles in isotropic turbulence. *Phys. Fluids*, **15**, 1776–1787 (2003)

[123] V. M. Alipchenkov, L. I. Zaichik: Statistical model of particle motion and dispersion in an anisotropic turbulent flow. *Fluid Dyn.*, **39**, 735–747 (2004)

[124] L. I. Zaichik, B. Oesterlé, V. M. Alipchenkov: On the probability density function model for the transport of particles in anisotropic turbulent flow. *Phys. Fluids*, **16**, 1956–1964 (2004)

[125] V. M. Alipchenkov, L. I. Zaichik: Dispersion and clustering of bidisperse particles in isotropic turbulence. *Fluid Dyn.*, **40**, 83–94 (2005)

[126] W. P. Jones, D. H. Sheen: A probability density function method for modelling liquid fuel sprays. *Flow Turbul. Combust.*, **63**, 379–394 (1999)

[127] O. Simonin: Statistical and continuum modeling of turbulent reactive particulate flows. Part I: theoretical derivation of dispersed phase Eulerian modeling from probability density function kinetic equation. *VKI Lectures On Combustion and Turbulence in Two-Phase Flows*, (1996)

[128] O. Simonin: Statistical and continuum modeling of turbulent reactive particulate flows. Part II: Application of a two-phase second-moment transport model for prediction of turbulent gas-particle flows. *VKI Lectures On Combustion and Turbulence in Two-Phase Flows*, (1996)

[129] J. Pozorski, J. P. Minier: On the Lagrangian turbulent dispersion models based on the Langevin equation. *Int. J. Multiphas. flow*, **24**, 913–945 (1998)

[130] J. P. Minier, E. Peirano: The pdf approach to turbulent polydispersed two-phase flows. *Phys. Rep.*, **325**, 1–214 (2001)

[131] E. Peirano, J. P. Minier: Probabilistic formalism and hierarchy of models for polydispersed turbulent two-phase flows. *Phys. Rev. E*, **65**, art. no. 046301 (2002)

[132] Z. Gao, F. Mashayek: Stochastic model for nonisothermal droplet-laden turbulent flows. *AIAA J.*, **42**, 255–260 (2004)

[133] Z.-H. Liu, C.-G. Zheng, L.-X. Zhou: A joint PDF model for turbulent spray evaporation/combustion. *Proc. Combust. Inst.*, **29**, 561–568 (2002)

[134] Z.-H. Liu: *The SOM-PDF transport equation model and PDPA measurements of turbulent gas-particle flows.* PhD Thesis, Huazhong University of Science and Technology, Wuhan, P.R.China (2002), in chinese

[135] M. S. Raju: Application of scalar Monte Carlo probability density function method for turbulent spray flames. *Numer. Heat Tr. A-Appl.*, **30**, 753–777 (1996)

[136] M. S. Raju: Scalar Monte-Carlo PDF computations of spray flames on unstructured grids with parallel computing. *Numer. Heat Tr. B-Fund.*, **35**, 185–209 (1999)

[137] M. S. Raju: On the importance of chemistry/turbulence interactions in spray computations. *Numer. Heat Trans. B-Fund.*, **41**, 409–432 (2002)

[138] C. Taut, C. Correa, O. Deutschmann, J. Warnatz, S. Einecke, C. Schulz, J. Wolfrum: 3D-modelling with Monte-Carlo-PDF methods and laser diagnostics of the cmbustion in a two-stroke engine. *Proc. Combust. Inst.*, **28**, 1153–1159 (2000)

[139] P. Durand, M. Gorokhovski, R. Borghi: An application of the probability density function model to diesel engine combustion. *Combust. Sci. Technol.*, **158**, 47–78 (2000)

[140] H.-W. Ge, E. Gutheil: PDF simulation of turbulent spray flows. *Atomiz. Sprays*, (2005), accepted

[141] H.-W. Ge, E. Gutheil: Joint velocity-scalar PDF modeling of turbulent spray flows. *Proc. 20th ILASS–Europe*, Orléans, France (September 2005)

[142] H.-W. Ge, E. Gutheil: PDF modeling coupled with the spray flamelet model for the simulation of a turbulent spray flame. *Proc. Combust. Inst.*, (2005), submitted

[143] M. Zhu, K. N. C. Bray, B. Rogg: PDF modelling of spray autoignition in high pressure turbulent flows. *Combust. Sci. Technol.*, **120**, 1996 (357-379)

[144] M. Zhu, K. N. C. Bray, O. Rumberg, B. Rogg: PDF transport equations for two-phase reactive flows and sprays *Combust. Flame*, **122**, 327–338 (2000)

[145] O. Rumberg, B. Rogg: Full PDF modelling of reactive sprays via an evaporation-progress variable *Combust. Sci. Technol.*, **158**, 211–247 (2000)

[146] B. Naud: *PDF modeling of turbulent sprays and flames using a particle stochastic approach.* PhD Thesis, Delft University of Technology, Delft, Netherland (2003)

[147] B. Naud, D. Roekaerts: Stochastic modelling of sprays and flames. *Proc. 20th ILASS–Europe*, 10–10 Orléans, France (September 2005)

[148] N. A. Beishuizen, D. Roekaerts: Numerical modeling of spray evaporation. *Int. Symp. Heat Mass Transfer in Spray Systems*, Antalya, Turkey (June 2005)

[149] R. Borghi: *Réactions chimiques en milieu turbulent.* PhD Thesis, Université Pierre et Marie Curie, Paris 6 (1978)

[150] C. W. Gear: The automatic integration of ordinary differential equations. *Comm. ACM*, **14**, 176–179 (1971)

[151] A. C. Hindmarsh, G. D. Byrne: *EPISODE: An effective package for the integration of systems of ordinary differential equations.* Tech. Rep. UCID-30112 Lawrence Livermore Laboratory (1977)

[152] D. B. Spalding: Mixing and chemical reaction steady confined turbulent flames. *Proc. Combust. Inst.*, **13**, 1971 (649-657)

[153] S. Magnussen, B. H. Hjertager: On the mathematical modeling of turbulent combustion with special emphasis on soot formation and combustion. *Proc. Combust. Inst.*, **16**, 719–729 (1977)

[154] F. C. Christo, A. R. Masri, E. M. Nebot: Artificial neural network implementation of chemistry with pdf simulation of H2/CO2 flames. *Combust. Flame*, **106**, 406–427 (1996)

[155] T. Turányi: Application of Repro-Modeling for the Reduction of Combustion Mechanisms. *Proc. Combust. Inst.*, **25**, 949–955 (1994)

[156] J. B. Bell, N. J. Brown, M. S. Day, M. Frenklach, J. F. Grcar, R. M. Propp, S. R. Tonse: The dependence of chemistry on the inlet equivalence ratio in vortex-flame interactions. *Proc. Combust. Inst.*, **28**, 107–113 (2001)

[157] F. Mauss, N. Peters: Reduced kinetic mechanisms for premixed methane-air flames. *N. Peters, B. Rogg (Eds.), Reduced Kinetic Mechanisms for Applications in Combustion Systems*, New York: Springer (1993)

[158] J. Warnatz, U. Maas, R. W. Dibble: *Combustion*, Berlin: Springer (1999)

[159] S. B. Pope, U. Maas: *Simplifying chemical kinetics: trajectory-generated low-dimensional manifolds.* Tech. Rep. FDA 93-11 Cornell University (1993)

[160] S. H. Lam: Using CSP to understand complex chemical kinetics. *Combust. Sci. Technol.*, **89**, 375–404 (1993)

[161] J. A. van Oijen, L. P. H. D. Goey: Modeling of premixed laminar flames using flamelet generated manifolds. *Combust. Sci. Technol.*, **161**, 113–137 (2000)

[162] O. Gicquel, N. Darabiha, D. Thévenin: Laminar premixed hydrogen/air counter-flow flames simulation using flame prolongations of ILDM. *Proc. Combust. Inst.*, **28**, 1901–1908 (2001)

[163] M. R. Roussel, S. J. Fraser: Global analysis of enzyme inhibition kinetics. *J. Phys. Chem.*, **97**, 8316–8327 (1993)

[164] J. C. Keck: Rate-controlled constrained-equilibrium theory of chemical reactions in complex systems. *Prog. Energy Combust. Sci.*, **16**, 125–154 (1990)

[165] Q. Tang, S. B. Pope: Implementation of combustion chemistry by *in situ* adaptive tabulation of rate-controlled constrained equilibrium manifolds *Proc. Combust. Inst.*, **29**, 1411–1417 (2002)

[166] Z.-Y. Ren, S. B. Pope: Species reconstruction using pre-image curves. *Proc. Combust. Inst.*, **30**, 1293–1300 (2005)

[167] J. B. Moss, K. N. C. Bray: A unified statistical model of the premixed turbulent flame. *Acta Astronaut.*, **4**, 291–319 (1977)

[168] C. Meneveau, T. Poinsot: Stretching and quenching of flamelets in premixed turbulent combustion. *Combust. Flame*, **81**, 311–332 (1991)

[169] N. Peters: *Turbulent combustion*, Cambridge: Cambridge University Press (2000)

[170] J. M. Richardson, H. C. Howard, R. W. Simth: The relation between sampling-tube measurements and concentration fluctuations in a turbulent gas jet. *Proc. Combust. Inst.*, **4**, 814–817 (1953)

[171] A. R. Kerstein, W. T. Ashurt: *Lognormality of gradients of diffusive scalars in homogeneous, two-dimensional mixing systems.* Tech. rep. Sandia National Laboratory (1983)

[172] A. Y. Klimenko: Multicomponent diffusion of various admixtures in turbulent flow. *Fluid Dyn.*, **25**, 327–334 (1990)

[173] R. W. Bilger: Conditional moment closure for turbulent reacting flow. *Phys. Fluids A*, **5**, 436–444 (1993)

[174] A. Y. Klimenko, R. W. Bilger: Conditional moment closure for turbulent combustion. *Prog. Energy Combust. Sci.*, **25**, 595–687 (199)

[175] W. T. Kim, K. Y. Huh: Numerical simulation of spray autoignition by the first-order conditional moment closure model. *Proc. Combust. Inst.*, **29**, 569–576 (2002)

[176] M. P. Musculus, C. J. Rutland: Coherent flamelet modeling of diesel engine combustion. *Combust. Sci. Technol.*, **104**, 295–337 (1995)

[177] A. Gill, E. Gutheil, J. Warnatz: Numerical investigation of the combustion process in a direct injection stratified charge engine. *Combust. Sci. Technol.*, **115**, 317–333 (1996)

[178] C. Hollmann, E. Gutheil: Modeling of turbulent spray diffusion flames including detailed chemistry. *Proc. Combust. Inst.*, **26**, 1731–1738 (1996)

[179] C. S. Chang, Y. Zhang, K. N. C. Bray, B. Rogg: Modeling and simulation of autoignition under simulated diesel-engine conditions. *Combust. Sci. Technol.*, **113-114**, 205–219 (1996)

[180] C. Hollmann, E. Gutheil: Flamelet-modeling of turbulent spray diffusion flames based on a laminar spray flame library. *Combust. Sci. Technol.*, **135**, 175–192 (1998)

[181] E. Gutheil, W. A. Sirignano: Counterflow spray combustion modeling including detailed transport and detailed chemistry. *Combust. Flame*, **113**, 92–105 (1998)

[182] D. Schlotz, E. Gutheil: Modeling of laminar mono-and bidisperse liquid oxygen/hydrogen spray flames in the counterflow configuration. *Combust. Sci. Technol.*, **158**, 195–210 (2000)

[183] E. Gutheil: Structure and extinction of laminar ethanol/air spray flames. *CTM*, **5**, 1–15 (2001)

[184] I. Düwel, H.-W. Ge, H. Kronemayer, R. Dibble, E. Gutheil, C. Schulz, J. Wolfrum: Experimental and numerical characterization of a turbulent spray flame. *Proc. Combust. Inst.*, (2005), submitted

[185] T. Poinsot, D. Veynante: *Theoretical and numerical combustion*, Philadelphia: Edwards (2001)

[186] M. W. Chase, C. A. Davis, J. R. Downey, D. J. Frurip, R. A. McDonald, A. N. Syverud: JANAF Thermochemical Tables, 3rd ed. *J. Phys. Chem. Ref. Data*, **14** (1985)

[187] A. Burcat, B. McBride: *1994 ideal gas thermodynamic data for combustion and air-pollutant use.* Tech. Rep. Report TAE 697 TECHNION - Israel Institute of Technology Haifa, Israel (1993)

[188] R. J. Kee, J. Warnatz, J. A. Miller: *A FORTRAN computer-code package for the evaluation of gas-phase viscosities, conductivities, and diffusion coefficients.* Tech. Rep. Report SAND 83-8209 Sandia Laboratory (1983)

[189] J. O. Hirschfelder, C. F. Curtiss, R. B. Bird: *Molecular theory of gases and liquids*, New York: John Wiley & Sons (1954)

[190] L. Prandtl: Bericht über Untersuchungen zur ausgebildeten Turbulenz. *Z. Angew. Math. Meth.*, **5**, 136–139 (1925)

[191] B. E. Launder, D. B. Spalding: *Mathematical models of turbulence.*, London/New York: Academic Press (1972)

[192] P. P. Spalart, S. R. Allmaras: A one-equation turbulence model for aerodynamics flows. *Rech. Aerospatiale*, **1**, 5–21 (1994)

[193] W. P. Jones, B. E. Launder: The prediction of laminarization with a two-equation model of turbulence. *Int. J. Heat Mass Tran.*, **15**, 301–314 (1972)

[194] C. Hollmann: *Modellierung turbulenter Sprayflammen unter Verwendung detaillierter chemischer Reaktionsmechanismen.* PhD Thesis, University Heidelberg, Heidelberg (1997)

[195] A. A. Amsden, P. J. O'Rourke, T. D. Butler: *KIVA-II: A computer program for chemically reactive flows with sprays.* Tech. Rep. UC-96 Los Alamos National Laboratory (May 1989)

[196] K. N. C. Bray, P. A. Libby, G. Masuya, J. B. Moss: Turbulence production in premixed turbulent flames. *Combust. Sci. Technol.*, **25**, 127–140 (1981)

[197] K. N. C. Bray, M. Champion, P. A. Libby: The interaction between turbulence and chemistry in prexmied turbulent flames. *P. A. Libby, F. A. Williams (Eds.), Turbulent Reactive Flows*, New York: Springer (1989)

[198] M. Vogelgesang: *Entwicklung eines Reynolds-Spannungs-Modells zur Modellierung turbulenter Sprayflammen.* PhD Thesis, University Heidelberg, Heidelberg (2005)

[199] D. C. Haworth, S. B. Pope: A generalized Langevin model for turbulent flows. *Phys. Fluids*, **29**, 387–405 (1986)

[200] S. B. Pope: Stochastic Lagrangian models of velocity in homogeneous turbulent shear flow. *Phys. Fluids*, **14**, 1696–1702 (2002)

[201] S. B. Pope: A stochastic Lagrangian model for acceleration in turbulent flows. *Phys. Fluids*, **14**, 2360–2375 (2002)

[202] C. Dopazo: Probability density function approach for a turbulent axisymmetric heated jet. Centerline evolution. *Phys. Fluids*, **18**, 397–404 (1975)

[203] J. Janicka, W. Kolbe, W. Kollmann: Closure of the transport equation for the probability density function of turbulent scalar fields. *J. Non-Equilib. Thermodyn.*, **4**, 47–66 (1979)

[204] V. Raman, R. O. Fox, A. D. Harvey: Hybrid finite-volume/transport PDF simulations of a partially premixed methane-air flame. *Combust. Flame*, **136**, 327–350 (2004)

[205] S. Tavoularis, S. Corrsin: Experiments in nearly homogeneous turbulent shear flows with a uniform mean temperature gradient. Part 1. *J. Fluid Mech.*, **104**, 311–347 (1981)

[206] G. E. P. Box, M. E. Muller: A note on the generation of random normal deviates. *Ann. Math. Stat.*, **29**, 610–611 (1958)

[207] W. H. Press, B. P. Flannery, S. A. Teukolsky, W. T. Vetterling: *Numerical recipes*, Cambridge: Combridge University Press (1986)

[208] J. B. Kennedy, A. M. Neville: *Basic statistical methods for engineerings and scientists.*, New York: Harper & Row Publishers, Inc. (1986)

[209] S. Nukiyama, Y. Tanasawa: Experiments on the atomization of liquids in an air stream. Report 3: on the droplet-szie distribution in an atomized jet. *Trans. Soc. Mech. Engrs. Jpn.*, **5**, 62–67 (1939)

[210] E. Babinsky, P. E. Sojka: Modeling drop size distribution. *Prog. Energy Combust. Sci.*, **28**, 303–329 (2002)

[211] R. A. Fisher, L. M. C. Tippett: Limiting forms of the frequency distribution of the largest or smallest member of a sample. *Proc. Cambridge Phil. Soc.*, **24**, 180–190 (1928)

[212] W. Weibull: A statistical theory of the strenth of materials. *Ing. Velemskaps Akas. Handl.*, **151**, 1–45 (1939)

[213] W. Weibull: A statistical distribution of wide applicability. *J. Applied Mech.*, **18**, 293–297 (1951)

[214] L. J. Bian: *Statistical analysis of reliability and life-testing mdels*, New York: Marcel Dekker, Inc. (1978)

[215] P. Rosin, E. Rammler: The laws governing the fineness of powdered coal. *J. Inst. Fuel*, **7**, 1933 (29-36)

[216] F. A. Williams: Spray combustion and atomization. *Phys. Fluids*, **1**, 541–545 (1958)

[217] S. Subramaniam: Statistical representation of a spray as a point process. *Phys. Fluids*, **12**, 2413–2431 (2000)

[218] G. M. Faeth: Current status of droplet and liquid combustion. *Prog. Energy Combust. Sci.*, **3**, 191–224 (1977)

[219] G. L. Hubbard, V. E. Denny, A. F. Mills: Droplet evaporation: effects of transient and variable properties. *Int. J. Heat Mass Tran.*, **18**, 1003–1008 (1975)

[220] A. D. Gosman, E. Ioannides: Aspects of computer simulation of liquid-fueled combustors. *AIAA paper*, 81–0323 (1981)

[221] B. Abramzon, W. A. Sirignano: Droplet vaporization model for spray combustion calculation. *Int. J. Heat Mass Transfer*, **32**, 1605–1618 (1989)

[222] R. Clift, J. R. Grace, M. E. Weber: *Bubbles, drops and particles*, New York: Academic Press (1978)

[223] D. B. Spalding: The combustion of liquid fuels. *Proc. Combust. Inst.*, **4**, 1952 (847-864)

[224] N. B. Vargaftik: *Handbook of physical properties of liquids and gases: Pure substances and mixtures.*, Washington: Hemisphere Publ. Corp. (1986)

[225] K. W. Mao, H. L. Toor: A diffusion model for reactions with turbulent mixing. *AIChE J.*, **16**, 49–52 (1970)

[226] C. H. Gibson, P. A. Libby: On turbulent flows with fast chemical reaction. Part II–The distribution of reactants and products near a reacting surface. *Combust. Sci. Technol.*, **8**, 29–35 (1972)

[227] H. Pitsch: Unsteady flamelet modeling of differential diffusion in turbulent jet diffusion flames. *Combust. Flame*, **123**, 358–374 (2000)

[228] H. Pitsch, M. Chen, N. Peters: Unsteady flamelet modeling of turbulent hydrogen-air diffusion flames. *Proc. Combust. Inst.*, **27**, 1057–1064 (1998)

[229] S. Mitarai, Kosály, J. J. Riley: A new Lagrangian flamelet model for local flame extinction and reignition. *Combust. Flame*, **137**, 306–319 (2004)

[230] E. Effelsberg, N. Peters: Scalar dissipation rates in turbulent jets and jet diffusion flames. *Proc. Combust. Inst.*, **22**, 693–700 (1988)

[231] D. A. Feikema, D. Everest, J. F. Driscoll: Images of dissipation layers to quantify mixing within a turbulent jet. *AIAA J.*, **34**, 2531–2538 (1996)

[232] S. H. Stårner, R. W. Bilger, M. B. Long, J. H. Frank, D. F. Marran: Scalar dissipation measurements in turbulent jet diffusion flames of air diluted methane and hydrogen. *Combust. Sci. Technol.*, **129**, 141–163 (1997)

[233] F. X. Demoulin, R. Borghi: Assumed PDF modeling of turbulent spray combustion. *Combust. Sci. Technol.*, **158**, 249–271 (2000)

[234] F. H. Harlow, J. E. Welch: Numerical calculation of time-dependent viscous incompressible flow of fluid with free surfaces. *Phys. Fluids*, **8**, 2182–2188 (1965)

[235] S. K. Srivatsa: CORA2: A computer code for axi-symmetrical combustion chambers. (May 1977), CHAM Ltd.

[236] C. A. J. Fletcher: *Computational techniques for fluid dynamics 2. Specific techniques for different flow categories*, Berlin/New York: Springer (1991)

[237] J. P. V. Doormal, G. D. Raithby: Enhancement of the SIMPLE method for predicting incompressible fluid flows. *Numer. Heat Transfer*, **7**, 147–163 (1984)

[238] S. B. Pope: Private communication. (2001)

[239] C. T. Crowe, M. P. Sharma, D. E. Stock: The particle-source-in cell (PSI-Cell) model for gas-droplet flows. *J. Fluid. Eng.-T. ASME*, **99**, 325–332 (1977)

[240] V. G. McDonell, G. S. Samuelsen: *Detailed data set: PDI and IRES measurements in methanol sprays under reacting and nonreacting conditions, case A-C.* Tech. Rep. UCI-ARTR-90-17A-C UCI Combustion Laboratory Irvine,CA (1990)

[241] V. G. McDonell, G. S. Samuelsen: An experimental data base for computational fluid dynamics of reacting and nonreacting methanol sprays. *J. Fluid. Eng.-T. ASME*, **117**, 145–153 (1995)

[242] K. Liu: *Joint velocity-turbulent frequency-composition probability density function (PDF) calculation of bluff body stabilized flames.* PhD Thesis, Cornell University, (2004)

[243] T.-M. Liou, W.-Y. Lien, P.-W. Hwang: Flammability limits and probability density function in simulated solid-fuel ramjet combustors. *J. Propul. Power*, **13**, 643–650 (1997)

[244] V. Eswaran, S. B. Pope: Direct numerical simulations of the turbulent mixing of a passive scalar. *Phys. Fluids*, **31**, 506–520 (1988)

[245] C. Chevalier: *Entwicklung eines detaillierten Reaktionsmechanismus zur Modellierung der Verbrennungsprozesse von Kohlenwasserstoffen bei Hoch- und Niedrigtemperaturbedingungen.* PhD Thesis, University Stuttgart, Stuttgart (1993)

[246] I. Düwel, H. Kronemayer, C. Schulz, J. Wolfrum, H.-W. Ge, E. Gutheil: Joint velocity-scalar PDF modeling of turbulent spray flows. *Proc. 20th ILASS–Europe*, 349–354 Orléans, France (September 2005)

[247] T. Kunzelmann: *Charakterisierung von Sprayflammen mittels abbildender Laserspektroskopie.* PhD Thesis, University of Heidelberg, Heidelberg (2002)

[248] R. Cabra, Y. Hamano, J.-Y. Chen, F. Acosta, D. Holve, R. W. Dibble: Ensemble diffraction measurements of spray combustion in a novel vitiated coflow turbulent jet flame burner. *Spring Meeting of the Western States Section of the Combustion Institute*, Golden, CO (March 2000)

[249] I. Düwel, T. Kunzelmann, J. Schorr, C. Schulz, J. Wolfrum: Application of fuel tracers with different volatilities for planar LIF/Mie drop-sizing in evaporating systems. *Proc. ICLASS 2003*, Sorrento, Italy (2003)

[250] W. G. Bessler, C. Schulz: Quantitative multiline NO-LIF temperature imaging. *Appl. Phys. B*, **78**, 519–533 (2004)

[251] H. Kronemayer, W. G. Bessler, C. Schulz: Gas-phase temperature imaging in spray systems using multi-line NO-LIF thermometry. *Appl. Phys. B*, **81**, 1071–1074 (2005)

[252] P. Lavieille, F. Lemoine, G. Lavergne, M. Lebourché: Evaporating and combusting droplet temperature measurements using two-color laser-induced fluorescence. *Exp. Fluids*, **31**, 45–55 (2001)

[253] H. Kronemayer, I. Düwel, C. Schulz: Temperature imaging in spray flames. *European Combustion Meeting*, Louvain-la-Neuve, Belgium (April 2005)

[254] H.-W. Ge, M. Vogelgesang, E. Gutheil, I. Düwel, H. Kronemayer, C. Schulz: Experimental and numerical investigation of turbulent spray flows. *Int. Symp. Heat Mass Transfer in Spray Systems*, 115–120 Antalya, Turkey (June 2005)